Noninvasive Measurement of Dynamic Correlations in Spin Systems

by

Philipp Johann Uhrich

Thesis presented in partial fulfilment of the requirements for the degree of Master of Science in Theoretical Physics in the Faculty of Science at Stellenbosch University

Supervisors:

Prof. M. Kastner

National Institute for Theoretical Physics
Stellenbosch Node

Dr. H. Uys

Department of Physics
Stellenbosch University

December 2017

Declaration

By submitting this thesis electronically, I declare that the entirety of the work contained therein is my own, original work, that I am the sole author thereof (save to the extent explicitly otherwise stated), that reproduction and publication thereof by Stellenbosch University will not infringe any third party rights and that I have not previously in its entirety or in part submitted it for obtaining any qualification.

Date: ..... December 2017 .....

Abstract

Dynamic correlations $\langle\psi| O_1(t_1)O_2(t_2) |\psi\rangle$ of quantum observables are useful quantities for the study of quantum dynamics. Attempts at measuring these correlations are however complicated, due to the measurement backaction (wave function collapse) incurred during measurements at the early time t_1. We propose a noninvasive measurement protocol, based on a weak ancilla–target coupling, which reduces this backaction at t_1. We show that both real and imaginary parts of the desired correlation can be extracted through appropriate choices of the initial ancilla state and of the ancilla–target coupling Hamiltonian. The protocol is applicable to arbitrary (pseudo)spin systems with arbitrary (non)equilibrium initial states. Errors arising in experimental implementations are analysed, and we show that deviations from the desired correlation can be minimised through an optimal choice of the ancilla–target coupling time. Implementation in linear ion trap experiments is discussed.

We derive the positive-operator-valued measure which describes the noninvasive measurement at t_1. For dynamic correlations of single-site spin-1/2 observables, this operator formalism shows that measurement backaction is of no concern. Real parts can be obtained with projective measurements of the target at t_1 and t_2. Imaginary parts are obtained by performing a local rotation of the target at t_1, followed by a projective measurement at t_2. These ancilla-free protocols are theoretically simpler than the noninvasive measurement protocol, but remain experimentally challenging. Rotations and projections performed at t_1 may be subject to noise, which propagates into the measured correlation. We use Lieb-Robinson theory to bound the size of the resulting error terms. An analysis of the spatio-temporal behaviour of these errors provides guidance for experimental implementation of the ancilla-free measurement protocols.

Uittreksel

Dinamiese korrelasies $\langle\psi| O_1(t_1)O_2(t_2) |\psi\rangle$ van kwantum waarneembares is nuttig in die studie van kwantum dinamika. Die meting van hierdie hoeveelhede word egter gekompliseer deur die meetingsterugreaksie (golffunksie ineenstorting), wat tydens die meting by die vroeër tyd t_1 plaasvind. Ons stel 'n nie-ingrypende metingsprotokol voor, gebaseer op 'n swak ancilla–teikenstelsel koppeling, wat die meetingsterugreaksie by t_1 verminder. Ons toon dat die reële en imaginêre dele van die korrelasiefunksie deur geskikte keuses van die ancilla begintoestand en van die ancilla–teikenstelsel koppeling bepaal kan word. Die protokol is van toepassing op (pseudo)spin stelsels met arbitrêre nie-ewewig begintoestande. Foute wat in eksperimentele implementering ontstaan word geanaliseer. Ons toon dat afwykings van die gewenste korrelasie geminimeer kan word deur 'n optimale ancilla–teikenstelsel koppelingstyd. Implementering in liniêre ioonputte word bespreek.

Ons herlei die positiewe operator-waardige maat wat die nie-ingrypende meting by t_1 beskryf. Hierdie formalisme toon dat die meetingsterugreaksie van geen belang is vir dinamiese korrelasies van enkelpunt spin-1/2 waarneembares nie. Die reële deel kan deur projektiewe meetings by t_1 en t_2 bepaal word. Die imaginêre deel word verkry deur 'n lokale rotasie by t_1, gevolg deur 'n projektiewe meting by t_2. Hierdie ancilla-vrye protokolle is teoreties eenvoudiger as die nie-ingrypende metingsprotokol, maar eksperimentele implementering bly uitdagend. Rotasies en projeksies wat by t_1 uitgevoer word kan onder steurings ly, wat dan ook die gemete korrelasies affekteer. Ons gebruik Lieb-Robinson teorie om die grootte van die resulterende foute te begrens. 'n Analise van die foute se tyd en ruimtelike gedrag bied leiding vir die eksperimentele implementering van die ancilla-vrye metingsprotokolle.

Acknowledgements

I would like to express my sincere gratitude to my supervisors, Michael Kastner and Hermann Uys, for inspiring discussions and guidance throughout this project.

I would also like to thank the Sam Cohen Trust, the NRF, and Stellenbosch University for their financial support during my studies.

Lastly, I would like thank NITheP, in particular the staff and students, for providing a stimulating research environment.

Dedications

To my parents.

Contents

1

Introduction

Dynamic two-point correlation functions $C(t_1, t_2) = \langle O_1(t_1)O_2(t_2)\rangle$ relate the state of a system with respect to some observable O_1 at an early time[1] $t_1 \geq 0$ to the state of a system with respect to another observable O_2 at a later time $t_2 > t_1$. They play an important role in many theoretical approaches, including fluctuation-dissipation theorems and the Kubo formula [1], optical coherence [2], glassy dynamics and aging [3], and many more.

In a classical (non-quantum mechanical) system, a straightforward—at least in principle—protocol for determining dynamic correlations consists of measuring the observable O_1 at time t_1 and correlating the outcome with the measured value of O_2 at time t_2. In a quantum mechanical system, however, such a naive approach is in general thwarted by the measurement backaction i.e. the disturbing effect that a measurement of O_1 at the earlier time t_1 has on the subsequent time evolution, due to the collapse of the wave function [4; 5; 6]. As a result of this disturbance, correlating the eigenvalue obtained from a measurement of O_1 at time t_1 with that obtained from a measurement of O_2 at t_2 does not yield the desired dynamic correlation function C.

As an example, consider a lattice system consisting of two spin-1/2 degrees of freedom, initially in a product state

$$|\psi\rangle = (\alpha\,|+\rangle + \beta\,|-\rangle) \otimes (\alpha\,|+\rangle + \beta\,|-\rangle) = |\psi_1\rangle\,|\psi_2\rangle \tag{1.0.1}$$

with $\alpha, \beta \in \mathbb{C}$. The subscripts 1 and 2 denote the lattice positions of the two spins and $|+\rangle$ and $|-\rangle$ denote eigenstates of the Pauli operator σ^z with eigenvalues $+1$ and -1, respectively. Assume the dynamics of the two spins to be governed by the Hamiltonian $H = \sigma^x \otimes \sigma^x$. It follows from the series expansion of the corresponding time-evolution operator that

$$U(t) = \exp(-iHt) = \cos(t) - i\sin(t)(\sigma^x \otimes \sigma^x), \tag{1.0.2}$$

in units where $\hbar = 1$. Suppose now that we wish to correlate spin observables $O_1 = \sigma^z \otimes \mathbb{1}$ and $O_2 = \mathbb{1} \otimes \sigma^z$ at times t_1 and t_2 respectively. For simplicity we

[1] $O(t)$ denotes the time-evolved observable $U^\dagger(t)OU(t)$ in the Heisenberg picture where $U(t)$ is the time evolution generated by the system's Hamiltonian H_s.

choose $t_1 = 0$ and $t_2 = t > 0$, in which case one obtains

$$\begin{aligned} C(0,t) &= \langle\psi| (\sigma^z \otimes \mathbb{1}) U^\dagger(t) (\mathbb{1} \otimes \sigma^z) U(t) |\psi\rangle \\ &= \cos(2t) \left(|\alpha|^2 - |\beta|^2\right)^2 - i \sin(2t) \left(\alpha^* \beta - \alpha \beta^*\right)^2 \end{aligned} \tag{1.0.3}$$

for the exact dynamic correlation function.

Following the naive (classical) approach we now attempt to measure this correlation via projective measurements of either observable. The measurement at $t_1 = 0$ is done in the eigenbasis of σ^a, which we denote as $\{|m_a\rangle\}$, and will yield an eigenvalue $m_a \in \{\pm 1\}$ of σ^a with probability

$$P^{\text{Proj}}_{m_a} = \langle\psi| \Pi^{m_a} \otimes \mathbb{1} |\psi\rangle = |\langle\psi_1|m_a\rangle|^2 \tag{1.0.4}$$

according to Born's rule. Here $\Pi^{m_a} = |m_a\rangle \langle m_a|$ is a projection operator and $\mathbb{1}$ is the identity. The normalised post-measurement[2] state is

$$|\psi_{m_a}\rangle = \Pi^{m_a} \otimes \mathbb{1} |\psi\rangle / \sqrt{P^{\text{Proj}}_{m_a}} \tag{1.0.5}$$

according to the von Neumann projection postulate. The measurement at $t_2 = t$ (done in the eigenbasis $\{|m_b\rangle\}$ of σ^b) is therefore conditioned on the eigenvalue measured at t_1, and yields an eigenvalue $m_b \in \{\pm 1\}$ with probability

$$P^{\text{Proj}}_{m_b|m_a} = \langle\psi| (\Pi^{m_a} \otimes \mathbb{1}) U^\dagger(t) (\mathbb{1} \otimes \Pi^{m_b}) U(t) (\Pi^{m_a} \otimes \mathbb{1}) |\psi\rangle / P^{\text{Proj}}_{m_a}. \tag{1.0.6}$$

Correlating the measured outcomes as

$$\mathscr{C}^{\text{Proj}}(0,t) = \sum_{m_a, m_b = \pm 1} m_a m_b P^{\text{Proj}}_{m_a} P^{\text{Proj}}_{m_b|m_a} \tag{1.0.7}$$

we find that

$$\mathscr{C}^{\text{Proj}}(0,t) = \cos(2t) \left(|\alpha|^2 - |\beta|^2\right)^2 \neq C(0,t). \tag{1.0.8}$$

In general then such a naive approach to measuring dynamic correlations fails to yield the correct dynamic correlation. The measurement backaction, or wave function collapse, inherent to projective measurements makes measurement of dynamic correlations challenging, both theoretically and experimentally.

An alternative approach which avoids multiple temporally separated measurements goes as follows: First, we notice that any operator product $O_1(t_1)O_2(t_2)$ may be written as a sum of two observables

$$O_1(t_1)O_2(t_2) = \Omega_1 + i\Omega_2 \text{ where } \Omega_1 = \frac{1}{2}\{O_1(t_1), O_2(t_2)\} \text{ and } \Omega_2 = \frac{-i}{2}[O_1(t_1), O_2(t_2)]. \tag{1.0.9}$$

[2] We require an initial state $|\psi_1\rangle$ satisfying $\langle \pm_a|\psi_1\rangle \neq 0$ in order to avoid division by zero in (1.0.5).

From this follows that

$$C = \langle\psi|\,\Omega_1\,|\psi\rangle + i\,\langle\psi|\,\Omega_2\,|\psi\rangle\,, \tag{1.0.10}$$

which implies that we can reconstruct C from measurements of the two expectation values in (1.0.10). To measure these expectation values one only needs to (repeatedly) prepare the system state $|\psi\rangle$ and perform a projective measurement of Ω_1 (or Ω_2) at a single point in time $t = 0$. Measurement backaction is thus not an issue.

The underlying assumptions in this approach are firstly that we can determine (calculate) the observables Ω_1 and Ω_2, and secondly that we can measure them in a given experiment. Both assumptions turn out to be impractical for an arbitrary many-body quantum system: Analytic calculation of Ω_1 and Ω_2 requires solving for the dynamics $U(t)$ generated by the system's Hamiltonian H_s. This is an arbitrarily difficult problem for a general (possibly time-dependent) Hamiltonian of a system consisting of N particles. Even if one has solved for Ω_1 and Ω_2, their dependence on $U(t)$ implies that they will in general be global observables i.e. sums over all possible n-particle correlations for $n \in \{1, \ldots N\}$. To measure $\Omega_{1,2}$ one therefore has to measure all of these correlations, a task which scales exponentially[3] with the size of the system. To avoid this scaling one could construct a measurement apparatus specifically to measure the global observables $\Omega_{1,2}$, in which case again only a single measurement is required. However, it is unclear whether constructing such an apparatus is possible in general for an arbitrary global observable. Furthermore, the design of the apparatus could vary with the observable considered, making this approach undesirable.

A theoretical description of a general procedure for the measurement of dynamic correlations has been hard to find in existing literature. This is in stark contrast to the vast number of references (some of which were mentioned at the beginning of this introduction) in which dynamic correlations play an essential role in characterising a given quantum system. A theoretical proposal for a measurement protocol which gives access to dynamic correlations in arbitrary quantum systems is clearly desirable. An interesting scheme, based on Ramsey interferometry and spin-shelving, for probing thermal equilibrium values of dynamic correlations has been put forward by Knap *et al.* [7]. This scheme however requires certain symmetries of the Hamiltonian, and gives access only to the imaginary part of certain dynamic correlations, and to the real part of others. Another protocol for measuring dynamic correlations, due to Romero-Isart *et al.* [8], proposes to weakly couple photons to ultracold atoms in an optical lattice, and to store the information imprinted on the photons in a quantum memory. Reading out the correlations between the system and the quantum memory at a later time then gives access to the real part of the dynamic correlation function. The imaginary component, however, remains inaccessible within their proposal.

[3] For a lattice consisting of N spin-s particles the total number of n-particle correlations is $\mathcal{O}(s^{2N})$.

The goal of this thesis is to improve on these ideas. We will analytically derive and characterise a measurement protocol which can be used to measure the full complex dynamic correlation of any two observables. We will show this protocol's validity within quantum spin systems with arbitrary geometry, dimension, Hamiltonian and (non)equilibrium initial states. Furthermore, our protocol does not scale with the size N of the system which makes its implementation within existing experimental platforms feasible.

1.1 Thesis outline and main results

Throughout this work, the setting we have in mind is a spatially extended system, and for simplicity we focus on lattice models. When the choice of observables is unspecified, or clear from the context, we will use the symbol C to refer to dynamic correlations $C(t_1, t_2) = \langle\psi| O_1(t_1)O_2(t_2) |\psi\rangle$. Our first main result, discussed in Chap. 2, is a protocol for determining C by means of *noninvasive measurements*, which we review below in Sec. 1.2. noninvasive measurements have been around for some time and under various names, including non-projective, generalized, unsharp, or weak measurements[4], and these names are used for slightly different concepts in some works, and interchangeably in others; see [9] for an introduction. Noninvasive measurements also play an important role in continuous measurements [10; 11] and quantum control [12], and they have also been used for quantum state estimation [13].

The key idea of our noninvasive measurement protocol (NIMP) is to indirectly probe the target system at t_1 by coupling a secondary *ancilla* system to it in such a way that information about the target system's state is retrieved through a subsequent projective measurement of the ancilla. By choosing an appropriate coupling unitary $\mathscr{U}(\lambda)$—where λ is the coupling time—for the ancilla–target coupling, a full projection of the target system's state onto an eigenstate of the measured observable can be avoided. At t_2 we measure the system directly since measurement backaction is of no concern. The ancilla–target coupling λ time must also be carefully chosen and we show in Sec. 2.2 that the information obtained through multiple repetitions of this protocol can, for sufficiently small λ, be assembled to construct a faithful estimator of the correlation C. The NIMP is versatile, but also experimentally demanding in that multiple repetitions of the experiment are required, and a high degree of control is needed to couple and decouple an ancilla to the target system. In Sec. 2.2.1 we characterize the performance of the NIMP by deriving error bounds on the estimators for C. For a given number of repetitions of the protocol, these error bounds allow us to determine the optimal coupling time which simultaneously minimizes statistical and systematic errors. In Sec. 2.3 we

[4] We refrain from using the terminology "weak measurement" in order to avoid confusion with the concept of a (post-selected) weak value, which plays no role in our protocol.

discuss generalizations of the NIMP. The first is based on deferred measurements where information about the system at an early time t_1 is stored in an ancilla but read out not before t_2. We show that this deferral yields no further reduction of the backaction. A second generalization uses multiple noninvasive measurements at times t_1, t_2, t_3, in order to extract multiple correlations. It turns out that such a scheme is less efficient than repeated applications of the NIMP.

Our second main result is discussed in Chap. 3. There we use *Kraus operators*—which are also reviewed in Sec. 1.2 below—to reformulate the ancilla-based measurement protocols of Chap. 2. Kraus operators capture the dynamics incurred by a target system during an ancilla-based measurement. As a result these operators elucidate, for specific cases, the equivalence of our NIMP to ancilla-free measurement protocols of dynamic correlations. The most notable (and counter-intuitive) result of Chap. 3 is specific to spin-1/2 systems: when using the NIMP (with a specific coupling time λ) to measure $\mathrm{Re}\, C$, the state of the target after the noninvasive measurement at t_1 is projected onto an eigenspace of the observable to be correlated at t_1. This implies that the real part of dynamic correlations C is not affected by measurement backaction incurred at early times, and projective (von Neumann) measurements can be used at times t_1 and t_2 to accurately measure $\mathrm{Re}\, C$. This does not mean that no collapse of the wave function takes place at the early time t_1, only that its effect precisely cancels out in $\mathrm{Re}\, C$. The details of this projective measurement protocol (PMP) are reported in Sec. 3.2.2. Similarly, the Kraus operator formalism shows that $\mathrm{Im}C$ can be measured in spin-1/2 systems by performing a localised rotation of the target system at t_1, followed by a projective measurement of the target at t_2. A detailed description of this rotation-based measurement protocol (RMP) is reported in Sec. 3.2.1.

Despite the theoretical simplicity of the ancilla-free PMP and RMP, experimental challenges remain. We discuss some of these in Chap. 4 at the hand of linear ion-trap and quantum gas microscope experiments (reviewed at the beginning of Chap. 4). Both platforms simulate spin lattices by trapping ultra-cold ions or atoms. Implementation of the PMP is particularly challenging since the necessary projective measurement at t_1 causes decoherence and particle loss due to heating. This disturbs the system dynamics beyond the expected wave function collapse. We discuss in Sec. 4.1.2 how this disturbance propagates into the measured correlation and analyse the size of the resulting deviation from the desired correlation component. The RMP is easier to implement as it only requires a unitary rotation to be performed at t_1. As shown in Sec. 3.2.1 the RMP yields $\mathrm{Im}\, C$ exactly when the rotation angle is set to an optimal value (see the paragraph following Eq. (3.2.3)). In a given experiment, it might be difficult to precisely hit this optimal angle, so that the rotations are susceptible to errors. We show in Sec. 4.1.3 how these errors propagate into the measurement of $\mathrm{Im}C$ and characterise the size of the resulting deviation. The main theoretical tool used in the error analysis of Secs. 4.1.2 and 4.1.3 is the theory of Lieb-Robinson bounds, which we review in

Sec. 4.1.1. Due to the experimental challenges created by repeated projective measurements, our NIMP is still relevant for spin-1/2 systems since the ancilla-based noninvasive measurement allows one to defer all measurements to the final time t_2. In this way destructive effects due to projective measurements—such as heating and particle loss—are avoided before t_2. In Sec. 4.2 we show that the NIMP can be readily implemented in linear ion-traps with existing experimental techniques.

We conclude on our findings and provide an outlook on possible avenues for future research in Chap. 5

Parts of the work presented in this thesis have been accepted for publication in *Physical Review A* (PRA) in the form of a peer-reviewed article [14] written by P.Uhrich, M. Kastner, H. Uys and S. Castrignano. In particular Chap. 2, Sec. 3.2.1, 3.2.2, 4.2 and App. B have been adapted from [14]. The calculations presented in those sections are a direct result of this author's efforts, with the exception of the Γ operator (B.0.6), as well as the related anti-Hermiticity requirement (B.0.11), of App. B. These were derived by S. Castrignano as part of the collaboration leading to our publication in PRA.

1.2 Quantum measurement theory

This review is based on Chapter 1 of the textbook *Quantum Measurement Theory and its Applications* by Kurt Jacobs [15] and Chapter 8 of the textbook *Quantum Computation and Quantum Information* by M. Nielsen and I. Chuang [16].

We begin with a reminder of what is known in quantum theory as a *projective* or *von Neumann* measurement: Let $|\psi\rangle \in \mathscr{H}_S$ denote the state of some system of interest, where for our purposes it is sufficient to consider the system's Hilbert space $\mathscr{H}_S$ to be of finite dimension N. Let O be a bounded[5], Hermitian operator acting on this Hilbert space i.e. $O^\dagger = O$ and $O : \mathscr{H}_S \mapsto \mathscr{H}_S$. Let $n \in \{0, 1, \ldots, N-1\}$ denote the N (non-degenerate) eigenvalues of O, with corresponding eigenstates $\{|n\rangle\}$. Assume that this eigenbasis forms a complete basis for $\mathscr{H}_S$. It then follows that $|\psi\rangle = \sum_{n=0}^{N-1} c_n |n\rangle$ for any complex coefficients $\{c_n\}$ which satisfy $\sum_{n=0}^{N-1} |c_n|^2 = 1$. Suppose now that we measure the observable O. The measurement basis is then $\{|n\rangle\}$. The *measurement postulate* of quantum theory states that although the system can be in any state $|\psi\rangle \in \mathscr{H}_S$ before the measurement, the measurement outcome will be exactly one of the eigenvalues n of O, and that the post-measurement state of the system is given by the corresponding eigenstate $|n\rangle$. Which of the eigenvalues n we obtain is random and the corresponding probability p_n is given

[5]Here we use the usual definition that a bounded operator is one with finite norm. For the case of a Hermitian operator this is equivalent to saying that all of its eigenvalues have finite absolute value.

by the expansion coefficients as $p_n = |c_n|^2$. Such a measurement, where the post-measurement state of the system is exactly one of the states of the measurement basis, is called a von Neumann measurement [15].

Let us denote the post-measurement state of the system as $|\psi_n\rangle$. We can then express $|\psi_n\rangle$ in terms of the pre-measurement state $|\psi\rangle$ by means of projection operators Π_n—where $\Pi_n = |n\rangle\langle n|$ for non-degenerate spectra—as $|\psi_n\rangle = \Pi_n|\psi\rangle/\mathcal{N}$. Here $\mathcal{N}$ is a normalisation factor which ensures that $|\psi_n\rangle = |n\rangle$ and can be shown to be $\mathcal{N} = |\langle n|\psi\rangle| = \sqrt{p_n}$. We can also express the corresponding probability p_n as an expectation value of the projector Π_n; $p_n = \langle\psi|\Pi_n|\psi\rangle = |\langle n|\psi\rangle|^2 = |c_n|^2$. This is known as Born's rule. The process whereby the pre-measurement state $|\psi\rangle$ evolves into the post-measurement state $|\psi_n\rangle$ by means of a projection is known as *wave function collapse* [17] and constitutes a non-linear evolution of the system's wave function (due to the necessary normalisation).

In the introductory example of a naive measurement of the dynamic correlation $\langle\psi|(\sigma^z\otimes\mathbb{1})U^\dagger(t)(\mathbb{1}\otimes\sigma^z)U(t)|\psi\rangle$ (Eqs. (1.0.3)–(1.0.8)), we made use of a von Neumann measurement at the early time $t_1 = 0$ (and at the final time t_2), and referred to the resulting non-linearity in the system dynamics as *measurement backaction*. To measure dynamic correlations successfully one must avoid this backaction. Our approach in this thesis is to perform a noninvasive measurement at t_1. Such a measurement falls under a broader class of measurements which are typically referred to as "generalised quantum measurements". In the next paragraph we describe these generalised measurements, and show how they can be used to perform noninvasive measurements.

Generalised quantum measurements Let us refer to the system $|\psi\rangle \in \mathscr{H}_S$ which is to be measured as the *target* system. Now we introduce an *ancilla* quantum system whose initial state $|\phi\rangle \in \mathscr{H}_A$ is prepared independently from that of the target. The combined ancilla–target state[6] is then $|\phi\rangle\otimes|\psi\rangle \in \mathscr{H} = \mathscr{H}_A\otimes\mathscr{H}_S$. The idea is now that we can extract information about the target's state by performing a von Neumann measurement of the ancilla's state, after the ancilla and target have interacted under the action of some unitary operator $\mathscr{U}$. The physical motivation for this indirect ancilla-based measurement is that in general the interaction $\mathscr{U}$ will create correlations (i.e. entanglement) between the ancilla and target states. The measured state of the ancilla then yields information on the state of the target. However, due to this entanglement the state of the target system is in general changed. This change depends on the the initial state $|\phi\rangle$ of the target, the ancilla–target interaction $\mathscr{U}$ and the outcome of the ancilla measurement. By varying $\mathscr{U}$ and $|\phi\rangle$ this dynamical change of the target can range from that of a von Neumann measurement (wave function collapse), to arbitrarily small perturbations.

[6] Note that throughout this thesis we use for tensor products the convention that ancilla states are written to the left of target system states.

As an example suppose that the target system consists of a single qubit. Our target Hilbert space is thus $\mathscr{H}_S = \mathbb{C}^2$, and we use the computational basis $\{|0\rangle, |1\rangle\}$ to span $\mathscr{H}_S$. For simplicity, we assume the qubit to be in the pure state $|\psi\rangle = (|0\rangle + |1\rangle)/\sqrt{2} \in \mathscr{H}_S$. It will be useful to use the geometrical representation of this state as a point on the surface of a *Bloch sphere*, of which the North and South poles respectively represent basis state $|0\rangle$ and $|1\rangle$. Up to an arbitrary phase, our choice of $|\psi\rangle$ then lies on the equator of the Bloch sphere, as shown in Fig. 1.2.1. For the ancilla system, we introduce a second qubit, prepared in the basis state $|0\rangle$. To perform a noninvasive measurement of the target qubit, we couple ancilla and target with the unitary

$$\begin{aligned} \mathscr{U} =& |0\rangle\langle 0| \otimes M_0 + |0\rangle\langle 1| \otimes (-iM_1) + |1\rangle\langle 0| \otimes M_1 + |1\rangle\langle 1| \otimes (iM_0), \\ \text{where } M_0 =& \sqrt{k}\,|0\rangle\langle 0| + \sqrt{1-k}\,|1\rangle\langle 1| \\ \text{and } M_1 =& \sqrt{1-k}\,|0\rangle\langle 0| + \sqrt{k}\,|1\rangle\langle 1| \text{ for } k \in [0,1]. \end{aligned} \tag{1.2.1}$$

The reason for representing $\mathscr{U}$ in terms of operators $M_{0,1}$ will become clear in the next paragraph where Kraus operators are discussed. The post-coupling ancilla–target state is then

$$\mathscr{U}|\phi,\psi\rangle = |0\rangle (M_0|\psi\rangle) + |1\rangle (M_1|\psi\rangle). \tag{1.2.2}$$

We now measure the ancilla in the computational basis. The (normalised) post-measurement states of the target, corresponding to outcome 0 or 1 of the ancilla measurement, are

$$\begin{aligned} |\psi_0\rangle &= \sqrt{k}\,|0\rangle + \sqrt{1-k}\,|1\rangle, \\ |\psi_1\rangle &= \sqrt{1-k}\,|0\rangle + \sqrt{k}\,|1\rangle. \end{aligned} \tag{1.2.3}$$

For $k = 0, 1$, the ancilla-based measurement has the same dynamical effect on the target as a von Neumann measurement: for $k = 0$ the target is projected, and is orthogonal to the ancilla qubit. For $k = 1$, the target is again projected, but its post-measurement state matches that of the ancilla. In either case the post-measurement state of the target lies at one of the poles of the Bloch sphere (see Fig. 1.2.1), and we obtain maximal information about its state. For $k = 1/2$, $|\psi_0\rangle, |\psi_1\rangle = |\psi\rangle$ i.e. the ancilla measurement leaves the target unchanged. The target remains on the equator of the Bloch sphere, and we obtain no information on its state. This ability to tune the dynamic change of the target is essential to the measurement protocol developed in Chap. 2. The main idea is to choose $\mathscr{U}$ and $|\phi\rangle$ such that we can extract information about the target state, but reduce the measurement backaction to an arbitrarily small perturbation of the target's

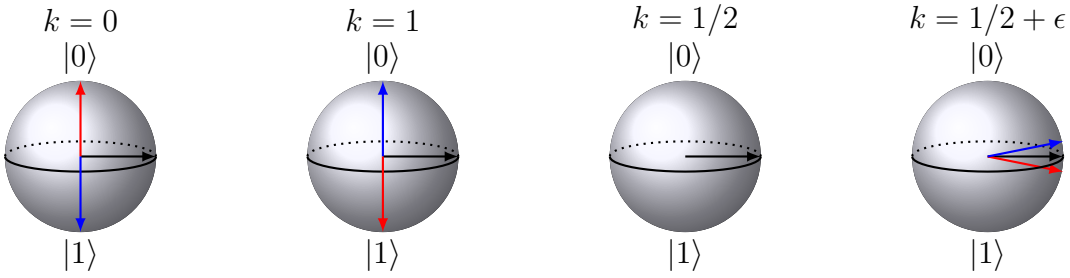

Figure 1.2.1: Bloch sphere representation of the target system's post-measurement state, for various values of $k \in [0, 1]$ in (1.2.1). North and South poles respectively represent the computational basis states $|0\rangle$ and $|1\rangle$. The equator represents an equal superposition of these basis states. The black arrow indicates the initial target state $|\psi\rangle = (|0\rangle + |1\rangle)/\sqrt{2}$, up to an arbitrary phase. For all values of k depicted here, blue (red) arrows represent the post-measurement state $|\psi_0\rangle$ ($|\psi_1\rangle$) of (1.2.3).

dynamics. For the current example, this is achieved by choosing $k = 1/2+\epsilon$, where $\epsilon > 0$. The normalised post-measurement states of the target are then

$$\begin{aligned} |\psi_0\rangle &= \sqrt{1/2 + \epsilon}\,|0\rangle + \sqrt{1/2 - \epsilon}\,|1\rangle\,, \\ |\psi_1\rangle &= \sqrt{1/2 - \epsilon}\,|0\rangle + \sqrt{1/2 + \epsilon}\,|1\rangle\,. \end{aligned} \tag{1.2.4}$$

These states are depicted in the right panel of Fig. 1.2.1. We see that both $|\psi_0\rangle$ and $|\psi_1\rangle$ lie close to the original state vector $|\psi\rangle$, but have been shifted slightly towards the North, respectively South, pole of the Bloch sphere. These shifted states correspond, respectively, to a measured eigenvalue 0 or 1, and we can use this information to construct a dynamic correlation, as shown in Sec. 2.1. By letting $\epsilon \to 0$, we reduce the measurement back-action on the target to an arbitrary degree and recover the pre-measurement state $|\psi\rangle$.

Whether the unitary (1.2.1) can be implemented, depends on the experimental set-up. In Chap. 2 our approach is to model the ancilla–target coupling unitary as a time-evolution of the ancilla–target state, generated by a coupling Hamiltonian H_c for some time λ. To achieve a noninvasive measurement we require the coupling time λ to be small. Further details are given in Sec. 2.1.

Kraus operators. Within quantum measurement theory the unitary ancilla–target coupling, followed by a projective measurement of the ancilla, is shown to be equivalent to the action of a set of *measurement operators* acting directly on the target Hilbert space $\mathscr{H}_S$. Measurement operators are frequently referred to as *Kraus* operators, and this is the name which we will use throughout this thesis. The utility of these Kraus operators is that they describe the same generalised measurement as above, but do not explicitly invoke an ancilla system. We will see

in Chap. 3 that this allows us to derive protocols for the measurement of dynamic correlations which do not require ancillas.

For a given ancilla-based measurement, the corresponding Kraus operators can be expressed in terms of the initial ancilla state $|\phi\rangle$ and the unitary interaction $\mathscr{U}$ [7], as we will now show. Let $M = \dim \mathscr{H}_A$ and $N = \dim \mathscr{H}_S$ be the ancilla and target Hilbert space dimensions, and let us denote respective bases as $\{|n\rangle\}$ and $\{|s_k\rangle\}$ where $n = 0, 1, \ldots, M-1$ and $k = 0, 1, \ldots, N-1$. A corresponding basis for the joint Hilbert space $\mathscr{H}$ is then $\{|n\rangle \otimes |s_k\rangle = |n, s_k\rangle\}$, with which express the unitary ancilla–target coupling as

$$\mathscr{U} = \sum_{n,n'} \sum_{k,k'} u_{nk,n'k'} \, |n, s_k\rangle \langle n', s_{k'}| \,, \tag{1.2.5}$$

where $u_{nk,n'k'} \in \mathbb{C}$ are the corresponding matrix elements of $\mathscr{U}$. In (1.2.5), for each pair of ancilla states n, n' there is an $N \times N$ sub-block $M_{nn'} = \sum_{k,k'} u_{nk,n'k'} \, |s_k\rangle \langle s'_k|$ which acts exclusively on the target Hilbert space. In terms of these sub-blocks, $\mathscr{U}$ is expressed as

$$\mathscr{U} = \sum_{n,n'} |n\rangle \langle n'| \otimes M_{nn'}. \tag{1.2.6}$$

This is the form used in (1.2.1) of the above example. To ensure unitarity of $\mathscr{U}$, as discussed in detail in Ref. [15], it suffices to choose the sub-blocks $M_n = M_{n0}$ such that they satisfy

$$\sum_n M_n^\dagger M_n = \mathbb{1}. \tag{1.2.7}$$

We now switch to the density matrix formalism to facilitate the partial trace in (1.2.9). We denote the combined ancilla–target state as $\chi = \alpha \otimes \rho$ where $\alpha = |\phi\rangle \langle\phi|$ and $\rho = |\psi\rangle \langle\psi|$. To simplify this derivation we assume $|\phi\rangle = |0\rangle$, but in general $|\phi\rangle$ may be any vector in $\mathscr{H}_A$ (or, in the language of density matrices, any pure state). The generalised ancilla-based measurement is achieved by applying $\mathscr{U}$ to χ and subsequently projecting the ancilla state. The (un-normalised) combined

[7] One may also proceed in the reverse direction: Given a set of Kraus operators satisfying condition (1.2.7) we can derive a unitary operator $\mathscr{U}$, which corresponds to the scenario of coupling an ancilla to a target and then projectively measuring the ancilla. This is shown, for instance in Box 8.1 of [16]. A more formal treatment goes under the name "Neumark's theorem", and can be found in section 9.-6. of [18].

post-measurement density matrix is then

$$\begin{aligned}\chi_n =&(\Pi_n \otimes \mathbb{1})\mathscr{U}(\alpha \otimes \rho)\mathscr{U}^\dagger(\Pi_n \otimes \mathbb{1}) \\ =&(|n\rangle\langle n| \otimes \mathbb{1})\left(\sum_{m,m'} |m\rangle\langle m'| \otimes M_{mm'}\right)(|0\rangle\langle 0| \otimes \rho)\left(\sum_{l,l'} |l\rangle\langle l'| \otimes M^\dagger_{ll'}\right) \\ &\times (|n\rangle\langle n| \otimes \mathbb{1}) \\ =&\,|n\rangle\langle n| \otimes M_n \rho M_n^\dagger,\end{aligned} \tag{1.2.8}$$

where we have used the block definition (1.2.6) of $\mathscr{U}$ in the second and third equality.

Due to the von Neumann measurement of the ancilla, the combined post-measurement state (1.2.8) is a product state from which we can extract (by tracing over $\mathscr{H}_A$) the normalised post-measurement state of the target system as

$$\rho_n = \frac{M_n \rho M_n^\dagger}{\mathrm{Tr}\left[M_n^\dagger M_n \rho\right]}. \tag{1.2.9}$$

The corresponding probability of the ancilla measurement yielding outcome n is

$$p_n = \mathrm{Tr}\left[(\Pi_n \otimes \mathbb{1})\mathscr{U}(\alpha \otimes \rho)\mathscr{U}^\dagger\right] = \mathrm{Tr}\left[M_n^\dagger M_n \rho\right]. \tag{1.2.10}$$

We see that the set of operators $\{M_n\}$, for $n = 0, 1, \ldots, N$—which stem from the definition (1.2.6) of $\mathscr{U}$—are sufficient to describe the target system's post-measurement state (1.2.9) as well as the probability (1.2.10) of finding it in that state once the generalised measurement is complete. The operators M_n are the aforementioned Kraus operators. Eqs. (1.2.9)–(1.2.10) show that the dynamic change of the target—due to the ancilla coupling $\mathscr{U}$ and the subsequent von Neumann measurement of the ancilla (1.2.8)—is captured by the Kraus operators. We note also that the Kraus operators can be expressed in terms of $\mathscr{U}$ and $|\phi\rangle$ as

$$M_n = \langle n|\,\mathscr{U}\,|\phi\rangle = \langle n|\,\mathscr{U}\,|0\rangle, \tag{1.2.11}$$

which follows from the first line of (1.2.8) with $|\phi\rangle = |0\rangle$.

Examples. The Kraus operators corresponding to the unitary $\mathscr{U}$ (1.2.1) of the ancilla-based example are M_0 and M_1. This follows directly from (1.2.11).

Using Kraus operators to directly describe a measurement procedure is often more useful than invoking the idea of an ancilla–target coupling. For instance, suppose again that we wish to measure a single qubit in the computational basis. We are given some measurement apparatus to do this. However, the apparatus may fail with probability p. Whenever the apparatus fails, it does not interact with the

target qubit, and we gain no knowledge about its state. This cannot be described with a von Neumann measurement procedure. Instead, the possible measurement outcomes can be described by the following set of Kraus operators (which satisfy (1.2.7))

$$M_1 = \sqrt{p}\mathbb{1},\ M_2 = \sqrt{1-p}\,|0\rangle\langle 0| \text{ and } M_3 = \sqrt{1-p}\,|1\rangle\langle 1|\,. \tag{1.2.12}$$

These operators capture the fact that with probability p the system state is unaffected, and is projected with probability $1-p$.

For any quantum measurement we now have two ways of thinking about the measurement procedure: Firstly, we may think of coupling an ancilla to the target and subsequently measuring this ancilla. This may be the more physically intuitive picture as it corresponds in many cases to the actual experimental procedure [19; 8]. We use this picture in developing the NIMP of Chap. 2. Secondly, we can use Kraus operators to describe quantum measurements in a purely mathematical way. In Chap. 3 we rephrase the NIMP in this mathematical picture, and show that it provides deeper insight into what the effective dynamics of the target system is.

POVM As a concluding remark on general quantum measurements we note that Kraus operators are related to *positive-operator valued measures* (POVM). The meaning of this name is explained in Chapter 1 of Ref. [15]: For any given set $\mathcal{S}$ of objects, a *measure* is a map which assigns a number to every subset of $\mathcal{S}$. A POVM is therefore a map which assigns a *positive operator* to every subset of $\mathcal{S}$. As an example, consider the quantum measurement above, where the relevant set consists of all possible outcomes n of the measurement. The probability to obtain outcome n is given by (1.2.10) as $p_n = \mathrm{Tr}\left[M_n^\dagger M_n \rho\right]$. Here the operator $M_n^\dagger M_n$ is the positive operator (often referred to as an "effect") of the POVM which is associated to the outcome n. In general, we may pick some subset $\mathcal{M}$ of outcomes, and the overall probability of measuring any outcome $n \in \mathcal{M}$ is then

$$P(n\in\mathcal{M}) = \sum_{n\in\mathcal{M}} p_n = \sum_{n\in\mathcal{M}} \mathrm{Tr}\left[M_n^\dagger M_n \rho\right] = \mathrm{Tr}\left[\left(\sum_{n\in\mathcal{M}} M_n^\dagger M_n\right)\rho\right]. \tag{1.2.13}$$

Since all the operators $M_n^\dagger M_n$ are positive, so is $\sum_{n\in\mathcal{M}} M_n^\dagger M_n$ and this is then the positive operator associated with the subset of outcomes $\mathcal{M}$.

2

Ancilla-based measurement protocols

The protocols developed in this chapter are derived and stated in the language of lattice spin systems with spin quantum number $s \in \mathbb{N}/2$, but generalizations to continuum systems should be possible. Within this general spin picture, our aim is to estimate dynamic correlations

$$C(t_1, t_2) = \left\langle S_i^a(t_1) S_j^b(t_2) \right\rangle = \langle\psi| \, e^{iH_s t_1} S_i^a e^{-iH_s t_1} e^{iH_s t_2} S_j^b e^{-iH_s t_2} \, |\psi\rangle \,, \tag{2.0.1}$$

where S_i^a denotes the a-component of a spin-s operator at lattice site i, with $a \in \{x, y, z\}$. The initial system state at time $t = 0$ is denoted by $|\psi\rangle$. We have assumed the system Hamiltonian H_s to be time-independent so that the system's time-evolution[1] is given by the unitary $U(t) = e^{-iH_s t}$. We will see in the following derivation that the explicit form of H_s plays no role, and generalisations to time-dependent Hamiltonians (as done in Ref. [19]) would alter only the form of $U(t)$. Generalizations to correlations at more than two times and/or more than two lattice sites are possible and straightforward.

We denote the possible outcomes of a projective measurement of either spin observable in (2.0.1) as $m_a, m_b \in \mathscr{S} = \{s, s-1, \ldots, -s+1, -s\}$. The correlation between a projective measurement at time t_1 and at t_2 is given by

$$\mathscr{C}^{\text{proj}} := \sum_{m_a, m_b \in \mathscr{S}} m_a m_b P_{m_a m_b}, \tag{2.0.2}$$

where P_{m_a, m_b} denotes the joint probability to projectively measure eigenvalue m_a and m_b at times t_1 and t_2, respectively. This projectively measured correlation suffers from two difficulties (see the example in Chap. 1 for a worked example). First, the expectation value (2.0.1) is in general complex, and can therefore not be directly described by the real (non-complex) measurement outcomes and their corresponding probabilities as in (2.0.2). Second, as discussed in Chap. 1, a projective measurement at the early time t_1 disturbs the unitary dynamics so that (2.0.1) and (2.0.2) differ in general. The following protocol, based on noninvasive measurements, successfully deals with both difficulties.

[1] All time evolution operators will be expressed in units with $\hbar = 1$.

2.1 Non-invasive measurement protocol (NIMP)

The basic idea of our noninvasive measurement protocol is simple: The system of interest is allowed to evolve unitarily until the time t_1. At that time, an ancillary quantum system is weakly coupled to lattice site i for a short period of time, after which a small amount of information about the system observable S_i^a is retrieved by performing a projective measurement on the ancilla. Then, with the ancilla decoupled, the system is evolved unitarily until time t_2, at which point S_j^b is measured projectively, directly on the target system. The novel technical finding presented in this section is to identify specific choices of the weak-coupling unitaries that give access to the real and imaginary parts of the correlation function (2.0.1) respectively.

For the noninvasive measurement of a spin-s target at time t_1, we make use of an ancillary spin-s degree of freedom (we show in Sec. 2.3.1 that the ancilla spin does, in general, not have to match that of the target spins). The total ancilla–target Hilbert space is therefore $\mathscr{H} = \mathscr{H}_\mathrm{A} \otimes \mathscr{H}_\mathrm{S} = \mathbb{C}^{2s+1} \otimes (\mathbb{C}^{2s+1})^{\otimes N}$, where N is the number of spins (lattice sites) in the lattice system. The system Hamiltonian $H = \mathbb{1}_\mathrm{A} \otimes H_\mathrm{s}$, which generates the unitary evolution in the dynamic correlation function (2.0.1), acts non-trivially on $\mathscr{H}_\mathrm{S}$ only. The main idea (which was introduced in the review of Sec. 1.2) is to weakly couple (entangle) the ancilla and the target system. We will use a Hamiltonian H_c, that acts on the total Hilbert space $\mathscr{H}$, to generate this coupling. By subsequently measuring the ancilla projectively, information about the system can be extracted without causing a complete collapse of the system's wave function. The noninvasive measurement protocol consists of the following steps.

(a) **Initial state preparation.** We assume ancilla and system to initially be in a product state,

$$|\Psi\rangle = |\phi\rangle \otimes |\psi\rangle \equiv |\phi, \psi\rangle \,. \tag{2.1.1}$$

The system initial state $|\psi\rangle$ is arbitrary and determined by the physical situation under investigation. We will determine the optimal choice of the ancilla initial state $|\phi\rangle$ in (2.1.11).

(b) **Time evolution until time t_1.** Time-evolve the initial state $|\Psi\rangle$ up to the time t_1 with the system Hamiltonian H_s,

$$|\Psi(t_1)\rangle = |\phi\rangle \otimes e^{-iH_\mathrm{s}t_1} |\psi\rangle \equiv |\phi, \psi(t_1)\rangle \,. \tag{2.1.2}$$

The ancilla state $|\phi\rangle$ is unaffected.

(c) **Weak coupling of ancilla and system site i.** Time evolution of $|\Psi(t_1)\rangle$ with a coupling Hamiltonian $H_\mathrm{c} := B \otimes A_i$ has the effect of generating entanglement between ancilla and target. The operator A_i acts non-trivially only on the spin

at lattice site i for which, according to (2.0.1), correlations at time t_1 are to be determined. This choice is expected to be most conducive towards our goal of imprinting information specifically about the state of the ith system spin onto the ancilla. We assume that the corresponding time evolution operator

$$\mathscr{U}(\lambda) = \exp(-i\lambda B \otimes A_i) \simeq \mathbb{1} - i\lambda B \otimes A_i \tag{2.1.3}$$

can be approximated to linear order in $|\lambda|\|B \otimes A_i\|$. Here and in the following we use the symbol $\simeq$ to denote validity up to linear order in λ. Physically, the required condition $|\lambda|\|B \otimes A_i\| \ll 1$ can be satisfied either by implementing a Hamiltonian of weak interaction strength $\|B \otimes A_i\|$, and/or by choosing the coupling time λ sufficiently small. We will take the point of view that $|\lambda| \ll 1$ and choose, without loss of generality, coupling operators such that $\|A_i\| = 1$ and $\|B\| = 1$. At the end of the coupling procedure, one obtains

$$|\Psi_\lambda(t_1)\rangle \simeq |\phi, \psi(t_1)\rangle - i\lambda\, |B\phi, A_i\psi(t_1)\rangle\,. \tag{2.1.4}$$

(d) **Measuring the ancilla.** The state of the ancilla is now probed by projectively measuring the observable $S^a \otimes \mathbb{1}_\mathrm{S}$, i.e. for the ancilla spin, the same observable that occurs in the correlation function (2.0.1) at time t_1 is probed. We denote the $2s+1$ eigenstates of S^a as $|m_a\rangle$ with corresponding eigenvalues $m_a \in \mathscr{S}$. According to Born's rule, one measures m_a with probability

$$\begin{aligned} P_{m_a} &\simeq \langle\Psi_\lambda(t_1)|\,(|m_a\rangle\langle m_a| \otimes \mathbb{1}_\mathrm{S})\,|\Psi_\lambda(t_1)\rangle \\ &\simeq |\langle m_a|\phi\rangle|^2 - i\lambda\,\langle A_i(t_1)\rangle_\psi\,(\langle\phi|m_a\rangle\langle m_a|\,B\,|\phi\rangle - \text{c.c.})\,, \end{aligned} \tag{2.1.5}$$

where c.c. denotes the complex conjugate and $\langle A_i(t_1)\rangle_\psi = \langle\psi|\,U^\dagger(t_1)A_iU(t_1)\,|\psi\rangle$. The post-measurement state is given by the normalized (and linearised with respect to λ) projection onto the subspace corresponding to the outcome m_a of the measurement,

$$|\Psi_{m_a}(t_1)\rangle \simeq \frac{(|m_a\rangle\langle m_a| \otimes \mathbb{1}_\mathrm{S})\,|\Psi_\lambda(t_1)\rangle}{\|(|m_a\rangle\langle m_a| \otimes \mathbb{1}_\mathrm{S})\,|\Psi_\lambda(t_1)\rangle\|} \simeq |m_a\rangle \otimes |\psi_{m_a}(t_1)\rangle \tag{2.1.6}$$

with

$$\begin{aligned} |\psi_{m_a}(t_1)\rangle \simeq \Bigg[&\frac{\langle m_a|\phi\rangle}{|\langle m_a|\phi\rangle|} - i\lambda\Bigg(\frac{\langle m_a|\,B\,|\phi\rangle}{|\langle m_a|\phi\rangle|}A_i - \frac{\langle m_a|\phi\rangle}{2\,|\langle m_a|\phi\rangle|^3} \\ &\times \langle A_i(t_1)\rangle_\psi\,(\langle\phi|m_a\rangle\langle m_a|\,B\,|\phi\rangle - \text{ c.c.})\Bigg)\Bigg]\,|\psi(t_1)\rangle\,. \end{aligned} \tag{2.1.7}$$

Ancilla and system are again in a product state.

(e) **Time evolution until time t_2.** Time-evolve the post-measurement state $|\Psi_{m_a}(t_1)\rangle$ up to the time t_2 with the system Hamiltonian H_s,

$$|\Psi_{m_a}(t_2)\rangle \simeq |m_a\rangle \otimes e^{-iH_\mathrm{s}(t_2-t_1)}\,|\psi_{m_a}(t_1)\rangle\,. \tag{2.1.8}$$

The ancilla state $|m_a\rangle$ remains unaffected.

(f) **Projective measurement at site j.** At the final time t_2, the disturbing effect due to a measurement is not of concern, and we can projectively measure the observable S_j^b at lattice site j without compromising the accuracy of the correlation function (2.0.1) which we wish to measure. The conditional probability of measuring the system in eigenstate $|m_b\rangle$ of S_j^b after having obtained eigenvalue m_a when measuring the ancilla is

$$\begin{aligned} P_{m_b|m_a} &\simeq \langle\Psi_{m_a}(t_2)|\,(\mathbb{1}_\mathrm{A}\otimes|m_b\rangle\langle m_b|)\,|\Psi_{m_a}(t_2)\rangle \\ &\simeq |\langle m_b|\,U(t_2)\,|\psi\rangle|^2 - i\lambda\Bigg[\frac{\langle\phi|m_a\rangle\,\langle m_a|\,\hat{B}\,|\phi\rangle}{|\langle m_a|\phi\rangle|^2}\Big(\langle\psi|\,U^\dagger(t_2)\,|m_b\rangle \\ &\quad\times\langle m_b|\,U(t_2-t_1)A_iU(t_1)\,|\psi\rangle\,\langle A_i(t_1)\rangle_\psi\,|\langle m_b|\,U(t_2)\,|\psi\rangle|^2\Big) - \text{c.c.}\Bigg]. \end{aligned} \tag{2.1.9}$$

(g) **Correlating the measured outcomes.** We use the probabilities (2.1.5) and (2.1.9) to calculate the correlation (2.0.2) between the measured ancilla spin at t_1 and the system spin j at t_2,

$$\begin{aligned} \mathscr{C}(t_1,t_2) &= \sum_{m_a,m_b\in\mathscr{S}} m_a m_b P_{m_b|m_a}P_{m_a} \\ &\simeq \langle S^a\rangle_\phi\,\langle S_j^b(t_2)\rangle_\psi - i\lambda\left(\langle S^aB\rangle_\phi\,\langle\psi|\,S_j^b(t_2)A_i(t_1)\,|\psi\rangle - \text{c.c.}\right), \end{aligned} \tag{2.1.10}$$

where we have absorbed the summations via the spectral representations of S^a and S_j^b. By setting $A_i = S_i^a$, the bracketed term in (2.1.10) is made to contain the desired correlation (2.0.1).

Isolating the bracketed term requires exact knowledge of the value $\langle S^a\rangle_\phi\,\langle S_j^b(t_2)\rangle_\psi$. Calculating $\langle S_j^b(t_2)\rangle_\psi$ is possible in principle, but can be very difficult for general initial states and Hamiltonians of a given many-body spin-lattice. To avoid this, our strategy is to choose the initial ancilla state

$$|\phi\rangle = \sum_{m_a\in\mathscr{S}} c_{m_a}\,|m_a\rangle \;\text{ with } c_{m_a}\in\mathbb{C} \tag{2.1.11}$$

such that

$$\langle S^a\rangle_\phi = 0. \tag{2.1.12}$$

This is achieved if the coefficients c_{m_a} satisfy

$$\sum_{m_a \in \mathscr{S}: m_a > 0} m_a \left(|c_{m_a}|^2 - |c_{-m_a}|^2 \right) = 0. \tag{2.1.13}$$

Physically relevant states satisfying this condition are, for instance, spin coherent states and equal superpositions which respectively have expansion coefficients

$$c_{m_a} = \frac{1}{2^s} \sqrt{\frac{(2s)!}{(s+m_a)!(s-m_a)!}} \text{ and } c_{m_a} = \frac{1}{\sqrt{2s+1}} \text{ for all } m_a \in \mathscr{S}. \tag{2.1.14}$$

We choose the latter for our derivation, noting that other choices only lead to modified prefactors $f^{(1)}, f^{(2)}$ in (2.1.17) and (2.1.19).

With condition (2.1.12) satisfied by our choice of $|\phi\rangle$, correlation (2.1.10) reduces to

$$\mathscr{C}(t_1, t_2) \simeq \frac{-2\lambda}{2s+1} \sum_{m_a, m'_a \in \mathscr{S}} m_a \mathrm{Im} \left[\langle m_a | B | m'_a \rangle C(t_1, t_2) \right]. \tag{2.1.15}$$

We can extract the real or imaginary part of $C(t_1, t_2)$ from (2.1.15) through suitable choices of B. Choosing B Hermitian and symmetric renders (2.1.15) proportional to $\mathrm{Im}\left[C(t_1, t_2)\right]$. A natural choice is

$$B = B^{(1)} := S^a, \tag{2.1.16}$$

which yields

$$\mathscr{C}^{(1)}(t_1, t_2) \simeq -\frac{2\lambda f^{(1)}}{2s+1} \mathrm{Im}\left[C(t_1, t_2)\right] \tag{2.1.17}$$

with $f^{(1)} = \sum_{m_a \in \mathscr{S}} m_a^2$. Choosing B Hermitian and antisymmetric makes (2.1.15) proportional to $\mathrm{Re}\left[C(t_1, t_2)\right]$. For $S^a = S^z$ a convenient choice is $B = S^y$. Analogously for general $a \in \{x, y, z\}$ the spin component

$$B = B^{(2)} := -\frac{i}{2} \left(S_a^+ - S_a^- \right) \tag{2.1.18}$$

is convenient. Here $S_a^{\pm}$ denote spin-lowering or -raising operators with respect to the m_a-eigenbasis. Then (2.1.15) reduces to

$$\mathscr{C}^{(2)}(t_1, t_2) \simeq -\frac{2\lambda f^{(2)}}{2s+1} \mathrm{Re}\left[C(t_1, t_2)\right] \tag{2.1.19}$$

with $f^{(2)} = i \sum_{m_a, m'_a \in \mathscr{S}} m_a \langle m_a | B^{(2)} | m'_a \rangle$. Inverting Eqs. (2.1.17) and (2.1.19), we can define

$$C^{\lambda}(t_1, t_2) = -\frac{2s+1}{2\lambda} \left(\frac{\mathscr{C}^{(2)}(t_1, t_2)}{f^{(2)}} + i \frac{\mathscr{C}^{(1)}(t_1, t_2)}{f^{(1)}} \right), \tag{2.1.20}$$

which approximates the exact correlation function $C(t_1, t_2)$ for sufficiently small λ.

Equation (2.1.20) is our first main result. It shows that the unitarily evolved correlation $C(t_1, t_2)$ (2.0.1) can be correctly obtained by using an ancilla system to perform a noninvasive measurement at the early time t_1 (steps c and d). Experimental implementation, discussed in Sec. 4.2, will require two measurement samples in order to construct the complex-valued correlation function (2.1.20). The first sample is obtained with ancilla–target coupling Hamiltonian $H_{\rm c}^{(1)} := B^{(1)} \otimes S_i^a$, and yields $\mathrm{Im}C$ (Eqs. (2.1.16)–(2.1.17)). The second sample is obtained with $H_{\rm c}^{(2)} := B^{(2)} \otimes S_i^a$ and yields $\mathrm{Re}\, C$ (Eqs. (2.1.18)–(2.1.19)). In both cases the initial ancilla state $|\phi\rangle$ must be chosen so as to satisfy condition (2.1.12). It is remarkable that the first-order (in λ) approximation of the ancilla–target coupling $\mathscr{U}$ leads to such a succinct relation between $C(t_1, t_2)$ and $\mathscr{C}(t_1, t_2)$. The protocol can be applied to any lattice spin model regardless of interaction type, spin number or dimensionality.

A number of measurement schemes discussed in the literature bear some superficial similarity to the above described protocol. In Ref. [20] two noninvasive measurements are made in succession, but not in a way suitable for, nor with the aim of, allowing for the full reconstruction of dynamical correlation functions. Other references use noninvasive measurements to show violations of Leggett-Garg inequalities, but the latter are inequalities for the dynamic correlations of (real) measurement outputs, so connecting the result to the (complex) dynamic correlation function (2.0.1) is not part of the agenda [21; 22]. A viable scheme for obtaining complex dynamical correlation functions is contained in none of these references, nor in any other we are aware of.

2.2 Finite-sample estimators and errors

The key formula (2.1.20) of the noninvasive measurement protocol contains the ancilla–target dynamical correlation function $\mathscr{C}$ defined in (2.1.10). This in turn requires knowledge of the outcome probabilities P_{m_a} (2.1.5) and $P_{m_b|m_a}$ (2.1.9). An exact calculation of these probabilities, which involve the time-evolution under the many-body Hamiltonian $H_{\rm s}$, is in almost all cases impossible. As an alternative, one can estimate these probabilities in a given experiment by doing multiple repetitions of the protocol of Sec. 2.1. The estimated probabilities can then be combined according to (2.1.10) to obtain estimators $\mathscr{C}_n^{(m)}$ of the ancilla–target correlation function $\mathscr{C}^{(m)}$, with $m = 1, 2$ [(2.1.17) and (2.1.19)]. The subscript n indicates the use of a finite sample of n measurements. Due to the finite sample size, the estimators will be error-prone and this error propagates into the estimated dynamic correlation function

$$C_n^{\lambda}(t_1, t_2) := -\frac{2s+1}{2\lambda}\left(\frac{\mathscr{C}_n^{(2)}(t_1, t_2)}{f^{(2)}} + i\frac{\mathscr{C}_n^{(1)}(t_1, t_2)}{f^{(1)}}\right). \tag{2.2.1}$$

From Eq. (2.2.1) it follows that the noise contained in signals $\mathscr{C}_n^{(m)}$ will be inherited by C_n^λ. Moreover, the $1/\lambda$ prefactor will strongly amplify this noise in the limit $\lambda \to 0$. We will refer to this amplified noise as a *statistical error*.

At this point an interesting optimisation problem arises: The noninvasive measurement protocol of Sec. 2.1 was derived to linear order in λ, and is hence accurate only for sufficiently weak ancilla–target couplings λ. Larger λ will lead to *systematic* errors in the estimators $\mathscr{C}_n^{(m)}$, and hence in C_n^λ. The *statistical* errors discussed in the previous paragraph show the opposite tendency, becoming smaller with increasing λ. The *total* error in C_n^λ, given by the sum of systematic and statistical errors, is therefore expected to take on a minimum at some intermediate value λ^* of the ancilla–target coupling. Since the systematic error is independent of the sample size n, whereas the statistical error decreases with increasing n, we expect λ^* to decrease as n increases. Realistically, however, limited resources (man power or time or money), will cap the maximum sample size n.

For the application of the NIMP, the following optimization problem is therefore of relevance: Given a finite sample size n, what is the optimal λ such that the sum of systematic and statistical error becomes minimal? In the remainder of this section we investigate this question by deriving a bound on the total error. For doing so, it may be convenient to recapitulate the different (estimators of) correlation functions that we have introduced.

C: Exact correlation function (2.0.1); this is the quantity we would like to extract by means of noninvasive measurements.

C^λ: Correlation function (2.1.20), defined in terms of the probabilities of system and ancilla measurement outcomes as in the second line of (2.1.10). Shown to be equal to C asymptotically in the limit of small λ. In principle, an infinite number of measurements would be required to determine the exact probabilities.

C_n^λ: Correlation function (2.2.1), defined like C^λ in terms of system and ancilla measurement outcomes, but with probabilities replaced by relative frequencies. This is the quantity one actually obtains from a sequence of $2n$ measurements (n measurements for each operator $B^{(m)}$, $m = 1, 2$).

The systematic, statistical, and total errors are then respectively given by

$$\epsilon_{\text{sys}} := \left|C - C^\lambda\right|, \tag{2.2.2a}$$

$$\epsilon_{\text{stat}} := \left|C^\lambda - C_n^\lambda\right|, \tag{2.2.2b}$$

$$\epsilon_{\text{tot}} := \left|C - C_n^\lambda\right| \leq \left|\epsilon_{\text{sys}}\right| + \left|\epsilon_{\text{stat}}\right|. \tag{2.2.2c}$$

The statistical error arises when the probabilities in the first line of (2.1.10) are replaced by the corresponding relative frequencies with which the different outcomes

are measured in a sequence of n measurements. This replacement is most directly done in the non-conditional probabilities

$$P_{m_a m_b} = P_{m_a} P_{m_b|m_a}, \tag{2.2.3}$$

which denote the joint probabilities of measuring m_a for the ancilla spin and m_b for the system spin at site j. In a sample of n measurements, one will observe the $(2s+1)^2$ possible outcome combinations (m_a, m_b) with relative frequencies $n_{m_a m_b}/n$, such that

$$\sum_{m_a,m_b} n_{m_a m_b} = n \quad \text{and} \quad \lim_{n\to\infty} \frac{n_{m_a m_b}}{n} = P_{m_a m_b}. \tag{2.2.4}$$

For sufficiently large n, one expects $n_{m_a m_b}/n$ to be Poisson-distributed with mean $P_{m_a m_b}$ and standard deviation $\sqrt{n_{m_a m_b}}/n$ [23]. Making use of $n_{m_a m_b}/n = P_{m_a m_b} \pm \sqrt{n_{m_a m_b}}/n$, we find

$$\mathscr{C}_n = \sum_{m_a,m_b} m_a m_b \frac{n_{m_a m_b}}{n} = \mathscr{C} + \sum_{m_a,m_b} m_a m_b \frac{\pm\sqrt{n_{m_a m_b}}}{n}. \tag{2.2.5}$$

Substituting (2.2.1) and (2.1.20) into (2.2.2b) we find

$$\begin{aligned} \epsilon_{\text{stat}} &\leq \frac{2s+1}{2|\lambda|} \left(\frac{|\,\mathscr{C}^{(2)} - \mathscr{C}^{(2)}_n\,|}{f^{(2)}} + \frac{|\,\mathscr{C}^{(1)} - \mathscr{C}^{(1)}_n\,|}{f^{(1)}} \right) \\ &\leq \frac{2s+1}{2|\lambda|} \sum_{m_a,m_b} |m_a m_b| \left(\frac{\sqrt{n^{(2)}_{m_a m_b}}}{f^{(2)}} + \frac{\sqrt{n^{(1)}_{m_a m_b}}}{f^{(1)}} \right), \end{aligned} \tag{2.2.6}$$

where (2.2.5) and the triangle inequality were used. From this estimate we expect that, for a fixed sample size n, the noise-to-signal ratio of the noninvasive measurement protocol diverges in the limit of small λ.

Estimating the systematic error ϵ_{sys} is much more challenging in general, as it involves the exact dynamic correlation function C, which is usually unknown. One possible approach is to redo the calculations of Sec. 2.1 to next-to-leading order in λ, from which we could estimate the linear (in λ) contribution to ϵ_{sys} in the regime of small λ. In the next section we will follow a different approach, trying to obtain an understanding of the interplay between systematic and statistical errors by discussing an exactly solvable minimal model, consisting of three spin-1/2 particles: one ancilla and two system degrees of freedom.

2.2.1 Example: two system spins, one ancilla

As a minimal model for investigating spatio-temporal correlations in spin-1/2 systems by means of noninvasive measurements, we require a system consisting of two

lattice sites, plus a single ancilla spin. The resulting Hilbert space of three spin-1/2 degrees of freedom is eight-dimensional, and all calculations can be performed numerically with little effort.

We choose a Hamiltonian with Ising-type spin–spin coupling,

$$H_{\mathrm{s}} = \sigma_1^x \sigma_2^x, \tag{2.2.7}$$

and consider dynamics starting from an initial product state

$$|\Psi\rangle = |\phi\rangle \otimes |\psi_1\rangle \otimes |\psi_2\rangle\,. \tag{2.2.8}$$

The system spin states are parametrized by angles $\alpha_i \in [0, \pi/2]$ and $\theta_i \in [0, 2\pi]$ as

$$|\psi_i\rangle = \cos(\alpha_i) e^{-i\theta_i/2} |+_z\rangle + \sin(\alpha_i) e^{i\theta_i/2} |-_z\rangle \quad \text{for } i = 1, 2. \tag{2.2.9}$$

The ancilla initial state $|\phi\rangle$ is given by (2.1.11) as $|\phi\rangle = (|+_z\rangle + |-_z\rangle)/\sqrt{2}$. Here $\{|\pm_z\rangle\}$ denotes the σ^z eigenbasis with corresponding eigenvalues ± 1. Our aim is to apply the NIMP for estimating the dynamical zz correlation function

$$\begin{aligned} C(t_1, t_2) &= \langle \psi_1 \psi_2 |\, \sigma_1^z(t_1) \sigma_2^z(t_2)\, |\psi_1 \psi_2\rangle \\ &= \cos(2\alpha_1)\cos(2\alpha_2)\cos(2(t_2 - t_1)) \\ &\quad + i \sin(2\alpha_1)\sin(2\alpha_2)\sin(\theta_1)\sin(\theta_2)\sin(2(t_2 - t_1)). \end{aligned} \tag{2.2.10}$$

To obtain the systematic error ϵ_{sys} (2.2.2a) one needs the probabilities (2.1.5) and (2.1.9), but without linear approximations in λ. Calculating these probabilities for the Hamiltonian (2.2.7) and combining them according (2.1.10) we can, to all orders in λ, construct

$$\begin{aligned} C^{\lambda}(t_1, t_2) = \frac{1}{2\lambda} \Big(& \cos(2\alpha_1)\cos(2\alpha_2)\sin(2\lambda)\cos(2(t_2 - t_1)) \\ & + i \sin(2\alpha_1)\sin(2\alpha_2)\sin(\theta_1)\sin(\theta_2)\sin(2\lambda)\sin(2(t_2 - t_1)) \Big) \end{aligned} \tag{2.2.11}$$

as defined in (2.1.20). In (2.2.11) $f^{(1)} = f^{(2)} = 2$ since we are using $m_z = \pm 1$ for this example. Substituting (2.2.10) and (2.2.11) into (2.2.2a) we obtain the systematic error

$$\begin{aligned} \epsilon_{\mathrm{sys}} = \frac{1}{2|\lambda|} \Big| (2\lambda - \sin(2\lambda)) \Big[& \cos(2(t_2 - t_1))\cos(2\alpha_1)\cos(2\alpha_2) \\ & + i \sin(2(t_2 - t_1))\sin(\theta_1)\sin(\theta_2)\sin(2\alpha_1)\sin(2\alpha_2) \Big] \Big|. \end{aligned} \tag{2.2.12}$$

A plot of the systematic error (2.2.12), which vanishes for $\lambda \to 0$, is shown in Fig. 2.2.1 (left, red line increasing from origin) for the parameter choice $\alpha_1 = \alpha_2 = \pi/3$. To be within the regime of small λ for which the NIMP holds (2.1.3), we plot

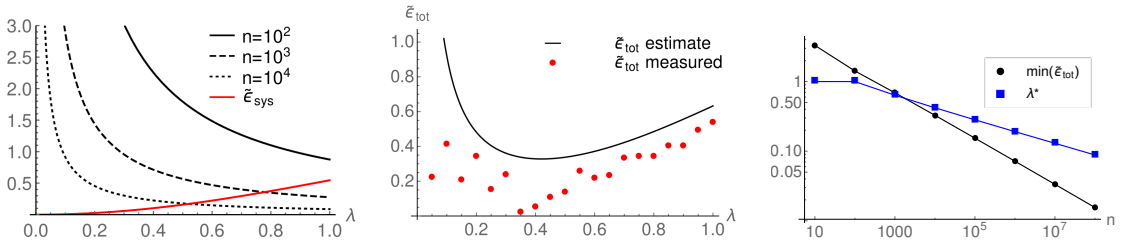

Figure 2.2.1: Error analysis for the example of Sec. 2.2.1 with parameter values $(t_1, t_2) = (1, 10)$, $\alpha_1 = \alpha_2 = \pi/3$ and $(\theta_1, \theta_2) = (\pi/7, \pi/5)$. All plots show relative errors $\tilde{\epsilon}_{\rm sys} = \epsilon_{\rm sys}/|C|$, and similarly for statistical and total errors. Left: Exact systematic error $\tilde{\epsilon}_{\rm sys}$ (red line, increasing from origin) and estimates (2.2.6) of $\tilde{\epsilon}_{\rm stat}$ for sample sizes $n = 10^2, 10^3, 10^4$ (solid, dashed, dotted black curves). The functional dependence of the bounds on the coupling time λ is as expected; The systematic error increases with λ and the stochastic error is inversely proportional to λ. Centre: Estimate for $\tilde{\epsilon}_{\rm tot}$ (line) together with numerically measured values for sample size $n = 10^4$ (dots). The estimated minimum error is 33% at $\lambda^* = 0.42$. The error estimate captures the qualitative behavior of the numerical data and is consistently larger. Right: Log-log plot of the estimated minimum error $\tilde{\epsilon}_{\rm tot}(\lambda^*)$ and its position λ^* as a function of sample size n. Straight lines indicate that the performance of the noninvasive measurement protocol improves like a power law with n.

the error for $\lambda \in (0, 1]$. The error is shown relative to $|C(t_1, t_2)|$, which we denote as $\tilde{\epsilon}_{\rm sys} = \epsilon_{\rm sys}/|C|$, and similarly for statistical and total errors. In the same plot the upper bound (2.2.6) on the statistical error, which decreases with increasing λ, is shown for various sample sizes n. For sufficiently large n the total error bound $\tilde{\epsilon}_{\rm tot}$ shows a minimum for some $\lambda = \lambda^*$ (solid line in Fig. 2.2.1, centre). Hence, assuming the error bounds to be reasonably tight, $\lambda^* = 0.42$ should be a good choice for the ancilla–target coupling when using a sample of $n = 10^4$ measurements. The corresponding error estimate is fairly large (33%) due to the conservative upper bound of the statistical error (2.2.6).

To check the tightness of the bounds, we numerically implemented the noninvasive measurement protocol of Sec. 2.1, using the exact time evolution (without expanding in λ) and drawing samples of random numbers according to the ancilla- and system-spin outcome probabilities [2]. As expected, the results of the numerical implementation (dots in Fig. 2.2.1 centre) are smaller than the conservatively estimated analytical error bounds. The influence of the statistical and systematic errors is evident in the numeric data. For $\lambda < \lambda^*$ the statistical error dominates, causing fluctuations whose sizes are of the same order as the total error. For $\lambda > \lambda^*$ the measured errors exhibit smaller fluctuations, and follow the trend of the error

[2] The relative frequencies $n_{m_a m_b}/n$ needed to determine (2.2.1) were obtained by binning 2×10^4 pseudo-random numbers drawn from the unit interval, with the probabilities $P_{m_a m_b}$ determining the bin widths.

bound. This reflects the increasingly dominant role of the systematic error at larger λ. To consistently achieve good accuracies, the ancilla–target coupling at t_1 should be chosen close to, but not smaller than λ^*.

The performance of the noninvasive protocol is characterized in Fig. 2.2.1 (right), where the minimum value $\tilde{\epsilon}_{\text{tot}}(\lambda^*)$ (dots) as well as the corresponding λ^* (squares) is shown for a range of sample sizes n. The minimum error decays like a power law with increasing sample size, as does the corresponding optimal coupling λ^*. This plot answers, at least on the level of error estimates, the optimization question posed at the beginning of Sec. 2.2. The conservative error estimates assume individual errors to not compensate each other, and experimental implementations are therefore expected to achieve accuracies higher than those predicted above.

2.3 Generalisations

In the NIMP of Sec. 2.1 we considered correlations of single-site observables, and used an ancilla whose spin s matched that of the individual spin degrees-of-freedom of the target lattice. In the first generalisation presented in this section, we show that the NIMP is valid for correlations of general observables $\langle\psi| O_1(t_1)O_2(t_2) |\psi\rangle$, and that we are free to choose the spin quantum number of the ancilla spin. The second and third generalisations aim to improve on the two key ingredients of the NIMP: weak ancilla–target coupling to reduce measurement backaction, and multiple repetitions of the protocol to achieve a sufficient signal-to-noise ratio.

2.3.1 General observables and ancilla spins.

Suppose that the target system is again a lattice of spin-$s \in \mathbb{N}/2$ degrees-of-freedom. Instead of specifying the type of observables correlated, we will allow any observables acting on the target's Hilbert space $\mathscr{H}_{\text{S}}$, and denote them as O_1, O_2. We will highlight only the pertinent differences in steps a–g of the NIMP.

The ancilla system is again a single spin degree-of-freedom, but we allow it to have any spin $\zeta \in \mathbb{N}/2$, i.e. we do not require $s = \zeta$. For the weak ancilla–target coupling $\mathscr{U}(\lambda)$ at t_1 (step c), we use Hamiltonian $H_{\text{c}} = B \otimes O_1$. Since the observable O_1 will generally not be a single-site observable, and since $s \neq \zeta$, we cannot measure the ancilla in the eigenbasis of O_1 (step d). Instead, we measure the ancilla in the eigenbasis $\{|m_\zeta\rangle\}$ of a spin-ζ observable S^α, where $\alpha \in \{x, y, z\}$.

At t_2 the target system is measured in the eigenbasis of observable O_2. Correlating the measurement outcomes as in (2.1.10) we obtain

$$\mathscr{C}(t_1, t_2) \simeq \langle S^\alpha \rangle_\phi \langle O_2(t_2) \rangle_\psi - 2\lambda \text{Im}\left[\langle BS^\alpha \rangle_\phi \langle\psi| O_1(t_1)O_2(t_2) |\psi\rangle\right]. \tag{2.3.1}$$

We eliminate the first term by choosing the initial ancilla state as an equal superposition of the ancilla measurement basis $|\phi\rangle = \sum_{m_\alpha \in \mathscr{S}} |m_\alpha\rangle / \sqrt{2\zeta+1}$. The resulting correlation is formally the same as (2.1.15)

$$\mathscr{C}(t_1,t_2) \simeq \frac{-2\lambda}{2\zeta+1} \sum_{m_\alpha, m'_\alpha \in \mathscr{S}} m_\alpha \mathrm{Im}\left[\langle m'_\alpha| B |m_\alpha\rangle \langle\psi| O_1(t_1) O_2(t_2) |\psi\rangle\right], \tag{2.3.2}$$

and the choices of B needed to extract $\mathrm{Re}\, C$ and $\mathrm{Im}C$ are analagous to those of the original NIMP (2.1.16), (2.1.18): With $B = S^\alpha$ correlation (2.3.2) reduces to $\mathrm{Im}C$, and with $B = -i(S^+_\alpha - S^-_\alpha)/2$ it reduces to $\mathrm{Re}\, C$. Since result (2.3.2) holds for any choice $\alpha \in \{x, y, z\}$, we are free to choose which spin-polarisation of the ancilla is to be measured at t_1. Choosing $\alpha = z$, for instance, $\mathrm{Im}C$ is obtained with $B = S^z$ and $\mathrm{Re}\, C$ is obtained with $B = S^y$.

The NIMP is therefore valid for correlations of arbitrary spin observables O_1, O_2, and the noninvasive measurement at t_1 does not depend on a specific choice for the spin quantum number ζ of the ancilla.

2.3.2 Deferral of ancilla measurement

Motivated by the use of deferred measurements of quantum memories (ancillas) in Ref. [19], we consider incorporating this technique into our noninvasive measurement protocol. The idea is that measurement backaction could be reduced by coupling (and then decoupling) an ancilla to the system at time t_1, but measuring the ancilla (step d in the protocol of Sec. 2.1) only at time t_2 or even later.

For a full comparison of such a deferred measurement protocol with the NIMP of Sec. 2.1 we will refrain from linearising the ancilla-system coupling unitary $\mathscr{U}(\lambda)$. Re-evaluating the correlation (2.1.10) of the NIMP to all orders of λ we have

$$\mathscr{C} = \langle \phi, \psi(t_1)| \mathscr{U}^\dagger(\lambda) \left(S^a \otimes e^{-iH_s t_1} S^b_j(t_2) e^{iH_s t_1}\right) \mathscr{U}(\lambda) |\phi, \psi(t_1)\rangle . \tag{2.3.3}$$

We will compare this correlation with that derived below for the deferred measurement procedure.

Up to (and including) step c of Sec. 2.1, the protocol remains unchanged, but since we refrain from linearisation of $\mathscr{U}(\lambda)$, the coupled ancilla–target state is

$$|\Psi_\lambda(t_1)\rangle = \mathscr{U}(\lambda) |\phi, \psi(t_1)\rangle . \tag{2.3.4}$$

Now, instead of projectively measuring the ancilla state at t_1, we keep $|\Psi_\lambda(t_1)\rangle$ unprojected, and proceed by time-evolving it with the system Hamiltonian H_s until time t_2,

$$|\Psi(t_2)\rangle = \mathbb{1}_A \otimes e^{-iH_s(t_2-t_1)} |\Psi_\lambda(t_1)\rangle . \tag{2.3.5}$$

This is the same time evolution as in step e of Sec. 2.1, but the ancilla state is not necessarilly preserved: the coupling $\mathscr{U}(\lambda)$ will in general entangle ancilla and target. Subsequent dynamics of the target (generated by H_s) will thus affect the ancilla state in a non-trivial way.

The deferred measurement protocol ends at t_2 with simultaneous projective measurements of the ancilla and the jth system spin. The joint probabilities for measurement outcomes (m_a, m_b) are

$$P_{m_a m_b} = \langle\Psi(t_2)| \left(|m_a\rangle\langle m_a| \otimes |m_b\rangle\langle m_b|\right) |\Psi(t_2)\rangle\,, \tag{2.3.6}$$

with the m_a projector acting on the ancilla, and the m_b projector only on site j of the system. Combining these probabilities according to (2.1.10) we obtain

$$\begin{aligned}\mathscr{C} &= \sum_{m_a,m_b\in\mathscr{S}} m_a m_b P_{m_a m_b} \\ &= \langle\Psi(t_2)| \sum_{m_a} m_a |m_a\rangle\langle m_a| \otimes \sum_{m_b} m_b |m_b\rangle\langle m_b| \,|\Psi(t_2)\rangle \\ &= \langle\phi,\psi(t_1)|\, \mathscr{U}^\dagger(\lambda) e^{iH_s(t_2-t_1)} \left(S^a \otimes S^b_j\right) e^{-iH_s(t_2-t_1)} \mathscr{U}(\lambda)\, |\phi,\psi(t_1)\rangle\,,\end{aligned} \tag{2.3.7}$$

where we have used the definition of $|\Psi(t_2)\rangle$ in the last line. The observable S^a acts only on the ancilla Hilbert space. Due to the trivial dynamics undergone by the ancilla from t_1 to t_2 (2.3.5), we have that $\left[e^{iH_s(t_2-t_1)}, S^a\right] = 0$. As a result (2.3.7) is identical to (2.3.3), to all orders in λ. Choosing the initial ancilla state $|\phi\rangle$ such that condition (2.1.13) is satisfied, both equations reduce to result (2.1.15) of Sec. 2.1 in the limit of $|\lambda| \ll 1$ where the linear expansion (2.1.3) of $\mathscr{U}$ is valid.

We conclude that the deferred measurement protocol described above is equivalent to the NIMP of Sec. 2.1, but that deferral of the ancilla measurement to times $t \geq t_2$ does not further improve the performance of the NIMP (i.e. backaction is unchanged). Nevertheless, either protocol may have distinct advantages over the other in experimental realisations: One may imagine experimental platforms in which storing the ancilla state until later times is difficult (favouring immediate measurement), or other situations in which the immediate measurement of the ancilla generates unwanted noise (favouring deferred measurement). We will see in Sec. 4.2 that the deferred measurement approach is favourable in linear ion-trap experiments as it avoids photon scattering and thus decoherence at t_1. From a theoretical point of view, deferred measurements have the advantage that no linearization of the post ancilla-measurement system state (as in (2.1.7)) is required. We will exploit this advantage in the next section.

2.3.3 Multiple measurements

In physical applications one will frequently be interested in correlations at more than one pair of times, or even in the functional dependence of C over a range of

times. The NIMP however describes a procedure to noninvasively measure only a single dynamic correlation function $C(t_1, t_2)$ at one pair of times (t_1, t_2). To measure more than one correlation, the NIMP must be repeated many times which translates into more time spent in the laboratory. In this section we attempt to make better use of experimental resources by comparing two strategies for noninvasively measuring multiple dynamic correlation functions. The key idea will be to perform multiple noninvasive measurements at times t_1, t_2, t_3, ... with the aim of extracting several dynamic correlation functions $C(t_1, t_2)$, $C(t_1, t_3)$, $C(t_2, t_3)$, ... from the same measurement samples.

To keep the presentation simple, we will discuss these strategies with respect to a minimal model consisting of two spin-1/2 degrees of freedom, and focus on dynamic correlation functions

$$C(t_1, t_2) = \langle\psi|\, \sigma_1^a(t_1)\sigma_2^b(t_2)\, |\psi\rangle\,, \tag{2.3.8a}$$
$$C(t_1, t_3) = \langle\psi|\, \sigma_1^a(t_1)\sigma_2^b(t_3)\, |\psi\rangle\,, \tag{2.3.8b}$$
$$C(t_2, t_3) = \langle\psi|\, \sigma_2^b(t_2)\sigma_1^a(t_3)\, |\psi\rangle\,, \tag{2.3.8c}$$

at three points in time, $t_3 > t_2 > t_1 \geq 0$. One way of noninvasively measuring these correlations is to repeat the NIMP of Sec. 2.1 separately for each correlation. We refer to this procedure as the single-noninvasive measurement protocol (sNIMP), as it involves only one noninvasive measurement before the final projective one. This approach however requires six, possibly very large, data samples (one sample per real and imaginary component). A possibly more efficient way to measure correlations (2.3.8a)–(2.3.8c) is to perform noninvasive measurements both at t_1 and t_2, followed by a projective measurement at t_3. We will refer to this protocol as the consecutive-noninvasive measurement protocol (cNIMP). The derivation of the cNIMP estimators (for general target systems of spin $s \geq 1/2$), the required coupling operators, and associated errors is similar to that of Sec. 2.1 and can be found in Appendix A.

While both variations of the NIMP turn out to be feasible in principle, they differ in their efficiency. Here we assume that, like in many experiments, the number of repetitions of the experiment is a limiting factor. We investigate in the following whether the sNIMP or the cNIMP is more efficient at determining all three correlations (2.3.8a)–(2.3.8c) to a desired accuracy.

To implement the cNIMP in our minimal model we need two[3] ancilla spins; One coupled to site 1 at t_1 with coupling time λ_1, the other to site 2 at t_2 with coupling time λ_2. Using the deferred measurement approach of the previous section, we measure both ancillas and lattice sites $i = 1$ and $j = 2$ at the final time t_3. Ancillas 1 and 2 are respectively measured in the eigenbasis of σ^a and σ^b, and this yields

[3] Choosing correlation functions other than those in Eqs. (2.3.8a)–(2.3.8c) may require more than two ancillas, but derivations go along similar lines (see App. A for a full discussion).

(see Eqs. (A.0.7)–(A.0.14))

$$C^{\lambda}(t_1,t_2)=\frac{\mathscr{C}^{(2)}(t_1,t_2)+i\,\mathscr{C}^{(1)}(t_1,t_2)}{4\lambda_1\lambda_2}. \tag{2.3.9}$$

Lattice site $j=2$ is measured in the eigenbasis of σ^b. Together with the measurement of ancilla 1, this yields (see Eqs. (A.0.15)–(A.0.18))

$$C^{\lambda}(t_1,t_3)=-\frac{\mathscr{C}^{(2)}(t_1,t_3)+i\,\mathscr{C}^{(1)}(t_1,t_3)}{2\lambda_1}. \tag{2.3.10}$$

Correlation $C^{\lambda}(t_2,t_3)$ is obtained from the measurement of ancilla 2 and that of site $i=1$, which is done in the eigenbasis of σ^a (see Eqs. (A.0.19)–(A.0.20)). Its form is

$$C^{\lambda}(t_2,t_3)=-\frac{\mathscr{C}^{(4)}(t_2,t_3)+i\,\mathscr{C}^{(3)}(t_2,t_3)}{2\lambda_2}. \tag{2.3.11}$$

The choices of coupling Hamiltonians required to construct (2.3.9)–(2.3.11) are summarised in table A.0.3. The table shows that the cNIMP requires only *three* measurement samples to obtain all six estimators in (2.3.9)–(2.3.11) of the real and imaginary parts of correlations (2.3.8a)–(2.3.8c).

Using these three finite measurement samples, the probabilities used to construct (2.3.9)–(2.3.11) can be approximated with relative frequencies (as in Sec. 2.2), and we again use a subscript n to denote quantities obtained from relative frequencies. Statistical, systematic and total errors (ϵ_{stat}, ϵ_{sys}, ϵ_{tot}) are defined as was done for the NIMP in Eqs. (2.2.2a)–(2.2.2c).

The estimator $C_n^{\lambda}(t_1,t_2)$ is obtained from two consecutive noninvasive measurements, and involves a division by both coupling times λ_1 and λ_2 (see (2.3.9)). As a consequence, the associated statistical error will be amplified much stronger than in the sNIMP in the limit $\lambda_1,\lambda_2\to 0$. Pushing this error below a certain desired level therefore requires larger sample sizes n, as shown in Fig. 2.3.2. This is the reason for the inferior performance of the cNIMP. The estimators $C_n^{\lambda}(t_1,t_3)$ and $C_n^{\lambda}(t_2,t_3)$ involve a division by only one of the coupling parameters (λ_1 or λ_2), so the statistical error is comparable to that of the sNIMP. The total error for these two correlations is however larger than in the sNIMP due to a larger systematic error which is incurred for non-zero λ_1 and λ_2.

Example: To illustrate our findings, and to compare the cNIMP and sNIMP, we revisit the example of Sec. 2.2.1 with Ising-type Hamiltonian (2.2.7) and zz correlation functions, i.e. $a=b=z$ in (2.3.8a)–(2.3.8c). Figure 2.3.1 shows the estimated total relative error $\tilde{\epsilon}_{\text{tot}}=\epsilon_{\text{tot}}/|C|$ for the cNIMP, as a function of both coupling times λ_1 and λ_2, for $C_n^{\lambda}(t_1,t_2)$ and $C_n^{\lambda}(t_1,t_3)$. For $C_n^{\lambda}(t_1,t_2)$ (left panel) a clear minimum deviation of 37% is indicated by the intersection of the black curves

at $(\lambda_1^*, \lambda_2^*) = (0.40, 0.41)$. Beyond this optimal coupling coordinate, the accuracy of the cNIMP estimator $C_n^{\lambda}(t_1, t_2)$ is bad as the total deviation grows to be of the order of $|C(t_1, t_2)|$. In the regime where either coupling time is small this large deviation is due to the above mentioned amplification of the statistical error brought about by the $1/(\lambda_1\lambda_2)$ factor in (2.3.9). For larger coupling times, systematic errors incurred from linear expansions with respect to λ_1 and λ_2 (A.0.9) add up to yield a larger systematic error than in the sNIMP. The estimator $C_n^{\lambda}(t_1, t_3)$ is obtained

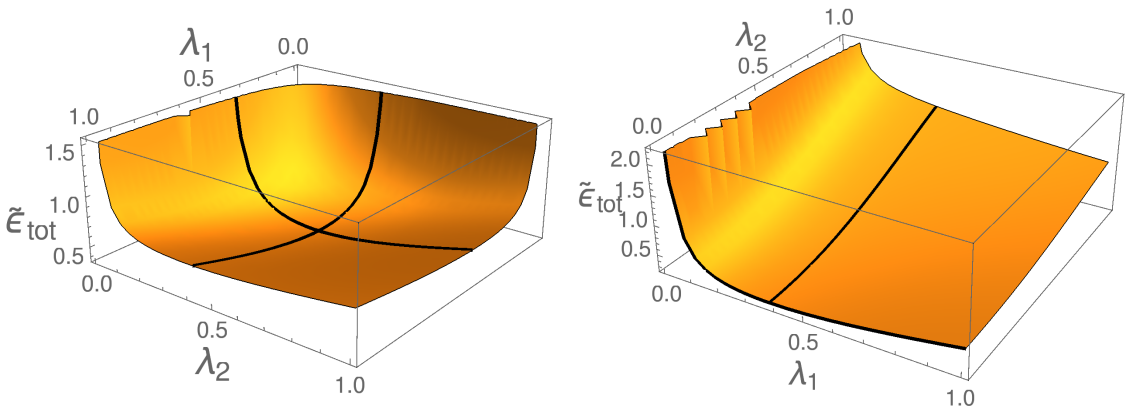

Figure 2.3.1: Predicted upper bounds on the relative error $\tilde{\epsilon}_{\text{tot}}$ for measurements of correlations $C(t_i, t_j)$ within the cNIMP for times $(t_1, t_2, t_3) = (0, 1, 10)$. The initial system state parameters are the same as in Fig. 2.2.1. The sample sizes are $n = 10^5$. Left: Estimated total relative error for measurements of $C_n^{\lambda}(t_1, t_2)$. The black curves are included to guide the reader's eye, and their intersection indicates the minimum error of 37% at $(\lambda_1^*, \lambda_2^*) = 0.40, 0.41)$. Right: Corresponding prediction for measurements of $C_n^{\lambda}(t_1, t_3)$, exhibiting a minimum error of 25% at $(\lambda_1^*, \lambda_2^*) = (0.37, 0.00)$. Although measurement of this correlation is performed in the cNIMP by measuring only the first ancilla (coupled to lattice-site 1 at t_1) and the spin at site 2, the additional coupling of the second ancilla to site 2 at intermediate time t_2 increases the systematic error. As a result the total error also increases with λ_2.

in the cNIMP from measurements of the first ancilla at t_1 and of site 2 at t_3. At the intermediate time t_2 the cNIMP perturbs the system dynamics by coupling a second ancilla to site 2. This perturbation is reflected in the error bound of $C_n^{\lambda}(t_1, t_3)$ (right panel of Fig. 2.3.1) which increases also with the coupling time λ_2. We omit the error bound of $C_n^{\lambda}(t_2, t_3)$ as it reflects a similar behaviour, only with the roles of λ_1 and λ_2 interchanged.

To measure (2.3.8a)–(2.3.8c) with accuracies as in Fig. 2.3.1 one needs a total of three samples of $n = 10^5$ measurements. In Fig. 2.2.1 we showed that the sNIMP achieves similar accuracies for samples of $n = 10^4$ measurements per real

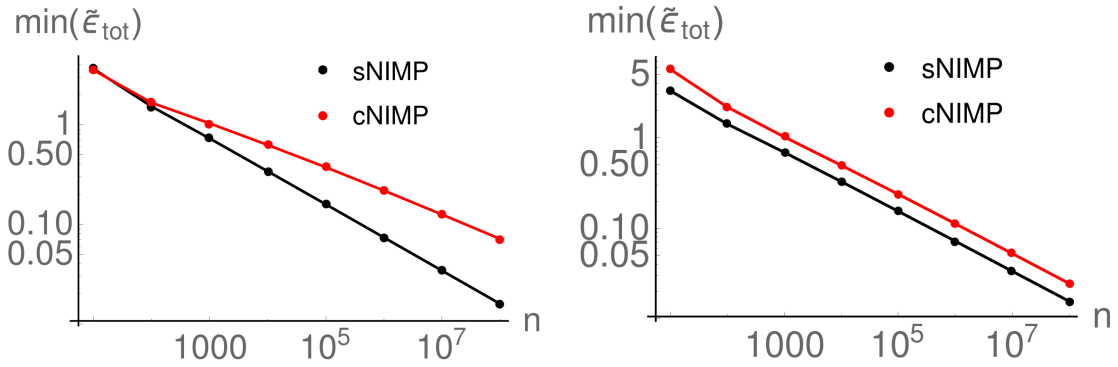

Figure 2.3.2: Minimum total error $\min_\lambda \tilde{\epsilon}_{\rm tot}(\lambda)$ as a function of sample size n. Times and system parameters are as in Fig. 2.3.1. Left: For $C_n^\lambda(t_1, t_2)$ the minimum error of the sNIMP decreases faster than that of the cNIMP. As a result, to construct an estimator with a total error of 10% or less, sample sizes in the sNIMP must be at least 10^6. This is about two orders of magnitude smaller than for the cNIMP. Right: For measurements of $C_n^\lambda(t_1, t_3)$ the minimum error of either protocol decreases at the same rate with the sample size, however the errors of the cNIMP are consistently larger than those of the sNIMP. Results for $C_n^\lambda(t_2, t_3)$ are similar (not shown).

and imaginary component. This is a first indication that the cNIMP is less efficient than the sNIMP.

To test this expectation we calculated numerically, for both protocols, the minima of the predicted estimator deviation $\tilde{\epsilon}_{tot}$ for increasing sample sizes. The results are shown in Fig. 2.3.2. Especially for the estimator $C_n^\lambda(t_1, t_2)$, which requires two noninvasive measurements in the cNIMP, the sNIMP is much more efficient in the large n regime (where the bound (2.2.6) is valid). The plot shows that the sNIMP error decreases at a faster rate than the cNIMP error, and an accuracy of 10% or less can be achieved in the sNIMP from 2×10^6 measurements, whilst in the cNIMP one would require 2×10^8 measurements. The minimum errors for the other two estimators decrease at the same rate in both protocols, but are consistently larger in the cNIMP. This is due to the greater systematic error incurred in the cNIMP.

In summary, both the cNIMP and sNIMP are feasible. However, to measure all correlations (2.3.8a)–(2.3.8c) with an accuracy of at least 10%, the cNIMP and sNIMP require, respectively, a net sample size $n_c = 3 \times 10^8$ and $n_s = 6 \times 10^6$. This example shows that multiple dynamic correlations are most efficiently measured with repeated implementations of the NIMP i.e. with the sNIMP.

3

Ancilla-free protocols

As reviewed in Sec. 1.2, general quantum measurements involving system-ancilla couplings and post-coupling projections of the ancilla can be described by Kraus operators and the related positive-operator valued measure (POVM). In this chapter we recast the noninvasive measurement protocol (NIMP) of Sec. 2.1 in the Kraus operator formalism, in order to gain deeper insight about the dynamic change induced by the noninvasive measurement on the target system. This insight will lead us to the remarkable and non-intuitive result that measuring dynamic correlations of spin-1/2 systems does not require any form of ancilla-based measurement: the real part can be measured by direct projective measurements of the system at both the early and final times. The imaginary part is obtained by performing rotations at the early times, followed by a single projective measurement at the final time.

3.1 Kraus operators for spin-$s \geq 1/2$ target systems

Keeping the notation of Chap.2, let $|\phi\rangle$ and $|\psi\rangle$ respectively denote the initial ancilla and target states. The initial product state at $t = 0$ is then $|\Psi\rangle = |\phi\rangle \otimes |\psi\rangle$, and the post-coupling state at $t_1 \geq 0$ (as follows from (2.1.4), step c of the NIMP) is

$$|\Psi_\lambda(t_1)\rangle = \mathscr{U}(\lambda)\,|\phi, \psi(t_1)\rangle\,. \tag{3.1.1}$$

Note that although the weak measurement of Sec. 2.1 requires $|\lambda| \ll 1$, we keep the unitary coupling $\mathscr{U}(\lambda)$ to all orders in λ for now so that we obtain the corresponding Kraus operators to all orders in λ too. For the subsequent ancilla measurement in the eigenbasis of S^a we use the projectors $\Pi^{m_a} = |m_a\rangle\langle m_a| \otimes \mathbb{1}_S$, and the (un-normalised) post-measurement state is then $\Pi^{m_a}\mathscr{U}(\lambda)\,|\phi, \psi(t_1)\rangle$.

As shown in (1.2.8) and (1.2.9), we obtain the (un-normalised) reduced density matrix of the target system in terms of the relevant Kraus operators by tracing over the ancilla degrees of freedom

$$\rho_{m_a}(t_1) = \mathrm{Tr}^{\neg S}\left[\Pi^{m_a}\mathscr{U}(\lambda)\,|\phi, \psi(t_1)\rangle\langle\phi, \psi(t_1)|\,\mathscr{U}^\dagger(\lambda)\Pi^{m_a}\right] = M_{m_a}\rho(t_1)M_{m_a}^\dagger, \tag{3.1.2}$$

where $\rho(t_1) = |\psi(t_1)\rangle\langle\psi(t_1)|$. The notation $\mathrm{Tr}^{\neg S}$ indicates that we trace over all degrees of freedom which do not belong to the target system i.e. we trace only over the ancilla Hilbert space $\mathscr{H}_A$. Using the matrix element form (1.2.11) of the Kraus operators, the ancilla initial state (2.1.11) (subject to constraint (2.1.13)) and the Taylor expansion of $\mathscr{U}(\lambda) = e^{-i\lambda H_c}$ we obtain

$$\begin{aligned} M_{m_a} &= \langle m_a|\,\mathscr{U}(\lambda)\,|\phi\rangle \\ &= \sum_{n=0}^{\infty}\frac{(-i\lambda)^n}{n!}\langle m_a|\,B^n\,|\phi\rangle\,A_i^n = \sum_{n=0}^{\infty}\frac{(-i\lambda)^n}{n!}\sum_{m'_a\in\mathscr{S}} c_{m'_a}\langle m_a|\,B^n\,|m'_a\rangle\,A_i^n. \end{aligned} \tag{3.1.3}$$

Recall that $\{c_{m_a}\}$ are the expansion coefficients of the initial ancilla state (2.1.11).

Expression (3.1.3) is the most general Kraus operator which describes the non-invasive measurement at t_1 in the NIMP. For $|\lambda| \ll 1$ and a given choice of $\{c_{m_a}\}$ and the ancilla–target coupling $H_c = B \otimes A_i$, it captures the dynamics induced on the target system by the noninvasive measurement (step c and d of Sec. 2.1). The set $\{M_{m_a}\}$ for all possible outcomes $m_a \in \mathscr{S}$ of the ancilla measurement forms the corresponding POVM. We will now consider the specific choices of $|\phi\rangle$ and H_c which were found in Sec. 2.1 to yield the dynamic correlation $C = \langle\psi|\,S_i^a(t_1)S_j^b(t_2)\,|\psi\rangle$ for a spin-$s \geq 1/2$ target system. Recall, that for both the real and imaginary part we found that $A_i = S_i^a$ and used the convention that $|\phi\rangle$ is an equal superposition of the eigenstates of S^a i.e.

$$|\phi\rangle = \frac{\sum_{m_a\in\mathscr{S}}|m_a\rangle}{\sqrt{2s+1}}. \tag{3.1.4}$$

3.1.1 Kraus operators for Im $\left[\langle\psi|\,S_i^a(t_1)S_j^b(t_2)\,|\psi\rangle\right]$

To extract Im $\left[\langle\psi|\,S_i^a(t_1)S_j^b(t_2)\,|\psi\rangle\right]$ we found that the coupling Hamiltonian should be chosen as $H_c = S^a \otimes S_i^a$ (see (2.1.10) and (2.1.16)). Substituting this into (3.1.3) we find that the Kraus operators corresponding to measurement outcomes $m_a \in \mathscr{S}$ are

$$\begin{aligned} M_{m_a} &= \sum_{n=0}^{\infty}\frac{(-i\lambda)^n}{n!}\langle m_a|\,(S^a)^n\,|\phi\rangle\,(S_i^a)^n \\ &= \langle m_a|\phi\rangle\sum_{n=0}^{\infty}\frac{(-i\lambda m_a)^n}{n!}(S_i^a)^n \\ &= \frac{1}{\sqrt{2s+1}}e^{-i(\lambda m_a)S_i^a}. \end{aligned} \tag{3.1.5}$$

In the second line we have used that the measurement basis for the ancilla is the eigenbasis of the operator $B = S^a$, and in the last line we have used our

conventional initial ancilla state (3.1.4). We find that the Kraus operators reduce to local rotations[1] of the target system. The axis of rotation is parallel to the spin component S^a which is to be correlated at t_1. The rotation angle is given by the coupling time λ scaled by the outcome m_a of the ancilla measurement.

This result provides major theoretical insight into the dynamic change of the target system's wave function when the weak measurement of the NIMP is set-up to measure $\mathrm{Im}\,[C]$; The net effect is that of a local *unitary* rotation of the target. The Kraus operators (3.1.5) then suggest that we should be able to measure $\mathrm{Im}\,[C]$ for all $s \geq 1/2$ without having to make use of an ancilla at t_1, but rather by means of local rotations of the target system at this early time. The weak-measurement condition $|\lambda| \ll 1$ which was necessary for the noninvasive measurement protocol should then translate to a condition on the rotation angle. Such an ancilla-free rotation protocol consists of the following steps:

(a) **Time evolution until time $t_1 \geq 0$.** The initial state of the target system $|\psi\rangle$ is allowed to evolve unitarily to t_1 with the dynamics $U(t_1)$ generated by the target's Hamiltonian

$$|\psi(t_1)\rangle = U(t_1)\,|\psi\rangle\,. \tag{3.1.6}$$

(b) **Local rotation of target at t_1.** As dictated by (3.1.5), we now apply a rotation to the ith lattice spin with the axis of rotation parallel to the spin component which is to be correlated at t_1 i.e. parallel to the unit vector $\boldsymbol{a}$. Similarly, (3.1.5) suggests the rotation angle to be λm_a where m_a is the eigenvalue obtained from the ancilla measurement. However, since we aim to measure $\mathrm{Im}\,[C]$ without invoking any ancilla coupling, we will denote the rotation angle as θ and assume no dependence on m_a or λ. The rotation operator is thus $R(\boldsymbol{a},\theta) = \exp(-i\frac{\theta}{2}S_i^a)$ and the rotated system state is

$$|\psi(t_1,\theta)\rangle = R(\boldsymbol{a},\theta)U(t_1)\,|\psi\rangle\,. \tag{3.1.7}$$

(c) **Time evolution until time $t_2 > t_1$.** In contrast to the NIMP, no measurement is performed at t_1. Rather, once the rotation has been completed the target is allowed to evolve unitarily under its Hamiltonian to $t_2 > t_1$

$$|\psi(t_2,\theta)\rangle = U(t_2-t_1)R(\boldsymbol{a},\theta)U(t_1)\,|\psi\rangle\,. \tag{3.1.8}$$

(d) **Projective measurement of site j.** At t_2, we projectively measure lattice spin j in the eigenbasis of observable S_j^b. The probability of measuring eigenvalue $m_b \in \mathscr{S}$ is

$$P_{m_b} = \langle\psi(t_2,\theta)|\,\Pi_j^{m_b}\,|\psi(t_2,\theta)\rangle\,, \tag{3.1.9}$$

[1] A quick check shows that (3.1.5) satisfies the completeness condition $\sum_{m_a\in\mathscr{S}} M_{m_a}^\dagger M_{m_a} = \mathbb{1}$ (1.2.7).

where the projection operator $\Pi_j^{m_b} = |m_b\rangle\langle m_b|$ acts non-trivially only on lattice site j. Using these probabilities we can construct the expectation value

$$\left\langle S_j^b(t_2,\theta)\right\rangle = \sum_{m_b\in\mathscr{S}} m_b P_{m_b} = \langle\psi(t_2,\theta)|\, S_j^b\,|\psi(t_2,\theta)\rangle\,. \tag{3.1.10}$$

(e) **Extract Im** $\left[\langle\psi|\, S_i^a(t_1)S_j^b(t_2)\,|\psi\rangle\right]$**.** Analogous to the weak-coupling requirement of the NIMP, let us now assume that the rotation angle is small i.e. $|\theta| \ll 1$. The motivation is that C is linear in both observables S_i^a and S_j^b, and this bi-linearity is achieved in the above expectation value (3.1.10) from a linear expansion of the rotation operators. This requires $|\theta/2|\|S_i^a\| = s|\theta/2|$ to be small. For a given spin-s system this is achieved by making the rotation angle small enough i.e. $|\theta| \ll 1$. We may then use $R(\boldsymbol{a},\theta) \simeq \mathbb{1} - i\frac{\theta}{2}S_i^a$, from which it follows that (3.1.10) reduces to

$$\begin{aligned}\left\langle S_j^b(t_2,\theta)\right\rangle &\simeq \left\langle S_j^b(t_2)\right\rangle_\psi - i\frac{\theta}{2}\left\langle S_j^b(t_2)S_i^a(t_1) - \text{h.c.}\right\rangle_\psi \\ &\simeq \left\langle S_j^b(t_2)\right\rangle_\psi - \theta\text{Im}\left[\langle\psi|\, S_i^a(t_1)S_j^b(t_2)\,|\psi\rangle\right].\end{aligned} \tag{3.1.11}$$

The last term contains the imaginary component of the desired dynamic correlation. Knowledge of the expectation value $\left\langle S_j^b(t_2)\right\rangle_\psi$ allows one to extract this component by a simple subtraction

$$\text{Im}\left[\langle\psi|\, S_i^a(t_1)S_j^b(t_2)\,|\psi\rangle\right] \simeq \left(\left\langle S_j^b(t_2,\theta)\right\rangle - \left\langle S_j^b(t_2)\right\rangle_\psi\right)/(-\theta). \tag{3.1.12}$$

Alternatively, one could exploit the fact that the first term of (3.1.11) is invariant under a sign change of θ and thus cancels when we take the difference $\left\langle S_j^b(t_2,-\theta)\right\rangle - \left\langle S_j^b(t_2,\theta)\right\rangle$

$$\text{Im}\left[\langle\psi|\, S_i^a(t_1)S_j^b(t_2)\,|\psi\rangle\right] = \left(\left\langle S_j^b(t_2,-\theta)\right\rangle - \left\langle S_j^b(t_2,\theta)\right\rangle\right)/(2\theta). \tag{3.1.13}$$

The Kraus operator formalism has thus allowed us to find a measurement protocol for $\text{Im}\,[C]$ that does not require an ancilla system for any spin-$s \geq 1/2$ target system. All operations performed before t_2 are unitary and performed directly on the target. Repeating all the steps above n times, we obtain a sample of n measurements from which we can construct an estimator of the the expectation value (3.1.11). $\text{Im}\,[C]$ can then be extracted either by using (3.1.12) (which requires separate measurement of an estimator of $\left\langle S_j^b(t_2)\right\rangle_\psi$), or by using (3.1.13) (which requires separate measurement of an estimator of $\left\langle S_j^b(t_2,-\theta)\right\rangle$). Which method is used within a given experimental platform is then a matter of convenience. Note that either option will be subject to statistical errors incurred from finite measurement samples. These errors propagate into the extracted imaginary component and are amplified since θ is small. The analysis of these statistical errors is the same as that presented in Sec. 2.2.

3.1.2 Kraus operators for Re $\left[\langle\psi| S_i^a(t_1)S_j^b(t_2) |\psi\rangle\right]$

We now derive the Kraus operators corresponding to the measurement of Re $[C]$ and consider their application to ancilla-free measurement protocols. In the previous section the unitary form of the Kraus operators (3.1.5) is due to the fact that the eigenbasis of the operator choice $B = S^a$ (which was found to yield Im $[C]$, see (2.1.16) and (2.1.17)) is also the basis in which the ancilla is measured during the NIMP (step d). To obtain Re $[C]$ with the NIMP, we found in Sec. 2.1 that the Hamiltonian generating the weak ancilla–target coupling should be $H_c = -i(S_a^+ - S_a^-)/2 \otimes S_i^a$ i.e. $B = -i(S_a^+ - S_a^-)/2 \neq S^a$ (see (2.1.18)). The ancilla is, however, still measured in the eigenbasis of S^a (the observable to be correlated at the early time). As a result the Kraus operators do not simplify in an obvious way

$$\begin{aligned} M_{m_a} =& \sum_{n=0}^{\infty} \frac{(-i\lambda)^n}{n!} \langle m_a| \left(-i(S_a^+ - S_a^-)/2\right)^n |\phi\rangle \, (S_i^a)^n \\ =& \frac{1}{\sqrt{2s+1}} \sum_{n=0}^{\infty} \frac{(-i\lambda)^n}{n!} \sum_{m'_a \in \mathscr{S}} \langle m_a| \left(-i(S_a^+ - S_a^-)/2\right)^n |m'_a\rangle \, (S_i^a)^n. \end{aligned} \tag{3.1.14}$$

In the last line we have again used our conventional choice for the initial ancilla state (3.1.4). Even upon considering the first order Taylor expansion of (3.1.14) with respect to λ (which is necessary for the weak-measurement of the target)

$$M_{m_a} \simeq \frac{1}{\sqrt{2s+1}} \left(\mathbb{1} - i\lambda \sum_{m'_a \in \mathscr{S}} \langle m_a| \left(-i(S_a^+ - S_a^-)/2\right) |m'_a\rangle \, (S_i^a) \right) \tag{3.1.15}$$

the dynamic effect of the Kraus operators on the target system is not at all obvious and so they do not provide insight towards an ancilla free measurement of Re $[C]$.

In an attempt to replicate the unitary ancilla-free measurement protocol of Im $[C]$ for any $s \geq 1/2$ target system, we considered changing the ancilla measurement of the NIMP (step d): Let us denote the eigenstates of B as $\{|b\rangle\}$ such that $B|b\rangle = b|b\rangle$. Observable B need not be a spin-polarised observable, but can be any bounded hermitian operator acting on the ancilla Hilbert space $\mathscr{H}_A$. Suppose now that in the NIMP we measure the ancilla in the eigenbasis of B, and not in the eigenbasis of the observable to be correlated at the early time S^a. Keeping the usual ancilla–target coupling Hamiltonian $H_c = B \otimes S_i^a$, the corresponding Kraus operators do then indeed reduce to rotations (ignoring the pre-factor) of the target system

$$M_b = \langle b| e^{-i\lambda B \otimes S_i^a} |\phi\rangle = \langle b|\phi\rangle \, e^{-i(\lambda b)S_i^a}. \tag{3.1.16}$$

However, when modifying step d of the NIMP accordingly, the measured correlation (2.1.10) becomes

$$\mathscr{C} \simeq \langle B\rangle_\phi \left\langle S_j^b(t_2)\right\rangle_\psi - 2\lambda \mathrm{Im}\left[\left\langle B^2\right\rangle_\phi C\right], \tag{3.1.17}$$

from which one can *never* extract the desired real component. This is due to the hermiticity of B (which is necessary to ensure unitarity of $\mathscr{U}$) which causes $\langle B^2\rangle_\phi \in \mathbb{R}$.

We must therefore conclude that for a given spin-s target system, one does in general require an ancilla-based noninvasive measurement at t_1 in order to measure $\mathrm{Re}\left[\langle\psi| S_i^a(t_1)S_j^b(t_2)|\psi\rangle\right]$. In contrast, the imaginary component can always be measured by means of a rotation-based (ancilla-free) measurement protocol if the rotation angles are small (as was shown in Sec. 3.1.1).

3.2 Specialisation to spin-1/2 target systems

We now discuss the results of Sec. 3.1.1 and 3.1.2 in the context of spin-1/2 systems.

3.2.1 Rotation-based measurement protocol for $\mathrm{Im}\left[\langle\psi| \sigma_i^a(t_1)\sigma_j^b(t_2)|\psi\rangle\right]$

From steps a to e of Sec. 3.1.1 we know that the imaginary part of dynamic correlations of any spin-s lattice system, with $s \geq 1/2$, can be measured by applying a rotation $R(\boldsymbol{a},\theta)$ locally to site i at t_1. A necessary condition was that the rotation angle θ is small (see step e). This lead to the expectation value (3.1.11) being linear in the operator S_i^a which is necessary for it to contain $\mathrm{Im}\left[\langle\psi| S_i^a(t_1)S_j^b(t_2)|\psi\rangle\right]$. This small angle condition is however not necessary when dealing with a spin-1/2 target system: For $s = 1/2$ the spin observables S^a for $a \in \{x,y,z\}$ are given by the Pauli matrices $(\hbar/2)\sigma^a$. Here and in the following discussions of spin-1/2 systems we will use the convention of dropping the prefactor so that the spin-1/2 observables are given by the unscaled Pauli matrices σ^a with eigensystem $\sigma^a|\pm_a\rangle = (\pm 1)|\pm_a\rangle$. Apart from being hermitian, the Pauli matrices are also unitary which gives them the special[2] property of being involutions i.e. $\sigma^a\sigma^a = \mathbb{1}$ for $a \in \{x,y,z\}$. Consequently, the rotation operator

$$R(\boldsymbol{a},\theta) = e^{-i\frac{\theta}{2}\sigma_i^a} = \cos(\theta/2) - i\sin(\theta/2)\sigma_i^a \tag{3.2.1}$$

is linear in the observable σ_i^a for *all* rotation angles $\theta \in [-\pi,\pi)$. In the rotation-based measurement protocol for $\mathrm{Im}\,[C]$, the expectation value (3.1.10) then becomes

$$\begin{aligned}\left\langle S_j^b(t_2,\theta)\right\rangle = &\cos^2(\theta/2)\left\langle\sigma_j^b(t_2)\right\rangle_\psi + \sin^2(\theta/2)\left\langle\sigma_i^a(t_1)\sigma_j^b(t_2)\sigma_i^a(t_1)\right\rangle_\psi \\ &- \sin(\theta)\mathrm{Im}\left[\langle\psi|\sigma_i^a(t_1)\sigma_j^b(t_2)|\psi\rangle\right],\end{aligned} \tag{3.2.2}$$

which contains $\mathrm{Im}\,[C]$ for *any* choice of θ. To extract $\mathrm{Im}\,[C]$ we had two options in Sec. 3.1.1: we could separately measure either $\left\langle\sigma_j^b(t_2)\right\rangle_\psi$ (3.1.12) or $\left\langle S_j^b(t_2,-\theta)\right\rangle$

[2] Special in the sense that spin observables for $s > 1/2$ are in general not involutions.

(3.1.13). In the special case of a spin-1/2 target system, the second option is favourable since both error terms (given in the first line of (3.2.2)) are cancelled so that the imaginary component is given by

$$\mathrm{Im}\left[\langle\psi|\,\sigma_i^a(t_1)\sigma_j^b(t_2)\,|\psi\rangle\right] = \left(\left\langle S_j^b(t_2,-\theta)\right\rangle - \left\langle S_j^b(t_2,\theta)\right\rangle\right)/\sin(\theta), \tag{3.2.3}$$

for any $\theta \in [-\pi,\pi)$.

We have thus shown that the rotation-based protocol of Sec. 3.1.1 can be utilised without any constraints on the rotation angle θ when correlating single-site spin-1/2 observables. In fact, from Eq. (3.2.3) it is clear that the optimal rotation angle is $\theta = \pi/2$ since then the denominator is 1. This has the benefit that statistical errors, which propagate into estimators (obtained from finite measurement samples) of (3.2.3), are not amplified. Assuming that the rotation angle can be tuned precisely to this value in a given experimental realisation, the only error incurred in the measurement of $\mathrm{Im}\left[\langle\psi|\,\sigma_i^a(t_1)\sigma_j^b(t_2)\,|\psi\rangle\right]$ is then due to statistical errors arising when estimating probabilities (3.1.9) from a finite sample of measurements. We will refer to the above measurement procedure which leads to (3.2.3) as the rotation-based measurement protocol (RMP).

3.2.2 Projective measurement protocol for $\mathrm{Re}\left[\langle\psi|\,\sigma_i^a(t_1)\sigma_j^b(t_2)\,|\psi\rangle\right]$

In the discussion of Sec. 3.1.2 we stated that the necessary choice of B (the operator acting on $\mathscr{H}_A$ in $H_\mathrm{c} = B\otimes S_i^a$) combined with the measurement basis for the ancilla measurement, prevented the Kraus operators (3.1.14) from describing physically clear dynamics on the target. We now reconsider these Kraus operators within the spin-1/2 context. To measure $\mathrm{Re}\left[\langle\psi|\,\sigma_i^a(t_1)\sigma_j^b(t_2)\,|\psi\rangle\right]$ with the NIMP, we know from (2.1.18) that the coupling Hamiltonian[3] should be $H_\mathrm{c} = -i(\sigma_a^+ - \sigma_a^-)\otimes\sigma_i^a$. Using the involution property of the Pauli matrices, and the fact that for any $a\in\{x,y,z\}$ the operator $-i(\sigma_a^+ - \sigma_a^-)/2$ is also a Pauli matrix, we can write the ancilla–target coupling $\mathscr{U}$ as a linear function of H_c for any $\lambda \geq 0$,

$$\mathscr{U} = \cos\lambda - i\sin\lambda\left(-i(\sigma_a^+ - \sigma_a^-)/2\otimes\sigma_i^a\right). \tag{3.2.4}$$

This linearity of the coupling operator, for all $\lambda \geq 0$, is analogous to the linearity of the rotation operators (3.2.1) in the RMP. This suggests that we should be able to measure the real part without making use of an ancilla. For spin-1/2, the initial ancilla state is $|\phi\rangle = (|+_a\rangle + |-_a\rangle)/\sqrt{2}$, and $\mathscr{U}$ is given by (3.2.4). The

[3] We have dropped the factor of 1/2 from the B operator of the coupling Hamiltonian since we are using the unscaled Pauli matrices.

corresponding Kraus operators are thus

$$\begin{aligned} M_{\pm_a} &= \langle \pm_a | \cos\lambda - i \sin\lambda \left(-i(\sigma_a^+ - \sigma_a^-) \otimes \sigma_i^a\right) |\phi\rangle \\ &= \frac{1}{\sqrt{2}} \left(\cos\lambda \mp \sin\lambda \sigma_i^a\right). \end{aligned} \tag{3.2.5}$$

The dynamics described by these two operators may not be immediately clear, but upon substituting $\lambda = 3\pi/4$ (which is allowed since (3.2.4) and thus (3.2.5) is valid to all orders of λ) we find that they reduce to local projection operators

$$M_{\pm_a} = \frac{1}{2}(\mathbb{1} \pm \sigma_i^a) = \Pi_i^{\pm_a} \text{ for } \lambda = 3\pi/4. \tag{3.2.6}$$

We may thus draw the surprising conclusion that when the NIMP is used to measure $\mathrm{Re}\, C$ for single-site spin-1/2 observables, the ancilla-based measurement at t_1 induces dynamics on the target which is equivalent to performing a projective measurement of the ith spin. Such a projective measurement protocol (PMP) for correlations of single-site observables $\mathrm{Re}\left[\langle\psi| \sigma_i^a(t_1)\sigma_j^b(t_2) |\psi\rangle\right]$ would be implemented as follows:

(a) **Time evolution until time t_1,**

$$|\psi(t_1)\rangle = U(t_1) |\psi\rangle, \tag{3.2.7}$$

where $|\psi\rangle$ is the initial state of the spin-1/2 target system.

(b) **Projective measurement at site i.** The state of the target is probed by projectively measuring the observable σ_i^a. The probabilities of measuring eigenvalue ± 1 are

$$P_{\pm_a}^{\mathrm{Proj}} = \langle\psi(t_1)| \Pi_i^{\pm_a} |\psi(t_1)\rangle, \tag{3.2.8}$$

and the corresponding normalised post-measurement states are

$$|\psi_{\pm_a}(t_1)\rangle = \Pi_i^{\pm_a} |\psi(t_1)\rangle / \sqrt{P_{\pm_a}^{\mathrm{Proj}}}. \tag{3.2.9}$$

(c) **Time evolution until time t_2.** Time-evolve the post-measurement state $|\psi_{\pm_a}(t_1)\rangle$ to time t_2,

$$|\psi_{\pm_a}(t_2)\rangle = U(t_2 - t_1) |\psi_{\pm_a}(t_1)\rangle. \tag{3.2.10}$$

(d) **Projective measurement at site j.** The conditional probability of measuring the system in eigenstate $|\pm_b\rangle$ of σ_j^b at time $t_2 > t_1$ after having obtained $|\pm_a\rangle$ when measuring σ_i^a at time t_1 is

$$\begin{aligned} P_{\pm_b|\pm_a}^{\mathrm{Proj}} &= \langle\psi_{\pm_a}(t_2)| \Pi_j^{\pm_b} |\psi_{\pm_a}(t_2)\rangle \\ &= \langle\psi| U^\dagger(t_1)\Pi_i^{\pm_a}U^\dagger(t_2 - t_1)\Pi_j^{\pm_b}U(t_2 - t_1)\Pi_i^{\pm_a}U(t_1) |\psi\rangle / P_{\pm_a}^{\mathrm{Proj}}. \end{aligned} \tag{3.2.11}$$

(e) **Correlating the measured outcomes.** Correlations are calculated according to

$$\mathscr{C}^{\mathrm{Proj}} = P^{\mathrm{Proj}}_{+_a+_b} + P^{\mathrm{Proj}}_{-_a-_b} - P^{\mathrm{Proj}}_{-_a+_b} - P^{\mathrm{Proj}}_{+_a-_b}, \tag{3.2.12}$$

where $P^{\mathrm{Proj}}_{+_a+_b} = P^{\mathrm{Proj}}_{+_a} P^{\mathrm{Proj}}_{+_b|+_a}$ denotes the joint probability to projectively measure outcome $+1$ for σ_i^a at time t_1 and outcome $+1$ for σ_j^b at t_2 (and similarly for the other indices). Inserting (3.2.8) and (3.2.11) into (3.2.12) and after some algebraic manipulations (reported in Appendix B) we obtain the final result

$$\mathscr{C}^{\mathrm{Proj}}(t_1,t_2) = \langle\psi|\, \sigma_i^a(t_1)\sigma_j^b(t_2)\,|\psi\rangle + 2i\mathrm{Im}\left[\langle\psi|\, \Pi_i^{+_a}(t_1)\sigma_j^b(t_2)\Pi_i^{-_a}(t_1)\,|\psi\rangle\right], \tag{3.2.13}$$

where we have abbreviated $U^\dagger(t_1)\Pi_i^{\pm_a}U(t_1) = \Pi_i^{\pm_a}(t_1)$. $\mathscr{C}^{\mathrm{Proj}}$ is real as per its definition (3.2.12) and the second term on the right-hand side of (3.2.13) is purely imaginary. Hence it follows that

$$\mathscr{C}^{\mathrm{Proj}}(t_1,t_2) = \mathrm{Re}\left[C(t_1,t_2)\right] \text{ where } C(t_1,t_2) = \langle\psi|\, \sigma_i^a(t_1)\sigma_j^b(t_2)\,|\psi\rangle\,. \tag{3.2.14}$$

For systems beyond spin-1/2 (as we saw from the Kraus operators of Sec. 3.1.2) and/or for general observables, this projective measurement protocol does not yield the real part of desired dynamic correlation functions. More precisely, we show in Appendix B that for dynamic correlations $\langle\psi|\, A(t_1)B(t_2)\,|\psi\rangle$ of arbitrary spin-$s \geq 1/2$ observables A and B, $\mathrm{Re}\left[\langle\psi|\, A(t_1)B(t_2)\,|\psi\rangle\right] = \mathscr{C}^{\mathrm{Proj}}$ holds only if the operator

$$\Gamma \equiv \sum_a a \sum_{a'\neq a} P^a_{\mathscr{A}}(t_1) B(t_2) P^{a'}_{\mathscr{A}}(t_1) \tag{3.2.15}$$

is anti-hermitian. Here we have used $\mathscr{A}$ to denote the support of A (for instance, if $s = 1/2$ and $A = \sigma_i^a$ then $\mathscr{A} = i$). The eigenvalues of A are denoted as $\{a\}$ and the projectors onto the corresponding (possibly degenerate) eigenspaces are given by $\{P^a_{\mathscr{A}}\}$, where the subscript $\mathscr{A}$ indicates that all lattice sites in the support of A are projected. The anti-hermiticity condition (B.0.11) is satisfied for correlations where A is a local spin-1/2 observable, and also for particular multi-site spin-1/2 observables (see (B.1.6) and (B.1.7)), but is violated in most other cases, for example for spin-1 models (see (B.0.13)).

The noninvasive measurement protocol of Sec. 2.1, which is valid for general spin models and observables, was developed with the aim of reducing, and essentially eliminating (in the limit of small coupling times λ) the disturbing effect of measurement backaction on the target system at the early measurement time t_1. In this chapter we have used the Kraus operator formalism to re-derive this NIMP. The motivation was to gain better insight into the dynamics induced on the target system during the noninvasive measurement at t_1. For the case of imaginary dynamic correlation components of general spin systems (Sec. 3.1.1) this insight

(summarised by result (3.1.5)) lead to an ancilla-free measurement protocol based on rotations of the lattice site whose state is to be correlated at t_1. Such a rotation is easily applied in experimental platforms, whereas preparation of a separate ancilla system and generation of the ancilla–target coupling requires a high level of control (although it is feasible as discussed in Sec. 4.2). Up to the constraint of a small rotation angle ($|\theta| \ll 1$) the rotation based protocol is thus a major simplification in our quest for measurement protocols of dynamic correlations.

Despite various efforts (some of which were discussed in Sec. 3.1.2), we were not able to derive a similar (or indeed any) ancilla-free measurement protocol for the real part of dynamic correlations for general spin systems. At this point in our research we thus conclude that noninvasive measurements are necessary in general to measure $\mathrm{Re}\, C$.

Nevertheless, we were able to shown in this section that spin-1/2 models present a special and indeed very interesting case. This is the second main result of this thesis: For general Hamiltonians, dynamic correlations of single-site observables $C(t_1, t_2) = \langle\psi|\, \sigma_i^a(t_1)\sigma_j^b(t_2)\, |\psi\rangle$ can be measured without any form of ancilla-based measurements. This is achieved by combining the RMP of Sec. 3.2.1 with the PMP of Sec. 3.2.2. Both protocols are valid for any spin-1/2 lattice model independent of dimension, geometry or Hamiltonian and is also valid for arbitrary (in general non-equilibrium) initial states. No ancilla systems are required at any point in the measurement of $C(t_1, t_2)$, and yet strictly no disturbance due to measurement backaction propagates into the measured correlation components. Note that the system does still experience measurement backaction, even of the strongest possible kind in the case of the PMP, but these disturbances cancel out when constructing the correlation components. We would like to stress again that this is a surprising and counter-intuitive result. It completely contradicts the premise which motivated the derivation of the NIMP, namely that backaction from projective measurements at early times disturbs the system dynamics and thus prevents accurate measurement of dynamic correlations. From a theoretical point of view, the ancilla-free RMP and PMP are a great simplification of the NIMP in the case of correlations of single-site spin-1/2 observables. From an experimental viewpoint one may imagine scenarios where the ancilla-based noninvasive measurement is very difficult to achieve since it requires a high level of control. The PMP and RMP avoid this problem. They also require a substantially smaller number of repetitions in order to accumulate sufficient measurement statistics: Systematic errors stemming from a weak coupling expansion are absent, and statistical errors are not amplified, leading to a higher accuracy of the protocol. As a closing remark we must however mention that projective measurements are generally challenging when it comes to experimental realisation. This is the motivation for the modified projective protocols presented in the next chapter, where we discuss implementation of Sec. 2.1's NIMP and of the ancilla-free protocols discussed in this chapter.

4

Experimental Implementation

In Chaps. 2 and 3 we established a theoretical framework describing how dynamic correlations can be measured. This is summarised by the NIMP of Sec. 2.1, the RMP of Sec. 3.2.1 and the PMP of Sec. 3.2.2. The goal of this chapter is to discuss implementation of these protocols in existing experimental platforms. While there are a number of experiments based on ultra-cold atoms, polar molecules, or ions with which quantum spin models can be simulated [24; 25; 26; 27], we will consider only linear ion traps and quantum gas microscopes. Both platforms provide single-site spin resolution and have been used to measure spatially resolved static spin correlations [28; 29]. This makes them ideal candidates for implementation of our measurement protocols to extract dynamic spin correlations.

Linear ion-traps (LIT) confine ions along a single axis in real-space within a vacuum chamber and are described, for instance, in Refs. [30; 31; 32]. The axial confinement is achieved by applying an oscillating radio-frequency voltage to two electrode pairs, arranged parallel to the trapping axis, thereby creating an anisotropic harmonic potential with the axial frequency much less then the two radial frequencies. As a result the motion of ions within the trap is radially restricted, but they are free to move along the trap axis. To prevent ion loss at the trap ends, a constant voltage is applied to an additional pair of "end-cap" electrodes situated at the trap ends. After having been sufficiently cooled [32], the trapped ions then naturally arrange themselves into a one-dimensional lattice due to their mutual Coulomb repulsion. Whilst this negates the need for a lattice potential, the resulting lattice period is not constant, but becomes larger towards the chain ends. The number of trapped ions is typically on the order of tens of ions, with $N = 53$ recently reported [28]. This one-dimensional lattice can then be modelled as a chain of N spin-1/2 particles: Designating two hyperfine levels[1] of a trapped ion's electronic ground state (for instance) as spin states $|\pm\rangle$, one can drive transitions from one to the other with an oscillating field whose frequency is tuned to the energy gap of the two states. State preparation is also possible [31]. Spin-spin interactions, and thus dynamics, are mediated by collective motional modes of the

[1] For the possible choices of electronic states see [31].

ions which are coupled to one-another due to their mutual Coulomb interaction. In order to address specific motional modes the ions are laser cooled [32] so that their motion is quantised. By applying external optical drive fields for a time interval τ, one can excite specific collective motional (phonon) modes of the ions, thereby generating many-body dynamics $e^{-i\tau H}$ under a desired Hamiltonian H [33; 34].

Quantum gas microscopes. Whereas linear ion traps specialise in the control of one-dimensional spin lattices, quantum gas microscopes (QGM) provide a platform in which two dimensional spin lattices can be simulated. They are based on high-resolution optical systems (microscopes) which are used to create a 2D trapping potential as well as to detect the trapped atoms. The lattice is created by using the microscope optics to project the periodic structure of a lithographically produced mask onto a 2D Bose-Einstein condensate (BEC). Imposing a lattice potential on a BEC allows for macroscopic ensembles, on the order of up to 10^4 atoms, to be trapped with near-unity fidelity (one atom per lattice site, see Ref. [35]). Arbitrary lattice geometries can be generated (within the limits of the optical system) by varying the pattern etched onto the mask. A major advantage of using such a mask is that the resulting lattice geometries are independent of the wavelength used to illuminate the mask, and this allows for precise control over tunnelling rates within the lattice by varying the laser wavelength. A direct application is to mitigate heating effects during projective measurements and we discuss this point in more detail in the next paragraph. The atomic lattice is positioned between 1.5 to $3\mu m$ from the first (hemi-spherical) lens of the optical system. This yields a diffraction limit well below the lattice period and thus provides single-site resolution of atomic densities within the lattice. Effective spins are created by optical addressing of the electronic hyperfine structure, similar to linear ion traps [28]. Spin-resolved imaging is achieved, for instance, by applying a magnetic field gradient which splits the trapping potential at each lattice site into a double well in which the potential minima of the two spin states are separated due to their differing magnetic moments. An atom's spin state is thus inferred from its position within this double-well (see Refs. [36; 29]).

Repeated projective measurements. To measure the spin state of an atom in either experiment, lasers are used to induce fluorescence of the trapped atoms. The emitted photons are recorded by a high resolution CCD camera (the optical set-up in QGMs yields a resolution higher than that achieved in LITs). In linear ion traps all ions are typically adressed simultaneously and the fluorescence is state dependent. The relative number of photons recorded from each ion is used to infer the spin state onto which the wave function of each individual ion has collapsed [31]. In QGMs the fluorescence is made to be state independent since one can infer spin states from the atom positions, as described in the previous paragraph.

The emitted photons however pose a challenge for repeated measurements in both experimental platforms. Each ion/atom scatters photons isotropically so that some of them interact with neighbouring spins. This decoheres the state of the spin chain. Scattered photons also impart momentum to the trapped particles and this can provide enough kinetic energy for the particles to escape from the trap. Spin densities are thus generally not preserved during measurement. Such heating effects can be mitigated in QGMs due to the high level of control which one has over the lattice geometry: Before performing a measurement the lattice depth, and thus the on-site trapping potential, can be increased by several orders of magnitude [35]. Nevertheless, repeated measurements of atomic densities show that a non-negligible fraction of atoms is lost (up to 16% is reported in Ref. [37]), or move along the lattice to be re-trapped elsewhere (hopping).

Experimental implementation of the otherwise theoretically simple PMP is a non-trivial task since it requires two repeated projective measurements. Our non-invasive measurement protocol is thus still relevant in spin-1/2 systems. Measurement of the ancilla can be deferred to the final time t_2 (see Sec. 2.3.2), and thus any destructive effects arising from projective measurements are postponed to the end of the protocol.

Organisation of this chapter. In Sec. 4.1 we discuss implementation of the ancilla-free RMP and PMP, which are specific to spin-1/2 systems. The non-trivial task of implementing the otherwise theoretically simple PMP is discussed in Sec. 4.1.2 with quantum gas microscopes in mind. We show how particle loss induced by the measurement at t_1 can alter the system dynamics and how this ultimately results in deviations of the measured correlation from the desired real correlation component. In Sec. 4.1.3 we discuss implementation of the RMP and consider the experimentally relevant question of how errors in the rotation angle at t_1 propagate into measurements of $\mathrm{Im}C$. In both sections our main result is a theoretical upper bound on the magnitude of the respectively incurred error. We discuss how this bound can be minimised through appropriate choices of measurement times and lattice sites. The main theoretical tool used is the theory of Lieb-Robinson bounds, which we review in Sec. 4.1.1.

In Sec. 4.2 we discuss implementation of our non-invasive measurement protocol. Although this ancilla based protocol is strictly speaking not necessary in spin-1/2 systems, we discuss implementation of the NIMP within linear ion traps. The motivation for doing so (beyond a proof-of-principle) is that the ancilla measurement can be deferred to t_2. As a result all projective measurements can be performed simultaneously at the end of the experiment, at which point decoherence and particle loss is of no concern. Note that the discussion of this last section is adapted from our publication [14] and focusses on existing techniques which can be readily utilised to implement the NIMP in linear ion traps. As such no novel technical

finding is presented, and this section should be read in particular as a proposal of how one can achieve the various coupling Hamiltonians necessary to extract real and imaginary correlation components from the non-invasive measurement (step c and the discussion following step g of Sec. 2.1).

4.1 Implementation of ancilla free protocols

4.1.1 Lieb-Robinson bounds

Here we provide a brief review of Lieb-Robinson theory, necessary for the derivations of Sec. 4.1.2 and 4.1.3.

Let Λ denote the set of all lattice sites within a given lattice. Suppose that at time $t = 0$ this lattice is subjected to a perturbation localised within some finite subset of lattice sites $X \subset \Lambda$. Suppose further that there is an observer who can perform measurements on some other finite set $Y \subset \Lambda$, disjoint with X i.e. $X \cap Y = \varnothing$. Let $d(X, Y) \geq 1$ denote the minimum separation of the two regions X and Y. A natural question to ask is how long the observer has to wait before he can detect in Y the perturbation which occurred in X at $t = 0$, if at all? The answer lies in the speed with which perturbations propagate within the quantum lattice. Intuitively this speed should depend on the type of interactions present in the quantum lattice, and Lieb and Robinson formalised this idea in 1972 [38].

The main ingredient in their work is to consider the dynamical change of the norm of a commutator of two observables: Using $X \cap Y = \varnothing$, the lattice's Hilbert space can be written as $\mathscr{H}_\Lambda = \mathscr{H}_X \otimes \mathscr{H}_Y \otimes \mathscr{H}_{\Lambda\setminus(X\cup Y)}$. Let A be an observable associated with the perturbation in X, and B an observable which the observer wishes to measure in Y. We then say that A is supported by the set of lattice sites X, denoted as $\mathrm{supp}(A) = X$, and it acts non-trivially only on the Hilbert space sector $\mathscr{H}_X$ i.e. $A = A \otimes \mathbb{1}_Y \otimes \mathbb{1}_{\Lambda\setminus(X\cup Y)}$. Similarly B, with $\mathrm{supp}(B) = Y$, acts non-trivially only on $\mathscr{H}_Y$ so that $B = \mathbb{1}_X \otimes B \otimes \mathbb{1}_{\Lambda\setminus(X\cup Y)}$. The two observables thus act on disjoint Hilbert space sectors at $t = 0$, from which follows that[2]

$$\|[A, B]\| = 0. \tag{4.1.1}$$

The converse is investigated in Lemma 3.1 of [40] which states[3]

Lemma 4.1.1 *Let $\mathscr{H}_1$ and $\mathscr{H}_2$ be Hilbert spaces, $A \in \mathcal{B}(\mathscr{H}_1 \otimes \mathscr{H}_2)$ and suppose there exists $\epsilon \geq 0$ such that*

$$\|[A, \mathbb{1} \otimes B]\| \leq \epsilon \|B\| \text{ for all } B \in \mathcal{B}(\mathscr{H}_2). \tag{4.1.2}$$

[2] Here $\|\cdot\|$ denotes the usual operator norm, of which a formal treatment can be found in [39], and we summarise some useful properties at the end of this subsection.

[3] We use $\mathcal{B}(\mathscr{H})$ to denote the set of bounded linear operators acting on Hilbert space $\mathscr{H}$.

Then, there exists an operator $A' \in \mathcal{B}(\mathscr{H}_1)$ *such that*

$$\|A' \otimes \mathbb{1} - A\| \leq \epsilon. \tag{4.1.3}$$

For a proof see [40]. From the lemma one can conclude that if $A \in \mathcal{B}(\mathscr{H}_\Lambda)$ and $B \in \mathcal{B}(\mathscr{H}_Y)$ nearly commute, A is approximately supported in $\Lambda \setminus Y$. Commutator norms thus quantify the extent to which the supports of two given observables overlap.

This is applicable in our work of Sec. 4.1.2 and 4.1.3, where we will encounter commutators in which one observable has undergone non-trivial dynamics in the Heisenberg picture i.e. $A(t) = e^{iHt}Ae^{-iHt}$ where H is the system Hamiltonian acting on $\mathscr{H}_\Lambda$. In such cases the commutator norm $\|[A(t), B]\|$ reduces to (4.1.1) for $t = 0$, but is non-vanishing in general; The interactions described by H will couple lattice sites within X to others in $X^c = (\Lambda \setminus X) \supset Y$ so that $A(t)$ acts on the entire Hilbert space $\mathscr{H}_\Lambda$ for $t > 0$ (assuming $[A, H] \neq 0$). Intuition then suggests that $\|[A(t), B]\|$ varies in time as the system interactions propagate the initial perturbation of X further into the remaining lattice X^c.

The original work of Lieb and Robinson [38] showed that in lattice systems with finite range or exponentially decaying interactions,

$$\|[A(t), B]\| \leq b_{LR}(t, r) = C_{lr}e^{(vt-r)/\xi}, \tag{4.1.4}$$

where $r = d(X, Y) > 0$. $C_{lr}, v, \xi > 0$ are constants defined in terms of the norms of operators A and B, as well as the size of their support, and the system interactions. These constants are independent of the lattice size $|\Lambda|$, so that (4.1.4) is valid for thermodynamically large systems. Considering coordinates (r, t) for which the bound $b_{LR}(t, r)$ is larger than some value $\kappa > 0$ defines an effective causal cone, outside of which the bound becomes negligibly small. This causal region, shown schematically in Fig. 4.1.1, is bounded by a linear relation between space and time

$$vt > r + \xi \ln(\kappa/C_{lr}), \tag{4.1.5}$$

analogous to the light-cone of relativistic theories. The gradient $1/v$ of the causal region's boundary places an upper limit on the speed at which perturbations may spread in the lattice Λ. Therefore, the bound $b_{LR}(t, r)$—and hence the commutator $\|[A(t), B]\|$—becomes negligible for all coordinates satisfying $r > vt$. Said differently, the group velocity V_g of lattice excitations is bounded from above by the rate v at which the bound (4.1.4) grows (exponentially) in time. The Lieb-Robinson bound (4.1.4) then tells us that for finite range or exponentially decaying interactions, the supports of $A(t)$ and B have negligible overlap for all times $t > 0$ for which $vt < r$ i.e. the initial perturbation, confined to X at $t = 0$, spreads with a constant maximum (interaction dependent) velocity $V_g < v$ and therefore reaches Y at $t = r/v$ at the earliest.

The work of Lieb and Robinson was extended in 2006 by Hastings and Koma [41] to lattices in which the interactions are long-ranged and decay only algebraically with distance as $1/r^{\alpha}$. Their work showed that for power laws satisfying $\alpha > D$, where D is the lattice dimension, the bound of (4.1.4) must be replaced by

$$b_{HK}(t,r) = C_{hk}\frac{e^{vt}-1}{(1+r)^{\alpha}}. \tag{4.1.6}$$

This bound decays only algebraically in space, as opposed to the exponential decay of (4.1.4). This reflects the intuition that long-range interactions transmit perturbations across greater distances in smaller time intervals. Considering again space-time coordinates (r,t) for which $b_{HK}(t,r) > \kappa$, we find a causal region which grows logarithmically for large distances r

$$vt > \ln\left[1+\frac{\kappa}{C_{hk}}(1+r)^{\alpha}\right]. \tag{4.1.7}$$

A schematic plot is shown in Fig. 4.1.1. As a result of the sub-linear growth of this logarithmic light-cone, the causal region in which $b_{HK}(t,r)$ is non-negligible, cannot be bounded by a linear space-time relation $t \sim r/v$. The implication is that, at least according to the bound, excitations may spread through the lattice faster as time t progresses i.e. (4.1.6) implies that the concept of a group velocity may not even be well defined [42]. Furthermore, the shape of light cone (4.1.7) remains logarithmic as $\alpha \to \infty$. The Hastings-Koma bound does thus not recover the result of Lieb and Robinson in the limit of nearest-neighbour interactions.

Foss-Feig *et al.* [43] recently refined the result of Hastings and Koma. For interactions with an algebraic decay satisfying $\alpha > 2D$, they showed that the causal region is bounded by a power law

$$t = r^{\zeta}, \text{where } 1/\zeta = 1 + (1+D)/(\alpha - 2D), \tag{4.1.8}$$

in the asymptotic regime of large distances r and times t (see Fig. 4.1.1). Whilst this polynomial light-cone still predicts an increasing group velocity, it places tighter constraints on its growth than the logarithmic light-cone of Hastings and Koma. Moreover, (4.1.8) recovers the linear light cone (4.1.4) of Lieb and Robinson in the limit of finite-range interactions $\alpha \to \infty$.

The choice of Lieb-Robinson bound when bounding commutator norms $\|[A(t),B]\|$ is thus not unique, but depends on the range of interactions present in the system under study, and these can vary from short-range (nearest neighbour, exponentially decaying) to long-range (algebraically decaying). Furthermore, in the case of long-range interactions, the bounds can be optimised (decreased) for specific regions in space-time, as shown by Foss-Feig and collaborators.

In Sec. 4.1.2 we deal with lattice systems fabricated in quantum gas microscopes which exhibit long-range interactions with $\alpha = 6$, and so the bound of Foss-Feig

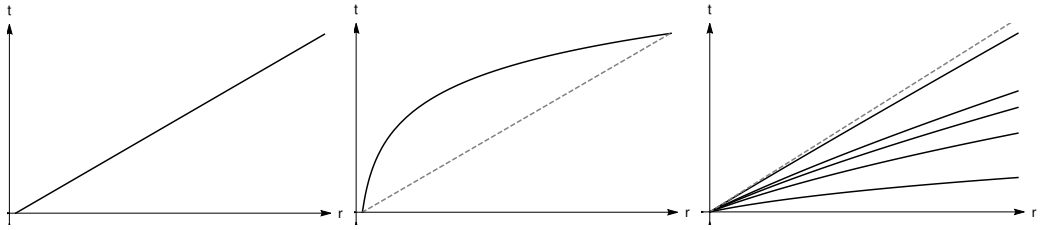

Figure 4.1.1: Schematic drawings of light-cone boundaries for various Lieb-Robinson bounds. Causal regions are restricted to the area above the curves in each plot. Outside of this causal region, for a fixed time t, the bounds decay exponentially or algebraically fast with increasing distance r. Left: For finite range, or exponentially decaying interactions, the original bound of Lieb and Robinson predicts a linear light cone boundary $t \sim r$ (4.1.5). Center: For long-range interactions decaying like a power law $r^{-\alpha}$ with $\alpha > D$, Hastings and Koma derived a bound which results in a logarithmic light cone $t \sim \log r$ (4.1.7). The dashed line indicates that no linear curve can bound the resulting causal region, so that the concept of a finite group velocity breaks down. Right: For the same long-range interactions, but with $\alpha > 2D$, Foss-Feig *et al.* showed that the causal region is bounded by a power-law $t \sim r^{\zeta}$ (4.1.8). For increasing α (solid lines from bottom to top), the power-law becomes increasingly linear (dashed line). In the limit $\alpha \to \infty$, where $r^{-\alpha}$ interactions go over to nearest-neighbour interactions, the linear light-cone of Lieb and Robinson is recovered.

et al. is applicable. However, their bound is restricted to single-site observables $A = A_i$, $B = B_j$ for lattice sites $i, j \in \Lambda$. In our work we deal with commutators of multi-site observables, so that a generalisation of Foss-Feig's bound, derived by Matsuta *et al.* [44], is more useful. This bound, stated in Theorem 2.1 of Ref. [44], is as follows.

Theorem 4.1.1 *Let A and B be bounded operators with respective supports $X \subset \Lambda$ and $Y \subset \Lambda$. Let $R \geq 1$ and $r = d(X, Y)$. Then*

$$\begin{aligned} \|[A(t), B]\| \leq b(t, r) =& 2\|A\|\|B\||X|\Big(e^{vt-r/R} + 2tg(r)f(R) \\ &+ C_2|X|R(r \vee R)^D f(R)te^{vt-r/R}\Big), \end{aligned} \tag{4.1.9}$$

for any $t \geq 0$, where $r \vee R := max\{r, R\}$, and v and C_2 are positive constants independent of Λ, t, R, X, Y, A and B.

The assumptions under which (4.1.9) is valid are:

(a) The Hamiltonian of the quantum spin system on a lattice Λ is given by

$$H_\Lambda = \sum_{X \subset \Lambda} h_X, \tag{4.1.10}$$

where h_X is a bounded local Hamiltonian with support $X \subset \Lambda$.

(b) There is a decreasing function f on $[0,\infty)$, such that

$$\sup_{x\in\Lambda}\sum_{\substack{Z\ni x:\\ \mathrm{diam}(Z)\geq R}}\|h_Z\|\leq f(R),\quad R\geq 0. \tag{4.1.11}$$

Here $Z\subset\Lambda$ and $\mathrm{diam}(Z):=\max\{d(x,y)|x,y\in Z\}$.

(c) The interactions between any lattice site and the remaining lattice must have finite norm

$$\sup_{x\in\Lambda}\sum_{y\in\Lambda}\sum_{Z\ni x,y}\|h_Z\|<\infty. \tag{4.1.12}$$

(d) There is a function g which increases monotonically on $[0,\infty)$ such that

$$|\{y\in\Lambda|d(x,y)\leq r\}|\leq g(r)\leq C(1+r)^D,\ \textit{for } r\geq 0 \textit{ and } x\in\Lambda. \tag{4.1.13}$$

Here $C>0$ is a constant and D is the lattice dimension.

The set in (4.1.13) is the neighbourhood of radius r for lattice site x, and so the function $g(r)$ can be thought of as an (over)estimate of the number of neighbours of x which are not further than some distance r.

To understand the physical meaning of (4.1.11) let us assume that all interactions in H_Λ are pair interactions i.e. $h_X=0$ if $|X|>2$. This is the case for the Hamiltonian (4.1.23) used in Sec. 4.1.2 below. The summation then yields the net strength with which a given lattice site $x\in\Lambda$ interacts with all lattice sites y satisfying $r=d(x,y)\geq R$. The supremum selects the largest of these net interactions in the lattice, and bounding this by the decreasing function f ensures that all interactions over a distance $r\geq R$ decay. A given choice of the parameter $R\geq 0$ thus defines a length scale and characterises the range of the lattice interactions. Ref. [44] shows that the bound $b(\tau,r)$ given by (4.1.9) can be optimised for large distances r and times τ by letting the R scale with distance r as

$$R=r^\kappa \text{ with } \kappa=\frac{1+D}{1+\alpha-D}, \tag{4.1.14}$$

where D is the lattice dimension and α is the exponent of the algebraic long-range interactions $1/r^\alpha$. Since $\alpha>2D$, parameter $\kappa<1$ so that R scales sub-linearly with distance r. Furthermore, in the case of a D-dimensional cubic lattice (i.e. $\Lambda\subset\mathbb{Z}^D$) the $(r\vee R)^D$ term of (4.1.9) can be replaced by $(r\vee R)^{D-1}$ which leads to a tighter bound (for a proof see Appendix. B of [44]). The optimised form of (4.1.9) for a cubic lattice is then

$$b(t,r)=2\|A\|\|B\||X|\Big(e^{vt-r^\eta}+2tg(r)f(r^\kappa)+C_2|X|r^{\kappa+D-1}f(r^\kappa)te^{vt-r^\eta}\Big), \tag{4.1.15}$$

where $\eta = 1 - \kappa$ and we have used that $\max\{r, r^\kappa\} = r$. We assume from here onwards that the target system's lattice geometry is cubic, so that we may make use of the optimised bound (4.1.15). Due to the sub-linear scaling of R with distance r, the dominant spatial contribution at large distances r is the exponential decay e^{-r^η}. As a result this bound is minimised when $r \gg 1$ and t is small. In Sec. 4.1.2 below we use the Hamiltonian (4.1.23) in which the interactions decay like $1/r^6$ for large distances r i.e. $\alpha = 6$. The derivation presented there is eventually specialised to $D = 1$, but it may be adapted to $D = 2$ since this too satisfies $\alpha > 2D$. Both cases are interesting as these are the lattice dimensions simulated in ion traps and quantum gas microscopes, but we expect that the essential physics described by the Lieb-Robinson bounds is the same in either case, only with different prefactors.

Useful properties of operator norms. Let O_1, O_2 be bounded operators acting on a Hilbert space $\mathscr{H}$. We will use $O = O_1$ when dealing with only one operator, and we denote the set of eigenvalues of O by $\{o_i\}$. Its norm is denoted by $\|O\|$, and satisfies:

$$|\langle\psi| O |\psi\rangle| \leq \|O\| \text{ for any } |\psi\rangle \in \mathscr{H}, \tag{4.1.16}$$

$$\|O\| = \max_i(|o_i|) \text{ if } O^\dagger = O, \tag{4.1.17}$$

$$\|O\| = 1 \text{ if } O^\dagger = O^{-1}, \tag{4.1.18}$$

$$\|O_1 + O_2\| \leq \|O_1\| + \|O_2\|, \tag{4.1.19}$$

$$\|O_1 O_2\| \leq \|O_1\|\|O_2\|. \tag{4.1.20}$$

It is useful to think of $\|O\|$ as the largest possible factor by which O can rescale any vector $|\psi\rangle \in \mathscr{H}$.

4.1.2 Implementation of PMP in quantum gas microscopes

Recall that the PMP can be used to measure real correlation components $\mathrm{Re}\,\langle\psi| A(t_1)B(t_2) |\psi\rangle$ if the observable A has only two distinct eigenvalues of opposite sign and equal magnitude (see (B.1.4) – (B.1.7)). We will consider here single- or multi-site spin-1/2 observables with eigenvalues $\{\pm 1\}$, and we denote their supports as $\mathrm{supp}(A) = X_A$ and $\mathrm{supp}(B) = X_B$ (if $A = \sigma_i^a$, for instance, $X_A = \{i\}$). We will assume in the following derivation that the supports of A and B are disjoint i.e. $X_A \cap X_B = \varnothing$. The spectral representation of the two observables is then

$$A = \sum_{m_a = \pm 1} m_a \Pi_{X_A}^{m_a} \text{ and } B = \sum_{m_b = \pm 1} m_b \Pi_{X_B}^{m_b}, \tag{4.1.21}$$

where, for instance, $\Pi_{X_A}^{m_a}$ is the projection operator onto $\mathrm{supp}(A)$ corresponding to eigenvalue m_a of A.

In quantum gas microscopes, projectively probing a region X_A of the trapped lattice at $t_1 \geq 0$ can cause particle loss within X_A and decoherence of lattice sites neighbouring X_A (see paragraph on repeated measurements in the introduction of this chapter). This is not accounted for in our original PMP of Sec. 3.2.2 and will alter the system state beyond the expected wave function collapse. In this section we present two theoretical adaptations of the PMP which aim to mitigate these additional disturbances of the system state. The main idea in both adaptations is to decouple lattice region X_A from the remaining lattice $X_A^c = \Lambda \setminus X_A$ at t_1. This decoupling is implemented by letting the system dynamics be generated by a modified Hamiltonian H'—from which all interaction terms between X_A and X_A^c have been removed—in the time interval $[t_1, t_2]$. The projective correlation $\mathscr{C}^{\mathrm{Proj}}_{H,H'}$ obtained with these modified dynamics will, in general, differ from the correlation $\mathscr{C}^{\mathrm{Proj}}_{H} = \mathrm{Re}\, C$ of the original PMP (3.2.12). To analyse the utility of either proposal, we will bound the deviation

$$\epsilon := \left| \mathscr{C}^{\mathrm{Proj}}_{H} - \mathscr{C}^{\mathrm{Proj}}_{H,H'} \right|, \tag{4.1.22}$$

by making use of Lieb-Robinson theory.

For our analysis we will utilise for H a long-range Hamiltonian which has been generated in the QGM experiments discussed in Ref. [29]. The long range interactions are created by off-resonant "Rydberg dressing": The hyperfine state of the trapped atoms which was chosen as the $|+\rangle$ spin state is off-resonantly coupled to a Rydberg state $|r\rangle$ of the atom, thereby leading to a "dressed" state $|+\rangle + \beta\,|r\rangle$, with $\beta \ll 1$. The large electric dipole [45] of Rydberg states facilitates long-range interactions between dressed states of different atoms in the lattice, and leads to a long-range Ising Hamiltonian

$$H = \sum_{m}^{N} h_m \sigma_m^z + \frac{1}{2} \sum_{m,n:m\neq n} U_{m,n} \sigma_m^z \sigma_n^z \,, \text{ with } U_{m,n} = \frac{U_0}{1 + (d(m,n)/R_c)^6}, \tag{4.1.23}$$

in units where $\hbar = 1$. The first sum is an on-site energy term arising from the interaction between spins and a site-dependent longitudinal field h_m. In the second sum, $U_{m,n}$ is the long-range spin-spin interaction arising from the Rydberg interactions in the QGM, and $d(m,n)$ is the distance (in units of the lattice constant) between sites m and n.

The parameter R_c is a length scale arising from the Rydberg-Rydberg interactions; The strong interaction between Rydberg atoms blocks simultaneous excitation of atoms into the dressed state if they lie within a critical distance R_c of one-another (Ref. [29] reports $R_c = 2$, in units of the lattice constant). This causes the soft-core shape of $U_{m,n}$ which saturates to a strength U_0 when $d(m,n) = 0$. The division by 2 in the second sum compensates for each pair interaction being counted twice. An advantage of Rydberg dressing over other long-range platforms,

such as ultra-cold polar molecules or trapped ions, is the highly tunable range and anisotropy of the spin-spin interaction. Proving the feasibility, from a theoretical side, of our PMP (and RMP in the next section) in QGMs would thus allow for measurement of dynamic correlations in various magnetic phases for a large class of magnetic Hamiltonians, such as the 2D (an)isotropic Heisenberg spin models simulated in [46].

To model the trap lattice of the QGM we again use Λ to denote the set of all lattice sites. Each site consists of a spin-1/2 particle so that the system Hilbert space is $\mathscr{H}_S = (\mathbb{C}^2)^{\otimes N}$, where $N = |\Lambda|$. $|\psi\rangle \in \mathscr{H}_S$ denotes the initial many-body spin-state of the lattice, and the initial lattice Hamiltonian H is given by (4.1.23). Steps a to b of the PMP remain unchanged: $|\psi\rangle$ evolves to t_1 under H and the probability $P_H^{\text{Proj}}(m_a)$ of measuring eigenvalue $m_a \in \{\pm 1\}$ of A is given by (3.2.8). The subsequent post measurement state (3.2.9) is a product state

$$|\psi_{m_a}\rangle = \Pi_{X_A}^{m_a} e^{-iHt_1} |\psi\rangle / \sqrt{P_H^{\text{Proj}}(m_a)} = |\psi_{X_A}(t_1)\rangle \otimes \left|\psi_{X_A^c}(t_1)\right\rangle \in \mathscr{H}_{X_A} \otimes \mathscr{H}_{X_A^c} = \mathscr{H}_S, \tag{4.1.24}$$

with $X_A^c = \Lambda \setminus X_A$ being the set-theoretic complement of X_A.

Adaptation 1: Locally destructive PMP

In our first adaptation of the PMP we assume that any disturbances of the system state (such as decoherence and particle loss), incurred during the projective measurement at t_1, are restricted to a small region X centred on X_A i.e. $X \supset X_A$. To mitigate the effect of these disturbances during the subsequent time-evolution, we propose to decouple X from the remaining lattice at t_1. For simplicity we will let $X = X_A$, but this does not affect our results beyond the size of some prefactors.

After the projective measurement at t_1, no entanglement exists between regions X_A and X_A^c in state $|\psi_{m_a}\rangle$. These regions can thus evolve independently during the time interval $[t_1, t_2]$ under action of a "decoupled" Hamiltonian $H' = H'_{X_A} \otimes \mathbb{1}_{X_A^c} + \mathbb{1}_{X_A} \otimes H'_{X_A^c}$. Theoretically we construct H' by removing from H all those terms which couple lattice sites $k \in X_A$ to sites $l \in X_A^c$ and we assume, without loss of generality, that the observables to be correlated are single-site observables with $X_A = i$ and $X_B = j$ for any two lattice sites $i \neq j$. The modified Hamiltonian is then

$$H' = H - \sum_{n \neq i} U_{i,n} \sigma_i^z \sigma_n^z = \sum_m^N h_m \sigma_m^z + \frac{1}{2} \sum_{\substack{m,n \neq i: \\ m \neq n}} U_{m,n} \sigma_m^z \sigma_n^z = H'_{X_A} \otimes \mathbb{1}_{X_A^c} + \mathbb{1}_{X_A} \otimes H'_{X_A^c}, \tag{4.1.25}$$

and this preserves the product structure of the post-measurement state (4.1.24) during the time interval $[t_1, t_2]$.

Calculating $\mathscr{C}^{\mathbf{Proj}}_{H,H'}$. The post measurement state (4.1.24) evolves from t_1 to t_2 with dynamics generated by H' (4.1.25). At t_2 we projectively measure observable B. The probability that this measurement yields eigenvalue $m_b \in \{\pm 1\}$ of B is

$$P^{\text{Proj}}_{H,H'}(m_b|m_a) = \langle\psi| e^{iHt_1}\Pi_i^{m_a} e^{iH'(t_2-t_1)}\Pi_j^{m_b} e^{-iH'(t_2-t_1)}\Pi_i^{m_a} e^{-iHt_1} |\psi\rangle / P^{\text{Proj}}_H(m_a). \tag{4.1.26}$$

This differs from the conditional probability of the original PMP (3.2.11) due to the modified dynamics in the time interval $[t_1, t_2]$. To distinguish the Heisenberg time evolution of an operator O under H or H', we use $O(t,H) = e^{iHt}Oe^{-iHt}$ and $O(t,H') = e^{iH't}Oe^{-iH't}$. The modified projective correlation can then be expressed as

$$\begin{aligned}\mathscr{C}^{\text{Proj}}_{H,H'} &= \sum_{m_a,m_b} m_a m_b P^{\text{Proj}}_H(m_a) P^{\text{Proj}}_{H,H'}(m_b|m_a) \\ &= \sum_{m_a} m_a \langle\psi| \Pi_i^{m_a}(t_1,H) e^{iHt_1} B(\Delta t, H') e^{-iHt_1} \Pi_i^{m_a}(t_1,H) |\psi\rangle ,\end{aligned} \tag{4.1.27}$$

where $\Delta t = t_2 - t_1$ and we have used the spectral representation of B (4.1.21).

Compare $\mathscr{C}^{\mathbf{Proj}}_{H,H'}$ and $\mathscr{C}^{\mathbf{Proj}}_{H}$. The deviation ϵ of the modified correlation $\mathscr{C}^{\text{Proj}}_{H,H'}$ from $\mathscr{C}^{\text{Proj}}_{H}$ (B.0.3) is obtained by substituting (B.0.3) and (4.1.27) into (4.1.22)

$$\begin{aligned}\epsilon = \Bigg| &\sum_{m_a} m_a \langle\psi| \Pi_i^{m_a}(t_1,H) \left(e^{iHt_1} B(\Delta t, H) e^{-iHt_1} - e^{iHt_1} B(\Delta t, H') e^{-iHt_1}\right) \\ &\times \Pi_i^{m_a}(t_1,H) |\psi\rangle \Bigg|.\end{aligned} \tag{4.1.28}$$

Whilst an exact calculation of (4.1.28) may be possible, it requires choosing a specific system state $|\psi\rangle$ so that the result would be applicable to only this state. To obtain a result which is valid for any initial state $|\psi\rangle$, we make use of operator norms to eliminate dependence of the bound on $|\psi\rangle$. Using the triangle inequality and $|m_a| = 1$ we obtain

$$\epsilon \leq \sum_{m_a} \left| \langle\psi| \Pi_i^{m_a}(t_1,H) \Big(e^{iHt_1} B(\Delta t, H) e^{-iHt_1} - e^{iHt_1} B(\Delta t, H') e^{-iHt_1}\Big) \Pi_i^{m_a}(t_1,H) |\psi\rangle \right|. \tag{4.1.29}$$

The operator norm properties listed at the end of Sec. 4.1.1 allows us to further bound this as

$$\begin{aligned}\epsilon &\leq \sum_{m_a} \|\Pi_i^{m_a}(t_1,H)\|^2 \|e^{iHt_1} \left(B(\Delta t, H) - B(\Delta t, H')\right) e^{-iHt_1}\| \\ &\leq 2\|B(\Delta t, H') - B(\Delta t, H)\|.\end{aligned} \tag{4.1.30}$$

As desired, this error bound is independent of the initial system state. It depends only on the difference of the Heisenberg representation of B—the observable to be projectively probed at t_2—under dynamics generated by H and H', respectively.

As shown in Eq. (11) of Ref. [47], $\|B(\Delta t, H) - B(\Delta t, H')\|$ can be upper bounded by a temporal integral over commutator norms

$$\begin{aligned} \|B(\Delta t, H') - B(\Delta t, H)\| &= \|e^{-iH\Delta t} B(\Delta t, H') e^{iH\Delta t} - B\| \\ &= \left\| \int_0^{\Delta t} d\tau \frac{d}{d\tau} e^{-iH\tau} B(\tau, H') e^{iH\tau} \right\| \\ &= \left\| \int_0^{\Delta t} d\tau e^{-iH\tau} \left[H - H', B(\tau, H') \right] e^{iH\tau} \right\| \\ &\leq \int_0^{\Delta t} d\tau \left\| [H - H', B(\tau, H')] \right\| . \end{aligned} \tag{4.1.31}$$

The third line results from application of the product rule, and the inequality follows from the triangle inequality and property (4.1.18). The error ϵ is therefore bounded as

$$\epsilon \leq 2 \int_0^{\Delta t} d\tau \left\| [H - H', B(\tau, H')] \right\| . \tag{4.1.32}$$

The integration variable τ is the the time elapsed between the projective measurement of observable A at t_1, and of observable B at t_2.

Substituting Hamiltonians H and H'. The Hamiltonians H and H', occurring in bound (4.1.32), are respectively defined in (4.1.23) and (4.1.25). From these definitions, it follows that $H - H' = \sum_{n \neq i}^{N} U_{i,n} \sigma_i^z \sigma_n^z$ and so (4.1.32) becomes

$$\epsilon \leq 2 \int_0^{\Delta t} d\tau \sum_{n \neq i} \| [B(\tau, H'), U_{i,n} \sigma_i^z \sigma_n^z] \| = 2U_0 \int_0^{\Delta t} d\tau \sum_{n \neq i} \frac{\| [B(\tau, H'), \sigma_i^z \sigma_n^z] \|}{1 + (d(i,n)/R_c)^6} . \tag{4.1.33}$$

For a given elapsed time $\tau \in [0, \Delta t]$, the commutator norm $\| [B(\tau, H'), U_{i,n}] \|$ quantifies the extent to which the decoupled dynamics have spread the support of B throughout the lattice, to include regions which were coupled to site i at t_1 via the long-range interactions $U_{i,n}$ (see the discussion of Sec. 4.1.1).

Bounding ϵ with Lieb-Robinson bounds. We now approximate the commutator norms in error bound (4.1.33) using the Lieb-Robinson theory reviewed in Sec. 4.1.1. For a given Lieb-Robinson bound $b(\tau, r)$, r is the minimum separation of the supports of the operators appearing in the commutator which is to be bounded. For the commutators in (4.1.33) we have $\text{supp}(B) = \{j\}$ and $\text{supp}(\sigma_i^z \sigma_n^z) = \{i, n\}$ so that

$$r = \min(d(j,i), d(j,n)) = \min(\rho, d(j,n)). \tag{4.1.34}$$

Those commutators for which $r = \rho$ will be bounded by a Lieb-Robinson bound $b(\tau, \rho)$ which is independent of the summation index n. Therefore, the spatial summation of (4.1.33) is split into two disjoint domains

$$\begin{aligned} r = \rho \text{ when } n \in D_1 &= \{n \in \Lambda : n \neq i \text{ and } d(j,n) \geq \rho\} \\ r = d(j,n) \text{ when } n \in D_2 &= \{n \in \Lambda : d(j,n) < \rho\}. \end{aligned} \tag{4.1.35}$$

Splitting the sum in (4.1.33) according to these two domains, we obtain

$$\epsilon \leq 2U_0 \int_0^{\Delta t} d\tau \left(b(\tau,\rho) \sum_{n \in D_1} \frac{1}{1 + (d(i,n)/R_c)^6} + \sum_{n \in D_2} \frac{b(\tau, r)}{1 + (d(i,n)/R_c)^6} \right). \tag{4.1.36}$$

To simplify our derivation we now assume that the lattice Λ is one-dimensional (further results are therefore also applicable to linear ion traps) i.e. $D = 1$. Suppose that lattice site i is situated to the left of site j, i.e. $i < j$. We then have $\rho = |i - j|$ and $d(i,n) = |i - n|$ in units of the lattice constant. Domain D_1 then lies to the left and right of D_2, and the error bound (4.1.36) can be written as

$$\epsilon \leq E(\Delta t, \rho) := 2U_0 \Big(\beta(\Delta t, \rho) \Big(\sum_{m=1}^{\infty} + \sum_{m=2\rho}^{\infty} \Big) \frac{1}{1 + (m/R_c)^6} + \sum_{m=1}^{2\rho-1} \frac{\beta(\Delta t, |\rho - m|)}{1 + (m/R_c)^6} \Big), \tag{4.1.37}$$

where $\beta(\Delta t, r) := \int_0^{\Delta t} d\tau b(\tau, r)$. The first two summations stem from the sum over D_1 in (4.1.36) and the third summation is over D_2. We have rewritten all distances occurring in these summations in terms of $m = |i - n|$.

Using the Lieb-Robinson bound of Matsuta *et al.* [44]. For the long-range interactions $U_{i,n}\sigma_i^z \sigma_n^z$ of Hamiltonians H (4.1.23) and H' (4.1.25), an appropriate choice for $b(\tau, r)$ is the Lieb-Robinson bound (4.1.15) of Ref. [44]. Recall that this bound has been optimised for a cubic lattice Λ (in our case of dimension $D = 1$), and large distances r (see discussion following Eq. (4.1.8) in Sec. 4.1.1). The temporal integral of this bound [defined beneath Eq. (4.1.37)] is

$$\begin{aligned} \beta(\Delta t, r) = 2\|B\| \Bigg(& \frac{1}{v} \left(e^{v\Delta t} - 1 \right) e^{-r^\eta} + 2g(r) f(r^\kappa) \Delta t \\ & + C_2 r^\kappa f(r^\kappa) \frac{1}{v^2} \left(e^{v\Delta t} (v\Delta t - 1) + 1 \right) e^{-r^\eta} \Bigg), \end{aligned} \tag{4.1.38}$$

where we have used $|X_B| = 1$, and $\|\sigma_i^z \sigma_n^z\| = 1$. Our choice for the functions $g(r)$ and $f(R)$ is discussed in Appendix. C [see Eqs. (C.0.1) – (C.0.4)]. Substituting this time-integrated optimised Lieb-Robinson bound into (4.1.37) we find that the overall error bound becomes

$$\begin{aligned}\frac{E(\Delta t,\rho)}{4\|B\|U_0} =& \frac{e^{v\Delta t}-1}{v}\left[e^{-\rho^\eta}\left(s(1)+s(2\rho)\right)+\sum_{m=1}^{\rho}\frac{e^{-(\rho-m)^\eta}}{1+(m/R_c)^6}+\sum_{m=\rho+1}^{2\rho-1}\frac{e^{-(m-\rho)^\eta}}{1+(m/R_c)^6}\right]\\ &+2\Delta t\left[g(\rho)f(\rho^\kappa)\left(s(1)+s(2\rho)\right)+\sum_{m=1}^{\rho}\frac{g(\rho-m)f((\rho-m)^\kappa)}{1+(m/R_c)^6}\right.\\ &\left.+\sum_{m=\rho+1}^{2\rho-1}\frac{g(m-\rho)f((m-\rho)^\kappa)}{1+(m/R_c)^6}\right]+\frac{C_2}{v^2}\left(e^{v\Delta t}(v\Delta t-1)+1\right)\left[\rho^\kappa\right.\\ &\times f(\rho^\kappa)e^{-\rho^\eta}\left(s(1)+s(2\rho)\right)+\sum_{m=1}^{\rho}\frac{(\rho-m)^\kappa f((\rho-m)^\kappa)e^{-(\rho-m)^\eta}}{1+(m/R_c)^6}\\ &\left.+\sum_{m=\rho+1}^{2\rho-1}\frac{(m-\rho)^\kappa f((m-\rho)^\kappa)e^{-(m-\rho)^\eta}}{1+(m/R_c)^6}\right].\end{aligned} \tag{4.1.39}$$

Here $\kappa=(1+D)/(1+\alpha-D)=2/6$, $\eta=1-\kappa=4/6$ since $D=1$ and $\alpha=6$. The physics of (4.1.39) is to be understood as follows: The three square brackets correspond to the three terms of the temporally integrated Lieb-Robinson bound (LRB) (4.1.38). The temporal dependence is captured by the prefactors of the bracketed expressions. In the limit of large time intervals $\Delta t=t_2-t_1$, these prefactors show that, for a fixed ρ, the overall error bound grows exponentially. The rate of this exponential growth is determined by the constant v. The spatial dependence of (4.1.39) is captured by the terms within the square brackets. These terms stem from the spatial dependence of the LRB (4.1.38) and from the long-range interactions $U_{i,n}$. The spatial contribution from the LRB is constant within domain D_1, so that the corresponding summation depends only on the algebraic decay of the long-range interactions and is summarised in (4.1.39) by $s(1)+s(2\rho)$, where

$$s(a)=\sum_{m=a}^{\infty}\frac{1}{1+(m/R_c)^6}. \tag{4.1.40}$$

In (4.1.39), the explicitly shown sums are those which run over domain D_2 and have been split into two physically distinct[4] parts

$$\begin{aligned}D_2 = d_1\cup d_2 \ \text{ satisfying } d_1\cap d_2=\varnothing,\\ \text{with } d_1=\{n\in D_2 : i<n\le j\} \text{ and } d_2=\{n\in D_2 : j<n\}.\end{aligned} \tag{4.1.41}$$

Within d_1, where $m=|i-n|\in[1,\rho]$, the spatial contributions of the long-range interactions and the LRB compete: For lattice sites close to i (i.e. summation index m close to 1) the algebraic terms are large and the exponential contribution

[4] This is also true for higher dimensions.

from the LRB is small. As one moves further from i and towards j, the algebraic interaction terms decay, but the exponential term of the LRB grows. This exponential contribution is large for lattice sites close to j (m close to ρ). Sub-domain d_2 contains all lattice sites in D_2 which lie to the right of j, so that the summation runs over $m \in [\rho+1, 2\rho-1]$. Within d_2, both the algebraic and the exponential terms decay as m increases. This reflects the fact that one moves further from both lattice sites i and j.

A trivial bound for ϵ. Instead of using Lieb-Robinson bounds to approximate bound (4.1.33), one can derive a trivial bound as follows. Since Pauli matrices and unitary matrices have unit norm, the commutator norm in (4.1.33) satisfies

$$\|[B(\tau, H'), \sigma_i^z \sigma_n^z]\| \leq 2\|B\|, \text{ for all } n \in \Lambda \text{ and any } \tau \in [0, \Delta t]. \tag{4.1.42}$$

We have used operator norm properties (4.1.17) – (4.1.20). Eq. (4.1.42) is independent of τ. The temporal integral in (4.1.33) therefore becomes trivial upon substituting (4.1.42) into (4.1.33)

$$\epsilon \leq \tilde{E}(\Delta t) := 4U_0\|B\|\Delta t \sum_{n \neq i} (1 + (d(i,n)/R_c)^6)^{-1}. \tag{4.1.43}$$

Compare $E(\Delta t, \rho)$ and $\tilde{E}(\Delta t)$. The simplicity of the trivial bound (4.1.43) for the error ϵ (4.1.28) is appealing. Moreover, $\tilde{E}(\Delta t)$ reflects the algebraic decay of the long-range interactions between $\text{supp}(A) = \{i\}$ and the remaining lattice. However, it neglects the temporal dependence of $\text{supp}(B(\tau, H'))$, and is independent of $\rho = d(X_A, X_B)$. As a result $\tilde{E}(\Delta t)$ predicts a constant error regardless of how far apart the supports of the correlated observables are. We thus expect that (4.1.43) is a very loose bound of ϵ for large separations ρ, and some domain of Δt values.

In contrast, error bound $E(\Delta t, \rho)$ (4.1.39) is optimised for large distances ρ and long times Δt (since we used the optimised Lieb-Robinson bound (4.1.38) for its derivation). Both $\tilde{E}(\Delta t)$ and $E(\Delta t, \rho)$ are suitable for numeric calculations, and Fig. 4.1.2 shows a comparison of the two error bounds. The figure shows contour plots of $\min(E(\Delta t, \rho), \tilde{E}(\Delta t))$ for a range of $(\rho, \Delta t)$ coordinates. Plotting this minimum value takes into account that the trivial bound $\tilde{E}(\Delta t)$ may perform better than $E(\Delta t, \rho)$ at short times and distances. All parameters appearing in E and $\tilde{E}$ have been set to 1, so the comparison is purely qualitative[5]. The plots show that in the asymptotic region of large distances and times, $E(\Delta t, \rho)$ is superior to (tighter than) the trivial error bound, whilst at early times and short distances the trivial bound performs better.

[5]Moreover, for a true quantitative comparison of $\mathscr{C}_H^{\text{Proj}}$ and $\mathscr{C}_{H,H'}^{\text{Proj}}$ one should consider the relative errors $E(\Delta t, \rho)/|\mathscr{C}_H^{\text{Proj}}|$ and $\tilde{E}(\Delta t)/|\mathscr{C}_H^{\text{Proj}}|$.

Recall that $\Delta t = t_2 - t_1$ is the time elapsed in our projective measurement protocol (PMP) between measurements of site i (at t_1) and j (at t_2). In the modification discussed in this section, the lattice experiences modified dynamics within time interval $[t_1, t_2]$, under a decoupled Hamiltonian H' (4.1.25). This leads to the error $\epsilon = |\mathscr{C}_H^{\mathrm{Proj}} - \mathscr{C}_{H,H'}^{\mathrm{Proj}}|$ which is bounded by (4.1.39). The plotted data shows that this error can be suppressed by choosing to measure correlations $C = \langle\psi| A(t_1)B(t_2) |\psi\rangle$ which correspond to space-time coordinates $(\rho, \Delta t)$ lying outside of the light cone (white area) defined by the contours in Fig. 4.1.2. In a given experiment there are two relevant scenarios: The duration of time between repeated measurements may be bounded from below (depending on the details of the experimental set-up e.g. response times of lasers) so that to suppress the error ϵ one must choose to correlate lattice sites i and j separated by a large distance ρ. Conversely, if the number of trapped particles does not allow for large separations ρ (as is the case in typical ion trap experiments), the error bound (4.1.37) can be used to determine the time durations Δt for which the incurred error remains below a desired threshold.

Error bound (4.1.39) and the corresponding plots in Fig. 4.1.2 provide a proof of principle. We may conclude that the correlation $\mathscr{C}_{H,H'}^{\mathrm{Proj}}$ obtained from the modified projective protocol, can in principle be used to approximate $\mathscr{C}_H^{\mathrm{Proj}} = \mathrm{Re}\, C$. The precision of this approximation is limited only by the domain of $(\rho, \Delta t)$ which is experimentally accessible. To use (4.1.39) quantitatively in a given experimental set-up, one must use the exact values of the constants appearing in the definition of the Lieb-Robinson bound (4.1.15). These are known in principle, or can be measured separately.

Adaptation 2: PMP with decoupling and deferral of measurements

The second adaptation of the PMP seeks to delay any destructive effects arising from particle loss or decoherence resulting from a projective measurement at t_1. The idea is similar to the deferred measurement approach of Sec. 2.3.2: At t_1 the lattice region $X_A = \mathrm{supp}(A)$ is not immediately measured (in contrast to the original PMP and the first adaptation of Sec. 4.1.2). Instead, X_A is decoupled from the remaining lattice at t_1 and its measurement is deferred to t_2, where $X_B = \mathrm{supp}(B)$ is probed. Both measurements are thus performed simultaneously, and any detrimental effects arising from these measurements are of no concern.

To model the decoupling of X_A at t_1 we again let the lattice evolve from t_1 to t_2 under a decoupled Hamiltonian H'. Since no measurement is performed at the early times, the system state will in general not be a product state at t_1 (in contrast to the adaptation of Sec. 4.1.2). Therefore, although regions X_A and X_A^c undergo decoupled dynamics under H' for $t > t_1$, there is no guarantee that the spins in X_A evolve independently from those in X_A^c for $t > t_1$: Time evolution generated by H during $0 \leq t \leq t_1$ will in general entangle spins in X_A and X_A^c with one-another. Dynamics of spins in X_A^c, generated by H' during $[t_1, t_2]$, will thus influence spins

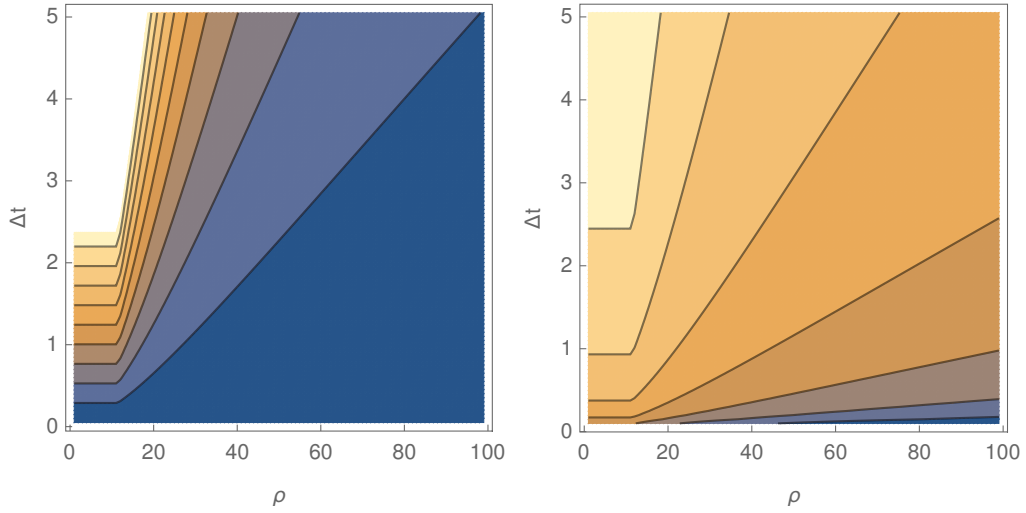

Figure 4.1.2: Left: Contour plot of $\min(\tilde{E}(\Delta t), E(\Delta t, \rho))$ for $\Delta t = t_2 - t_1 \in [0, 5]$ and $\rho = |i - j| \in [2, 100]$. Right: Contour plot of $\min(\log(\tilde{E}(\Delta t)), \log((E(\Delta t, \rho)))$ over the same domain of space-time points. All parameters were set to one, except for $\alpha = 6$. The various spatial sums of $\tilde{E}(\Delta t)$ (4.1.43) and $E(\Delta t, \rho)$ (4.1.39) were numerically evaluated. Horizontal contours in either plot are attributed to the trivial bound $\tilde{E}$, which is constant for varying ρ. The colour scales for either plot are not the same, but darker colours represent smaller values in both cases. In the regime of large Δt and ρ, the contours show that for a given value of Δt, the error bound decreases as ρ increases. Conversely, for a fixed value of ρ, the error bound remains under a given threshold value (represented by the contours) for a limited amount of time Δt, growing exponentially thereafter.

in X_A, and vice versa. We therefore expect that the deviation of $\mathscr{C}^{\text{Proj}}_{H,H'}$ from $\mathscr{C}^{\text{Proj}}_{H}$ will be larger than in the first adaptation of the PMP.

Much of the following error analysis is similar to that of Sec. 4.1.2 and the goal is again to bound ϵ (4.1.22) by commutator norms, which can be further approximated with Lieb-Robinson bounds. We therefore discuss only the pertinent differences to the error derivation of Sec. 4.1.2 and App. C.

Since X_A and X_B are probed simultaneously, we deal with joint probabilities instead of conditional ones. At t_2 the probability of measuring eigenvalues m_a and m_b of A and B is

$$P^{\text{Proj}}_{H,H'}(m_a, m_b) = \langle\psi| e^{iHt_1} e^{iH'(t_2-t_1)} \left(\Pi^{m_a}_{X_A} \otimes \Pi^{m_b}_{X_B}\right) e^{-iH'(t_2-t_1)} e^{-iHt_1} |\psi\rangle\,, \quad (4.1.44)$$

from which the modified correlation follows

$$\begin{aligned} \mathscr{C}^{\text{Proj}}_{H,H'} &:= \sum_{m_a, m_b \in \{\pm 1\}} m_a m_b P^{\text{Proj}}_{H,H'}(m_a, m_b) \\ &= \sum_{m_a \in \{\pm 1\}} m_a \langle\psi| e^{iHt_1} e^{iH'(t_2-t_1)} \left(\Pi^{m_a}_{X_A} \otimes B\right) e^{-iH'(t_2-t_1)} e^{-iHt_1} |\psi\rangle\,. \end{aligned} \quad (4.1.45)$$

At this point it is necessary to discuss how the system Hamiltonian is modified at t_1. Our only requirement is that H' does not contain any interactions between spins $m \in X_A$ with spins $n \in X_A^c$. A simple option is to impose trivial (in the theoretical sense of the word) dynamics on X_A. The corresponding modified Hamiltonian is

$$H'_{\text{triv}} := \mathbb{1}_{X_A} \otimes H_{X_A^c} \tag{4.1.46}$$

In this case $\left[e^{iH'(t_2-t_1)}, \Pi_{X_A}^{m_a}\right] = 0$, and (4.1.45) is identical to the modified correlation of Adaptation 1 (4.1.27). Therefore, with $X_A = \{i\}$ and $X_B = \{j\}$, the deviation from the desired correlation component is bounded by $E(\Delta t, \rho)$ (4.1.37).

To model a more general scenario in which spins within X_A still interact with one-another and/or an external field, we use (4.1.25) for H'. This leads to a non-trivial commutator $\hat{c}(m_a, \Delta t) := \left[e^{iH'\Delta t}, \Pi_{X_A}^{m_a}\right]$, so that (4.1.45) is not equal to (4.1.27). In this case the error ϵ (obtained by substituting (4.1.27) and (4.1.45) into (4.1.22)) is bounded by

$$\begin{aligned}
\epsilon =& \left| \mathscr{C}_H^{\text{Proj}} - \mathscr{C}_{H,H'}^{\text{Proj}} \right| \\
\leq & \sum_{m_a \in \{\pm 1\}} \Big\| m_a e^{iHt_1} \Pi_{X_A}^{m_a} e^{iH(t_2-t_1)} B e^{-iH(t_2-t_1)} \Pi_{X_A}^{m_a} e^{-iHt_1} \\
& - m_a e^{iHt_1} e^{iH'(t_2-t_1)} \left(\Pi_{X_A}^{m_a} \otimes B\right) e^{-iH'(t_2-t_1)} e^{-iHt_1} \Big\| \\
\leq & \sum_{m_a \in \{\pm 1\}} \|\Pi_{X_A}^{m_a}(t_1, H)\|^2 \|B(\Delta t, H) - B(\Delta t, H')\| \\
& + \sum_{m_a \in \{\pm 1\}} \left(\|\Pi_{X_A}^{m_a} e^{iH'\Delta t} B \hat{c}^\dagger + \text{h.c}\| + \|\hat{c} B \hat{c}^\dagger\| \right) \\
\leq & E'(\Delta t, \rho) := E(\Delta t, \rho) + \sum_{m_a \in \{\pm 1\}} \left(\|\Pi_{X_A}^{m_a} e^{iH'\Delta t} B \hat{c}^\dagger + \text{h.c}\| + \|\hat{c} B \hat{c}^\dagger\| \right).
\end{aligned} \tag{4.1.47}$$

In the third line we have used the triangle inequality and the definition of $\hat{c}$. The first summation matches (4.1.30) and can therefore be approximated by (4.1.37), as indicated by the last line of (4.1.47). The additional terms in the last line show that the error incurred in this adaptation of the PMP is in general larger than that of the first adaptation discussed in Sec. 4.1.2.

Since $E'(\Delta t, \rho) > E(\Delta t, \rho)$ for all Δt and ρ, we conclude that Adaptation 1 of Sec. 4.1.2 is superior to the second adaptation proposed in this section. This is interesting because in the current adaptation no projection is performed at t_1, and intuition would suggest that decoupling X_A from the remaining lattice is less disturbing than subjecting the lattice to particle loss and/or decoherence (as is the case in Adaptation 1). A possible reason why Adaptation 1 leads to smaller errors ϵ, is that the projective measurement at the early time t_1 destroys any entanglement between the supports of the observables to be correlated, i.e. at t_1 X_A

and $X_A^c \supset X_B$ are decoupled. This also occurs in the original PMP, for which $\mathscr{C}_H^{\mathrm{Proj}} = \mathrm{Re}\, C$. Comparing the two adaptations discussed in this section, the modified system dynamics of Adaptation 2 therefore deviate more from those of the original PMP.

4.1.3 Imperfect implementation of the RMP

In section 3.2.1 we showed that $\mathrm{Im}\,[C]$—where C is a dynamic correlation of single-site spin-1/2 observables—could be measured by replacing the ancilla-based measurement of the NIMP at t_1 with a rotation of the ith lattice spin. The imaginary component was then constructed from the difference of two expectation values of $S_j^b(t_2)$ with respect to this rotated state [one obtained with angle $\theta_1 = \theta \in [-\pi, \pi)$ and the other with $\theta_2 = -\theta$, as shown in (3.2.3)]. In this section we will consider the experimentally relevant question of how well this protocol works when there is an inaccuracy in the rotation angles θ_1, θ_2. The following derivation is applicable to quantum gas microscopes and linear ion traps (and any other platforms simulating spin lattices).

Adapting our notation from (3.2.2), let us denote the two expectation values in result (3.2.3) as

$$E_{\theta_m} = (\langle 1\rangle - \langle 2\rangle)\cos^2(\theta_m/2) + \langle 2\rangle - \frac{1}{2}\mathrm{Im}\,[C]\sin(\theta_m), \text{ for } m = 1, 2. \tag{4.1.48}$$

Here we have used $\sin^2 x = 1 - \cos^2 x$, $\langle 1\rangle = \langle \sigma_j^b(t_2)\rangle_\psi$ and $\langle 2\rangle = \langle \sigma_i^a(t_1)\sigma_j^b(t_2)\sigma_i^a(t_1)\rangle_\psi$. Using this notation with $\theta_1 = \theta$ and $\theta_2 = -\theta$, Eq. (3.2.3) becomes

$$\Delta E = E_{\theta_2} - E_{\theta_1} = \mathrm{Im}\,[C]\sin(\theta) = \mathrm{Im}\,[C] \text{ for } \theta = \pi/2. \tag{4.1.49}$$

So we obtain $\mathrm{Im}\,[C]$ when

$$(\theta_1, \theta_2) = (\pi/2, -\pi/2) = (\pi/2, 3\pi/2) \mathrm{mod}(2\pi). \tag{4.1.50}$$

To model an inaccuracy in both rotation angles, we modify them as

$$\theta_1 = \theta + \delta_1 \text{ and } \theta_2 = -\theta + \delta_2, \tag{4.1.51}$$

where δ_1, δ_2 represent the deviations from the optimal rotation angle $\theta = \pm\pi/2$. These deviations can result from a systematic inaccuracy of the experimental equipment, in which case δ_1, δ_2 would have the same value in every implementation of the RMP, i.e. $\delta_1, \delta_2 = \delta > 0$. A more likely source of error could be noise in the optical fields used to generate qubit rotations. This noise would vary in each run of the experiment, and follow a statistical distribution. Assuming this distribution to have zero mean and standard deviation $\sigma > 0$, the resulting rotation angles will follow the same distribution, only with the mean shifted to $\pm\theta$. In this case

$\delta_1, \delta_2 = \sigma$. The following derivation is valid in either case, and we will continue to distinguish δ_1 and δ_2, to keep track of the errors incurred in the forward (θ_1) and backward (θ_2) rotations.

Substituting the modified angles (4.1.51) into (4.1.48), we have

$$\begin{aligned} E_{\theta_1} &= (\langle 1\rangle - \langle 2\rangle)\cos^2(\frac{\theta+\delta_1}{2}) + \langle 2\rangle - \frac{1}{2}\mathrm{Im}\,[C]\sin(\theta+\delta_1), \\ E_{\theta_2} &= (\langle 1\rangle - \langle 2\rangle)\cos^2(\frac{-\theta+\delta_2}{2}) + \langle 2\rangle - \frac{1}{2}\mathrm{Im}\,[C]\sin(-\theta+\delta_2), \end{aligned} \tag{4.1.52}$$

of which the difference (4.1.49) becomes

$$\Delta E = (\langle 1\rangle - \langle 2\rangle)\left(\cos^2(\frac{\theta-\delta_2}{2}) - \cos^2(\frac{\theta+\delta_1}{2})\right) + \frac{1}{2}\mathrm{Im}\,[C]\left(\sin(\theta-\delta_2) + \sin(\theta+\delta_1)\right). \tag{4.1.53}$$

We now assume that deviations from the optimal rotation angles are small. We may then Taylor-expand (4.1.53) with respect to δ_1, δ_2 as

$$\begin{aligned} \Delta E =& \frac{\langle 2\rangle - \langle 1\rangle}{2}\sum_{k=0}^{\infty}(-1)^k\left[(\delta_1^{2k+1} + \delta_2^{2k+1})\sin\theta - (\delta_1^{2k} - \delta_2^{2k})\cos\theta\right] \\ &+ \frac{1}{2}\mathrm{Im}\,[C]\sum_{k=0}^{\infty}(-1)^k\left[(\delta_1^{2k} + \delta_2^{2k})\sin\theta + (\delta_1^{2k+1} - \delta_2^{2k+1})\cos\theta\right]. \end{aligned} \tag{4.1.54}$$

Setting θ to the optimal choice of rotation angle (4.1.50), the above reduces to

$$\begin{aligned} \Delta E(\theta = \pi/2) =& \frac{\langle 2\rangle - \langle 1\rangle}{2}\sum_{k=0}^{\infty}(-1)^k(\delta_1^{2k+1} + \delta_2^{2k+1}) + \frac{1}{2}\mathrm{Im}\,[C]\sum_{k=0}^{\infty}(-1)^k(\delta_1^{2k} + \delta_2^{2k}) \\ =& \mathrm{Im}\,[C] + \epsilon, \end{aligned} \tag{4.1.55}$$

with

$$\epsilon := \frac{\mathrm{Im}\,[C]}{2}\sum_{k=1}^{\infty}(-1)^k(\delta_1^{2k} + \delta_2^{2k}) + \frac{\langle 2\rangle - \langle 1\rangle}{2}\left((\delta_1+\delta_2) + \sum_{k=1}^{\infty}(-1)^k(\delta_1^{2k+1} + \delta_2^{2k+1})\right). \tag{4.1.56}$$

Equation (4.1.55) yields the desired imaginary correlation component with an overall error ϵ (4.1.56). When $|\delta_1|, |\delta_2| \ll 1$, this error reduces to

$$\epsilon \simeq \frac{\delta_1 + \delta_2}{2}(\langle 2\rangle - \langle 1\rangle). \tag{4.1.57}$$

If the errors in the rotation angles are systematic, $\delta_1 + \delta_2 = 2\delta > 0$. If they are statistical, $\delta_1 + \delta_2 = 2\sigma > 0$. In either case the prefactor $\delta_1 + \delta_2$ in (4.1.57) is small, but cannot vanish. To determine the size of the error ϵ, it is therefore necessary to characterise the size of the scaling term

$$\langle 2\rangle - \langle 1\rangle = \langle\psi|\, \sigma_i^a(t_1)\sigma_j^b(t_2)\sigma_i^a(t_1) - \sigma_j^b(t_2)\,|\psi\rangle\,. \tag{4.1.58}$$

Within a given experimental platform one could measure the two expectation values above in additional experimental runs. This would however cost more (time, money, manpower). Therefore, a theoretical analysis of the size of (4.1.58) is desirable. A straightforward calculation of these expectation values may be possible, but to obtain a general result which is independent of the initial many-body system state $|\psi\rangle$ we again make use of Lieb-Robinson bounds (reviewed in Sec. 4.1.1). Using property (4.1.16) we upper bound (4.1.58) as

$$\begin{aligned}\langle 2\rangle - \langle 1\rangle \leq& \|\sigma_i^a(t_1)\sigma_j^b(t_2)\sigma_i^a(t_1) - \sigma_j^b(t_2)\| \\ \leq& \|\sigma_i^a(t_1)\left(\sigma_j^b(t_2)\sigma_i^a(t_1) - \sigma_i^a(t_1)\sigma_j^b(t_2)\right)\| \\ \leq& \|U(t_1)\left(U^\dagger(t_1)\sigma_j^b(t_2)U(t_1)\sigma_i^a - \sigma_i^a U(t_1)\sigma_j^b(t_2)U^\dagger(t_1)\right)U(t_1)\| \\ \leq& \left\|\left[\sigma_j^b(\Delta t), \sigma_i^a\right]\right\|.\end{aligned} \tag{4.1.59}$$

In the second line we have used that $\sigma_i^a(t_1)\sigma_i^a(t_1) = \mathbb{1}$. In the third and fourth line we have used property (4.1.20) and $\|\sigma_i^a(t_1)\| \leq 1$ and $\|U(t_1)\| = 1$. The commutator norm in the final line can be upper bounded with a Lieb-Robinson bound $b(\Delta t, \rho)$, as shown in Sec. 4.1.1, and so we may upper bound the net error (4.1.57) as

$$\epsilon \leq \frac{\delta_1 + \delta_2}{2} b(\Delta t, \rho), \text{ for } \delta_1, \delta_2 \ll 1. \tag{4.1.60}$$

We have seen in the preceding sections of this chapter that the choice of Lieb-Robinson bound is not unique, and depends on the type of interaction given by the system Hamiltonian as well as the space-time domain for which one wants to minimise the error. Therefore, result (4.1.60) is the most general form of the net error ϵ—applicable to any spin lattice—and should be interpreted qualitatively: The errors δ_1, δ_2 in the rotation angles can be thought of as unwanted perturbations of the system state at t_1. The Lieb-Robinson bound $b(\Delta t, \rho)$ defines a light-cone region in the $(\Delta t, \rho)$ parameter space, within which these perturbations cause a significant deviation of the measured correlation component i.e. where ϵ is on the order of $|\mathrm{Im}C|$. Outside of this light-cone, $b(\Delta t, \rho)$ decays exponentially so that the net error ϵ is suppressed.

For a quantitative characterisation of ϵ, the many-body interactions in a given experimental set-up must be known, so that the optimal choice of $b(\Delta t, \rho)$ can be made. This however goes beyond the scope of what we wanted to achieve, namely to show how errors in the rotation angles θ_1, θ_2 propagate into the final signal as a net error ϵ (4.1.60) and that this error can in principle be brought below a desired threshold value through appropriate choices of ρ and Δt.

4.2 Implementing the NIMP in ion-traps

The ability of linear ion traps (LITs) to simulate many-body spin dynamics under a given Hamiltonian H_{s}, and the high level of control which one has over individual ions, makes them a good candidate for implementation of the ancilla-based NIMP of Sec. 2.1. In this section we consider simulations of spin-1/2 chains in LITs. Although the NIMP is strictly speaking not necessary for spin-1/2 systems, there are two reasons for considering its implementation in the spin-1/2 setting. First as a proof of principle, and second to avoid complications which arise in the PMP due to a projective measurement of the target system at the early time t_1.

Suppose that we want to measure the dynamic correlation $\langle\psi|\,\sigma_i^a(t_1)\sigma_j^b(t_2)\,|\psi\rangle$, between the ith and jth spin[6]. To do so the NIMP requires an ancilla particle to be prepared in a well-defined state, followed by a controlled weak coupling to the ith system ion at t_1 (step c of the protocol). Both steps can be readily achieved in LITs with currently available techniques: Assume that $N+1$ ions are trapped in a given experiment. We propose to designate one of these ions as the spin-1/2 ancilla particle, with the remaining N ions forming the target system. The ancilla's Hilbert space is $\mathscr{H}_A = \mathbb{C}^2$, and the required initial ancilla state $|\phi\rangle \in \mathscr{H}_A$ (2.1.11) can be prepared via single-ion laser addressing [31] if the qubit transition is in the optical regime. The remaining N ions which form the target system will have a collective initial state $|\psi\rangle \in \mathscr{H}_S = (\mathbb{C}^2)^{\otimes N}$. Their dynamics under action of a desired Hamiltonian H_{s} can be initiated and driven for some time t_1 by applying optical drive fields. To achieve the pre-coupling product state (2.1.2) of step b, the initial ancilla state must be excluded from these dynamics. This can be done with a "spin-shelving" procedure [30]. This involves placing the ancilla ion in a different hyperfine state which is off-resonant with the dynamics-generating driving field. As a result the drive field does not couple to the ancilla ion, thereby preserving its state.

For the non-invasive measurement, the ancilla spin must interact with *only* the ith lattice spin, and this coupling must be generated by the unitary operator $\mathscr{U} = \exp(-i\lambda B \otimes \sigma_i^a)$ (step c of Sec. 2.1). In deriving the NIMP we assumed that the system undergoes no dynamics due to H_{s} during this coupling. This can be achieved in LITs by temporarily switching off the driving fields at t_1. The coupling between the ancilla and the target ions is mediated by collective phonon modes of the ion lattice (see the review on LITs in this chapters introduction). Restricting these interactions to a specific ion pair (the ancilla and the ith spin) requires sophisticated but well-established techniques, as described in [48; 49; 34; 50], and we will elaborate on this point in Sec. 4.2.1 below. Note that no spatial proximity is required between the ancilla ion and the ith lattice ion; since interactions are

[6] Since the trapped ions are distinguishable by their equilibrium position one can simply label them from left to right as $1, \ldots, N$.

mediated by phonons, the ancilla may be located at any site, including the ends of the trapped ion chain. To avoid decoherence at t_1, we suggest to defer measurement of the ancilla ion to t_2. This requires the ancilla to undergo trivial dynamics from t_1 to t_2 (see Sec. 2.3.2), which can again be achieved through shelving techniques. Once the ancilla–target coupling has been completed, the system dynamics must be resumed. Time evolution of the (post-coupling) state from t_1 to t_2 is achieved by applying the same optical drive fields which generated the time evolution up to t_1.

4.2.1 Ancilla–target coupling in linear ion traps

To generate the ancilla–target coupling $\mathscr{U}$ (2.1.3) at t_1 under Hamiltonian $H_c = B \otimes \sigma_i^a$, a suitable technique is to use an entangling gate mediated by phonon modes transverse to the trap axis [50; 51]. These transverse phonon mode (TPM) gates can, for a chosen coupling strength λ, entangle the spin states of arbitrary ion pairs by producing a $\sigma^z\sigma^z$ interaction. The ancilla–target coupling is then restricted to $\mathscr{U}(\lambda) = \exp(-i\lambda\sigma^z \otimes \sigma_i^z)$. This is sufficient to measure $\operatorname{Im}\langle\psi|\,\sigma_i^a(t_1)\sigma_j^b(t_2)\,|\psi\rangle$ with $a = z$ and $b \in \{x, y, z\}$, but not for other spin components. We will show in this section that the various coupling Hamiltonians (outlined in (2.1.15)–(2.1.20)) can be implemented by augmenting the TPM coupling with rotations of the ancilla and system spins. As a result one can measure dynamic correlations with any combination of $a, b \in \{x, y, z\}$. As stated above, we use the deferred measurement approach of Sec. 2.3.2.

Let

$$R_S(\theta, \boldsymbol{n}) = \prod_{k=1}^{N} R_k(\theta, \boldsymbol{n}) = \prod_{k=1}^{N} \exp\left(-\frac{i\theta}{2}\boldsymbol{n}\cdot\boldsymbol{\sigma}_k\right) \text{ and} \tag{4.2.1}$$

$$R_A(\alpha, \boldsymbol{m}) = \exp\left(-i\frac{\alpha}{2}\boldsymbol{m}\cdot\boldsymbol{\sigma}\right), \tag{4.2.2}$$

respectively denote rotation operators acting on the system and ancilla Hilbert spaces. Note that the system rotation is global i.e. all spins are rotated by the same angle θ and about the same axis defined by the unit vector $\boldsymbol{n}$. Consider then the following rotated ancilla–target state, propagated to t_2,

$$|\Psi_R(t_2)\rangle = U(t_2 - t_1)(R_A(\alpha, \boldsymbol{m})R_S(\theta, \boldsymbol{n}))^\dagger \mathscr{U}(\lambda) R_A(\alpha, \boldsymbol{m})R_S(\theta, \boldsymbol{n})\,|\phi, \psi(t_1)\rangle\,. \tag{4.2.3}$$

Let us keep the coupling Hamiltonian general for now, so that $\mathscr{U} = \exp(-i\lambda B \otimes A_i)$. If this coupling satisfies the non-invasive measurement requirement $\lambda \ll 1$, we may expand (4.2.3) to linear order in λ as

$$|\Psi_R(t_2)\rangle = |\phi, \psi(t_2)\rangle - \lambda B(\alpha)\,|\phi\rangle \otimes U(t_2 - t_1)A_i(\theta)\,|\psi(t_1)\rangle\,, \tag{4.2.4}$$

where we have defined $B(\alpha) = R_A^\dagger(\alpha, \boldsymbol{m}) B R_A(\alpha, \boldsymbol{m})$ and $A_i(\theta) = R_i^\dagger(\theta, \boldsymbol{n}) A_i R_i(\theta, \boldsymbol{n})$. From a theoretical point of view, a local rotation of only the ith spin yields the same state as above, and the decision whether to perform a global rotation of the system or a local rotation of only the ith spin depends on the experimental set up at hand. Combining probabilities $P_{\pm_a \pm_b}$ for a simultaneous measurement of the ancilla and jth spin at t_2 as in (2.1.10) we get

$$\mathscr{C}(t_1, t_2) \simeq \langle \sigma^a \rangle_\phi \left\langle \sigma_j^b(t_2) \right\rangle_\psi - i\lambda \Big(\langle \phi | \, \sigma^a B(\alpha) \, | \phi \rangle \, \langle \psi | \, \sigma_j^b(t_1) A_i(\theta, t_1) \, | \psi \rangle - \text{ c.c.} \Big), \tag{4.2.5}$$

where $A_i(\theta, t_1) = U^\dagger(t_1) A_i(\theta) U(t_1)$.

Recall now that the TPM coupling restricts the coupling Hamiltonian H_c to $B \otimes A_i = \sigma^z \otimes \sigma_i^z$, so that

$$\begin{aligned} A_i(\theta, t_1) &= U^\dagger(t_1) e^{i\theta/2 \boldsymbol{n}\cdot\boldsymbol{\sigma}_i} \sigma_i^z e^{-i\theta/2 \boldsymbol{n}\cdot\boldsymbol{\sigma}_i} U(t_1) \text{ and} \\ B(\alpha) &= e^{i\alpha/2 \boldsymbol{m}\cdot\boldsymbol{\sigma}} \sigma^z e^{-i\alpha/2 \boldsymbol{m}\cdot\boldsymbol{\sigma}}. \end{aligned} \tag{4.2.6}$$

For a given choice of $a, b \in \{x, y, z\}$ the measured correlation (4.2.5) then contains the desired dynamic correlation $\langle \psi | \, \sigma_i^a(t_1) \sigma_j^b(t_2) \, | \psi \rangle$ if $\boldsymbol{n}$ and θ can be chosen such that $A_i(\theta, t_1) = \sigma_i^a(t_1)$. To extract the corresponding imaginary and real components ((2.1.17) and (2.1.19)), the ancilla rotation $R_A(\alpha, \boldsymbol{m})$ must be chosen such that $B(\alpha)$ satisfies conditions (2.1.16) and (2.1.18), respectively. The appropriate choices of $\boldsymbol{n}, \boldsymbol{m}, \theta$ and α are given below in Table 4.2.1, and can be summarised as follows: Condition $A_i(\theta, t_1) = \sigma_i^a(t_1)$ is achieved for $a = x, y$ by choosing the system rotation axis $\boldsymbol{n}$ orthogonal to the a–z plane. If $a = z$ no system rotation is needed since $A_i = \sigma_i^z$ is already fulfilled by the TPM coupling. We know from (2.1.16) and (2.1.17) that the imaginary correlation component, for any $a \in \{x, y, z\}$, can be extracted by choosing $B = \sigma^a$. $B(\alpha) = \sigma^a$ is achieved by choosing $\boldsymbol{m}$ orthogonal to the a–z plane. In contrast, to extract $\operatorname{Re} C$, the NIMP requires $B(\alpha) = -i(\sigma_a^+ - \sigma_a^-)$. When $a = x, y$, this is achieved by rotating the ancilla parallel to the a-axis i.e. $\boldsymbol{m} = \boldsymbol{a}$ (see (2.1.18) and (2.1.19)). When $a = z$, a rotation around the x-axis is necessary i.e. $\boldsymbol{m} = (1, 0, 0)$.

We have thus shown that the various ancilla–target couplings which are crucial to the functioning of the NIMP, can be generated in linear ion traps with well-documented techniques. Considering also the discussion of Sec. 4.2 before this subsection, we may conclude that implementation of the NIMP is feasible in linear ion traps.

Table 4.2.1: Summary of rotation parameters needed to measure components of $\langle\psi|\,\sigma_i^a(t_1)\sigma_j^b(t_2)\,|\psi\rangle$

a	Component	$\boldsymbol{n}$	θ	$A_i(\theta)$	$\boldsymbol{m}$	α	$B(\alpha)$
x	$\mathrm{Re}\left\langle\sigma_i^x(t_1)\sigma_j^b(t_2)\right\rangle$	$(0,1,0)$	$3\pi/2$	σ_i^x	$(1,0,0)$	$\pi/2$	σ^y
	$\mathrm{Im}\left\langle\sigma_i^x(t_1)\sigma_j^b(t_2)\right\rangle$				$(0,1,0)$	$3\pi/2$	σ^x
y	$\mathrm{Re}\left\langle\sigma_i^y(t_1)\sigma_j^b(t_2)\right\rangle$	$(1,0,0)$	$\pi/2$	σ_i^y	$(0,1,0)$	$3\pi/2$	σ^x
	$\mathrm{Im}\left\langle\sigma_i^y(t_1)\sigma_j^b(t_2)\right\rangle$				$(1,0,0)$	$\pi/2$	σ^y
z	$\mathrm{Re}\left\langle\sigma_i^z(t_1)\sigma_j^b(t_2)\right\rangle$		0	σ_i^z	$(1,0,0)$	$\pi/2$	σ^y
	$\mathrm{Im}\left\langle\sigma_i^z(t_1)\sigma_j^b(t_2)\right\rangle$					0	σ^z

5

Conclusion and Outlook

In this thesis we have provided a theoretical description of how dynamic two-point correlations $C = \langle\psi| O(t_1)O(t_2) |\psi\rangle$ can be measured in many-body quantum systems. Measuring such correlations is challenging in general, since the system under study must be probed at different points in time. We showed in Chap. 1 that a naive approach of directly probing the system projectively is not feasible in general, due to the associated wave function collapse at the early measurements. Despite the ubiquitous use of dynamic correlations in many-body quantum physics, proposals of how they can be measured in experiments are few, and limited to specific Hamiltonians and/or equilibrium initial states. Moreover, they do not give access to the full complex value of the dynamic correlation.

In Chap. 2 we developed a noninvasive measurement protocol (NIMP) which addresses these issues. It is valid for quantum lattices of arbitrary geometry, dimension, and spin-$s \in \mathbb{N}/2$. The main technical ingredient in the NIMP is to reduce measurement backaction at the early time t_1 by using an ancilla system to perform a noninvasive measurement. The novel achievement is that our NIMP is independent of the target system's Hamiltonian and initial state, and allows for both the real and imaginary parts of C to be extracted. This requires a careful choice of the ancilla–target coupling $\mathscr{U} = e^{-i\lambda H_c}$ (2.1.3), and of the initial ancilla state (2.1.11). This was shown in Sec. 2.1. In Sec. 2.2 we characterised the accuracy of the NIMP. We derived a theoretical upper bound on deviations from the desired correlation components, and showed that these can be minimised through an optimal choice of the coupling time λ^*. This was verified numerically in Sec. 2.2.1. Generalisations of the NIMP were discussed in Sec. 2.3: In Sec. 2.3.1 we showed that the NIMP can be used to measure correlations of arbitrary (multi-site) spin observables, and that the size of the ancilla spins can be any $s \in \mathbb{N}/2$. We showed in Sec. 2.3.2 that the ancilla measurement can be deferred to the end of the noninvasive protocol. This can be useful in experiments where measuring the ancilla at early times introduces unwanted noise such as that arising from photon scattering (parasitic light) [31]. In Sec. 2.3.3 we showed that extending the NIMP to include repeated noninvasive measurements (cNIMP) does not improve its efficiency.

In Chap. 3 we used Kraus operators to analyse the dynamics induced on the target system by the noninvasive measurement at t_1. The main result is specific

to spin-1/2 systems: When measuring ImC, the Kraus operators describing the noninvasive measurement reduce to a rotation of the target. This lead to the rotation-based measurement protocol (RMP) of Sec. 3.2.1. More surprisingly, the Kraus operators showed that the noninvasive measurement is equivalent to a projection when measuring Re C. This counter-intuitive result lead to the projective measurement protocol (PMP) of 3.2.2. We proved in App. B that this PMP is valid for single-site spin-1/2 observables, as well as tensor products of these.

In Chap. 4 we have considered implementations of our measurement protocols in linear ion-traps and quantum gas microscopes. Although the NIMP, PMP and RMP are all feasible, experimental challenges modify our original theoretical results. Particle loss and decoherence occur as side effects of projective measurements, and this leads to errors when using the PMP to measure Re C. In Sec. 4.1.2 we approximated the size of this error using Lieb-Robinson bounds, and showed that it can be made small through careful choices of measurement times and lattice sites. For the RMP we discussed, in Sec. 4.1.3, how systematic errors in the rotation operators propagate into the measured value of ImC. We again used Lieb-Robinson bounds to prove that the net error can be brought below a desired threshold. We concluded the chapter by showing that the ancilla-based measurements of the NIMP can be readily implemented with existing techniques in linear ion-traps.

One avenue for future research is to simulate the NIMP when applied to a true many-body system. Comparing the correlations "measured" with a simulation of the NIMP to those calculated from existing numeric techniques would provide further benchmarking, and would build on the numeric results of Sec. 2.2.1. Some work in this direction was done during the course of this thesis. We coded a known numeric technique (reported in Refs. [52; 53; 54]) to calculate dynamic spin correlations in the one-dimensional transverse-field Ising model (TFIM). The technique consists of an exact diagonalisation of the TFIM Hamiltonian for a finite chain with open boundary conditions. Coding this benchmarking tool took longer than expected, and a numeric implementation of the NIMP for the TFIM remains to be done.

Analytic extensions of our work in Chap. 2 could seek to generalise the ancilla-based NIMP to continuous quantum systems. Another interesting scenario to consider is whether the weak-coupling requirement ($|\lambda| \ll 1$) can be eliminated when the observable to be correlated at t_1 is a spin-l observable, with $l \gg 1/2$. The idea is to use a spin-1/2 ancilla and coupling Hamiltonian $H_c = \boldsymbol{S} \cdot \boldsymbol{L}$. By expressing the initial ancilla–target product state in the coupled spin basis, one can calculate the post-coupling state $\exp(-\lambda \boldsymbol{S} \cdot \boldsymbol{L}) \, |\phi, \psi\rangle$ to all orders in λ. Transforming $\exp(-\lambda \boldsymbol{S} \cdot \boldsymbol{L}) \, |\phi, \psi\rangle$ back to the uncoupled spin-basis would then allow one to calculate the projective measurement of the ancilla state. The idea is that the distribution of the target states' expansion coefficients in this basis is not drastically altered by the ancilla measurement (due to the Clebsch-Gordan selection rules). Investigating how large l should be such that the target-state changes only negligibly at t_1 is an interesting line of inquiry.

Recently, there has been a large interest in "out-of-time-order correlations" (OTOCs, see for instance Refs. [55; 56; 57]). They can be used to describe the spread of chaos in quantum lattice systems. Some schemes to measure OTOCs have been proposed, but are difficult to implement as they require time-reversal [58] or interferometric techniques which yield correlators that are related to the OTOCs only at early times [59]. The structure of OTOCs is similar to that of the three-point correlators occurring in our RMP (see Eq. (3.2.2)), and proposals [58] to use ancillas to achieve the necessary time-reversal exist. This motivated us to attempt derivations of equivalent ancilla-free protocols by using Kraus operators. Thus far we have not been successful, and future work could rigorously study the use of ancillas in OTOC measurements with the ultimate goal of deriving a measurement protocol which does not require ancillas (similar to our PMP and RMP).

The work presented in this thesis has lead to an experimental PhD project (at Stellenbosch University) which aims to use our NIMP to measure dynamic correlations of spin-1/2 systems simulated in a linear ion-trap.

Appendices

A

Derivation of the cNIMP

In this appendix we present the derivation of the consecutive noninvasive measurement protocol (cNIMP) of Sec. 2.3.3. As outlined there, the cNIMP consists of multiple (ancilla based) noninvasive measurements, performed at early times $t < t_f$, and ends with a projective measurement of the target system at $t = t_f$. Our goal is to extract information on correlations of observables at multiple pairs of times. For the sake of brevity, we will consider only three times $0 \leq t_1 < t_2 < t_3$ and correlations $C_1 = C(t_1, t_2), C_2 = C(t_1, t_3)$ and $C_3 = C(t_2, t_3)$. However, generalisations to more times and correlations are straightforward extensions of the derivation presented below.

The NIMP, developed in Sec. 2.1, would require six distinct measurement samples to measure the imaginary and real components of C_1, C_2, C_3. Our goal in developing the cNIMP is therefore to extract these six components from less than six measurement samples. Although the cNIMP is not restricted to any particular choice of correlations, we will consider correlations

$$C_1 = C(t_1, t_2) = \langle\psi| S_i^a(t_1) S_j^b(t_2) |\psi\rangle \tag{A.0.1}$$

$$C_2 = C(t_1, t_3) = \langle\psi| S_i^a(t_1) S_j^b(t_3) |\psi\rangle \tag{A.0.2}$$

$$C_3 = C(t_2, t_3) = \langle\psi| S_i^a(t_3) S_j^b(t_2) |\psi\rangle\,, \tag{A.0.3}$$

in a spin-s lattice system with arbitrary Hamiltonian H_s and spin $s \in \mathbb{N}/2$.

We will show that estimating correlation C_1 (see (A.0.1)) requires two noninvasive measurements, one at t_1 and one at t_2, so that at least two ancilla particles are required, coupled to sites i and j respectively. We will refer to either ancilla by the index of the time at which they are coupled to the principle system, and denote their initial states as $|\phi_1\rangle$ and $|\phi_2\rangle$. Together with the noninvasive measurement at t_1, a projective measurement of lattice spin j at t_3 will lead to an estimator (A.0.18) of C_2. Similarly, the second noninvasive measurement, combined with a projective measurement of lattice spin i at t_3 will yield an estimator (A.0.20) of C_3. The two noninvasive measurements should therefore suffice to estimate (A.0.1) – (A.0.3). Note that the number of noninvasive measurements (i.e. ancillas) required to measure three correlations with the cNIMP is not unique: had we instead chosen to consider the correlation $C_3 = \langle\psi| S_i^a(t_2) S_j^b(t_3) |\psi\rangle$, we would require a third noninvasive measurement—namely of lattice spin i at t_2—and thus require three ancilla

particles. The number of required ancillas depends on the number n of points in time considered, and the number of correlations which one wishes to extract. For instance, if one is interested in exactly one correlation per distinct pair of time points, one would require at most $\binom{n}{2}$ ancillas.

Measuring the system. Since we require only two ancilla spins, the total ancilla–target Hilbert space is $\mathscr{H} = \mathscr{H}_{\mathrm{A}_1} \otimes \mathscr{H}_{\mathrm{A}_2} \otimes \mathscr{H}_{\mathrm{S}}$. The Hilbert space of ancilla $m = 1, 2$ is denoted by $\mathscr{H}_{\mathrm{A}_m} = \mathbb{C}^{2s+1}$. The Hilbert space for a target system of N spin-s lattice spins is $\mathscr{H}_{\mathrm{S}} = (\mathbb{C}^{2s+1})^{\otimes N}$. As in the NIMP, we assume system and ancillas to initially be in a product state $|\Psi\rangle = |\phi_1, \phi_2, \psi\rangle$, with ancilla initial states $|\phi_m\rangle$ to be determined.

For the cNIMP, the relevant time evolution operators on $\mathscr{H}$ are

$$U(t) = \mathbb{1}_{A_1} \otimes \mathbb{1}_{A_2} \otimes \exp(-iH_{\mathrm{s}}t), \tag{A.0.4a}$$

$$\mathscr{U}(\lambda_1) = \exp(-i\lambda_1 B_1 \otimes \mathbb{1}_{A_2} \otimes A_i), \tag{A.0.4b}$$

$$\mathscr{U}(\lambda_2) = \exp(-i\lambda_2 \mathbb{1}_{A_1} \otimes B_2 \otimes A_j), \tag{A.0.4c}$$

which describe the system dynamics, the coupling to the first ancilla, and the coupling to the second ancilla, respectively. The coupling operators A_i, A_j act nontrivially only on lattice sites i and j, respectively. In terms of the time evolution operators (A.0.4a)–(A.0.4c), the ancilla–target state at time t_3 is

$$|\Psi(t_3)\rangle = U(t_3 - t_2)\mathscr{U}(\lambda_2)U(t_2 - t_1)\mathscr{U}(\lambda_1)U(t_1)\,|\Psi\rangle\,. \tag{A.0.5}$$

We use the deferred measurement approach[1] to measure both ancillas as well as sites i and j, at time t_3. Ancilla 1 and site i are measured in the eigenbasis $\mathscr{S}_a = \{|m_a\rangle\}$ of S^a. Ancilla 2 and site j are measured in the eigenbasis $\mathscr{S}_b$ of S^b. The joint probabilities for this 4-particle measurement are then

$$P = \langle\Psi(t_3)|\,\Pi_{A_1}^{m_a} \otimes \Pi_{A_2}^{m_b} \otimes \Pi_i^{m_a} \otimes \Pi_j^{m_b}\,|\Psi(t_3)\rangle\,, \text{ for } m_a \in \mathscr{S}_a \text{ and } m_b \in \mathscr{S}_b. \tag{A.0.6}$$

Extracting C_1. In C_1 we wish to correlate the states of sites i and j at the early times t_1 and t_2. The relevant measurement outcomes are therefore those of the ancilla measurements. The first step in correlating these measurements outcomes is to marginalise the 4-particle distribution (A.0.6) over the eigenvalues corresponding to measurements of sites i and j at the final time t_3. This yields the marginal distribution

$$\begin{aligned} P_1 &= \langle\Psi(t_3)|\,\Pi_{A_1}^{m_a} \otimes \Pi_{A_2}^{m_b} \otimes \left(\sum_{m_a \in \mathscr{S}_a} \Pi_i^{m_a}\right) \otimes \left(\sum_{m_b \in \mathscr{S}_b} \Pi_j^{m_b}\right) |\Psi(t_3)\rangle \\ &= \langle\Psi(t_3)|\,\Pi_{A_1}^{m_a} \otimes \Pi_{A_2}^{m_b} \otimes \mathbb{1}_{\mathrm{S}}\,|\Psi(t_3)\rangle\,. \end{aligned} \tag{A.0.7}$$

[1] Which was shown in Sec. 2.3.2 to yield the same results as immediate measurements of the ancilla spins.

As in (2.1.10) we now construct a correlation from this marginalised distribution

$$\mathscr{C}(t_1,t_2)=\sum_{\substack{m_a\in\mathscr{S}_a,\\ m_b\in\mathscr{S}_b}} m_a m_b P_1=\langle\Psi(t_3)|\, S^a_{A_1}\otimes S^b_{A_2}\otimes \mathbb{1}_S\,|\Psi(t_3)\rangle\,, \tag{A.0.8}$$

which, to linear order in the coupling times λ_1,λ_2, is equal to

$$\begin{aligned}\mathscr{C}(t_1,t_2)\simeq&\langle S^a\rangle_{\phi_1}\langle S^b\rangle_{\phi_2}+2\lambda_1\langle S^b\rangle_{\phi_2}\langle A_i(t_1)\rangle_\psi \operatorname{Im}\left[\langle S^aB_1\rangle_{\phi_1}\right]\\&+2\lambda_2\langle S^a\rangle_{\phi_1}\langle A_j(t_2)\rangle_\psi \operatorname{Im}\left[\langle S^bB_2\rangle_{\phi_2}\right]\\&+4\lambda_1\lambda_2\operatorname{Im}\left[\langle B_2S^b\rangle_{\phi_2}\right]\operatorname{Im}\left[\langle B_1S^a\rangle_{\phi_1}\langle\psi|\,A_i(t_1)A_j(t_2)\,|\psi\rangle\right].\end{aligned} \tag{A.0.9}$$

By choosing $A_i=S^a_i$ and $A_j=S^b_j$ the desired correlation (A.0.1) is contained in the last line. This is a first condition on the coupling Hamiltonians of (A.0.4b) and (A.0.4c). The terms of the first two lines can be eliminated by choosing initial ancilla states $|\phi_1\rangle,|\phi_2\rangle$ such that $\langle S^a\rangle_{\phi_1},\langle S^b\rangle_{\phi_2}=0$. As in the NIMP, we achieve this by choosing the initial ancilla states as equal superpositions[2] of the eigenbases of S^a and S^b

$$|\phi_1\rangle=\frac{1}{\sqrt{2s+1}}\sum_{m_a\in\mathscr{S}_a}|m_a\rangle\ \text{ and }\ |\phi_2\rangle=\frac{1}{\sqrt{2s+1}}\sum_{m_b\in\mathscr{S}_b}|m_b\rangle\,. \tag{A.0.10}$$

Since we wish to use the same measurement samples for estimators of C_2 and C_3, the initial ancilla states are now fixed by the above equations for the remainder of the cNIMP.

To retain the term containing correlation C_1 in (A.0.9), we require that

$$\operatorname{Im}\left[\langle B_2S^b\rangle_{\phi_2}\right]\neq 0, \tag{A.0.11}$$

and this must be taken into account when choosing the coupling Hamiltonian of $\mathscr{U}(\lambda_2)$ (A.0.4c). Having specified $|\phi_2\rangle$ in (A.0.10), the condition (A.0.11) is met when $B_2=-i(S^+_b-S^-_b)/2$, in which case

$$\operatorname{Im}\left[\langle B_2S^b\rangle_{\phi_2}\right]=\frac{1}{2s+1}\sum_{m_b,m'_b\in\mathscr{S}_b}m_b\operatorname{Im}\left[\langle m'_b|-i(S^+_b-S^-_b)/2\,|m_b\rangle\right]=\frac{g}{2s+1}. \tag{A.0.12}$$

With $A_i=S^a_i$, $A_j=S^b_j$, $B_2=-i(S^+_b-S^-_b)/2$ and ancilla states (A.0.10) we obtain

$$\mathscr{C}(t_1,t_2)\simeq\frac{4\lambda_1\lambda_2 g}{(2s+1)^2}\sum_{m_a,m'_a\in\mathscr{S}_a}m_a\operatorname{Im}\left[\langle m'_a|\,B_1\,|m_a\rangle\,C_1\right], \tag{A.0.13}$$

[2] See Sec. 2.1 for a discussion on viable ancilla states.

from which we can extract imaginary and real parts of C_1 by respectively choosing B_1 as $B_1^{(1)}$ (2.1.16) and $B_1^{(2)}$ (2.1.18). Finally then, we can construct the estimator

$$C^{\lambda}(t_1,t_2) = \frac{(2s+1)^2}{4\lambda_1\lambda_2 g}\left(\frac{\mathscr{C}^{(2)}(t_1,t_2)}{f^{(2)}} + i\frac{\mathscr{C}^{(1)}(t_1,t_2)}{f^{(1)}}\right), \tag{A.0.14}$$

which approximates C_1 in the limit of weak ancilla–target couplings (i.e. small coupling times λ_1 and λ_2). In (A.0.14), $f^{(1)}, f^{(2)}$ are defined as in Sec. 2.1 and the superscripts indicate whether $B^{(1)}$ or $B^{(2)}$ has been used for B_1 in the coupling of ancilla 1 to site i (A.0.4b).

Table A.0.1 summarises the requirements for extracting C_1 from the 4-particle distribution (A.0.6). The table shows that we need at least two measurement samples S_1 and S_2, corresponding to the second and third row of the table. The initial ancilla states are given by (A.0.10) for both samples. In what follows, the operator choices used to obtain S_1 and S_2 must be taken into account when we extract estimators for C_2 and C_3. The hope is that we can extract these estimators from S_1 and S_2 by marginalising the outcome distributions of either sample over different eigenvalues.

Correlation component	B_1	A_i	B_2	A_j	Sample
$\mathrm{Re}\,[C_1]$	$-i(S_a^+ - S_a^-)/2$	S_i^a	$-i(S_b^+ - S_b^-)/2$	S_j^b	S_1
$\mathrm{Im}\,[C_1]$	S^a	S_i^a	$-i(S_b^+ - S_b^-)/2$	S_j^b	S_2

Table A.0.1: Conditions on ancilla–target couplings to extract real and imaginary parts of C_1 (A.0.1).

Extracting C_2. The derivation of $C^{\lambda}(t_1,t_3)$ is much the same as for $C^{\lambda}(t_1,t_2)$ above. The relevant measurement outcomes are now those of ancilla 1 and site j so that the appropriate marginalisation is over the eigenvalues corresponding to measurements of ancilla 2 and lattice spin i

$$\begin{aligned} P_2 &= \langle\Psi(t_3)|\,\Pi_{A_1}^{m_a}\otimes\left(\sum_{m_b\in\mathscr{S}_b}\Pi_{A_2}^{m_b}\right)\otimes\left(\sum_{m_a\in\mathscr{S}_a}\Pi_i^{m_a}\right)\otimes\Pi_j^{m_b}\,|\Psi(t_3)\rangle \\ &= \langle\Psi(t_3)|\,\Pi_{A_1}^{m_a}\otimes\mathbb{1}_{A_2}\otimes\Pi_j^{m_b}\,|\Psi(t_3)\rangle\,. \end{aligned} \tag{A.0.15}$$

We now correlate the outcomes of measurements of ancilla 1 and lattice site j, and again linearise with respect to both coupling parameters. Taking into account the

initial ancilla states (A.0.10), and choosing B_2 such that $\langle B_2 \rangle_{\phi_2} = 0$, we obtain

$$\begin{aligned} \mathscr{C}(t_1, t_3) = \sum_{\substack{m_a \in \mathscr{S}_a, \\ m_b \in \mathscr{S}_b}} m_a m_b P_2 = \langle \Psi(t_3) | \, S^a \otimes \mathbb{1}_{A_2} \otimes S_j^b \, | \Psi(t_3) \rangle \\ \simeq \frac{-2\lambda_1}{2s+1} \sum_{m_a, m_a' \in \mathscr{S}_a} m_a \mathrm{Im} \left[\langle m_a' | \, B_1 \, | m_a \rangle \, C_2 \right]. \end{aligned} \tag{A.0.16}$$

Appropriate choices for ensuring $\langle B_2 \rangle_{\phi_2} = 0$ are

$$B_2 = S^b \text{ or } B_2 = -i(S_b^+ - S_b^-)/2. \tag{A.0.17}$$

Estimators of imaginary and real components of C_2 are obtained with the same choices of B_1 as for (A.0.14) and so the overall estimator of C_2 is

$$C^\lambda(t_1, t_3) \simeq -\frac{2s+1}{2\lambda_1} \left(\frac{\mathscr{C}^{(2)}(t_1, t_3)}{f^{(2)}} + i \frac{\mathscr{C}^{(1)}(t_1, t_3)}{f^{(1)}} \right), \tag{A.0.18}$$

where $f^{(1)}, f^{(2)}$ are as in (A.0.14).

Table A.0.2 compares the new conditions on coupling operators $\mathscr{U}(\lambda_1), \mathscr{U}(\lambda_2)$ required for (A.0.18), to those required for (A.0.14). Due to the freedom of choice for B_2 (A.0.11) when constructing $C^\lambda(t_1, t_3)$ we require no additional measurement sample: $\mathrm{Re}\,[C_2]$ can be extracted from S_1 and $\mathrm{Im}\,[C_2]$ from S_2 by marginalising over measurement outcomes of ancilla 2 and site i instead of sites i and j [as was done for (A.0.14)]. In contrast, using the NIMP would require four distinct measurement samples, one per correlation component.

Correlation component	B_1	A_i	B_2	A_j	Sample
$\mathrm{Re}\,[C_1]$	$-i(S_a^+ - S_a^-)/2$	S_i^a	$-i(S_b^+ - S_b^-)/2$	S_j^b	S_1
$\mathrm{Im}\,[C_1]$	S^a	S_i^a	$-i(S_b^+ - S_b^-)/2$	S_j^b	S_2
$\mathrm{Re}\,[C_2]$	$-i(S_a^+ - S_a^-)/2$	S_i^a	$-i(S_b^+ - S_b^-)/2$ or S^b	S_j^b	S_1
$\mathrm{Im}\,[C_2]$	S^a	S_i^a	$-i(S_b^+ - S_b^-)/2$ or S^b	S_j^b	S_2

Table A.0.2: Comparison of operator choices required to construct $C^\lambda(t_1, t_2)$ (A.0.14) and $C^\lambda(t_1, t_3)$ (A.0.18).

Extracting C_3. The estimator $C^\lambda(t_2,t_3)$ is obtained from marginalising over eigenvalues corresponding to measurement of ancilla 1 and site j. Therefore, the roles of B_1 and B_2 are reversed compared to $C^\lambda(t_1,t_3)$, and $C^\lambda(t_2,t_3)$ is obtained with

$$B_1 = S^a \text{ or } B_1 = -i(S_a^+ - S_a^-)/2. \tag{A.0.19}$$

Estimators for the imaginary and real parts of C_3 then require $B_2 = B^{(3)} = S^b$ and $B_2 = B^{(4)} = -i(S_b^+ - S_b^-)/2$, respectively, so that

$$C^\lambda(t_2,t_3) \simeq -\frac{2s+1}{2\lambda_2}\left(\frac{\mathscr{C}^{(4)}(t_2,t_3)}{f^{(4)}} + i\frac{\mathscr{C}^{(3)}(t_2,t_3)}{f^{(3)}}\right). \tag{A.0.20}$$

Here

$$f^{(3)} = \sum_{m_b \in \mathscr{S}_b} m_b^2 \text{ and } f^{(4)} = i \sum_{m_b, m_b' \in \mathscr{S}_b} m_b \langle m_b | B^{(4)} | m_b' \rangle , \tag{A.0.21}$$

analogous to the definitions of $f^{(1)}, f^{(2)}$ in Sec. 2.1 (and above).

Conclusion. Adding the operator conditions required for construction of (A.0.20) to Table A.0.2, we obtain a full summary of the cNIMP in Table A.0.3 (the choices for operators A_i and A_j and initial ancilla states are constant throughout the cNIMP, so we only present the conditions imposed on operators B_1, B_2). From the table we may conclude that the cNIMP requires three distinct measurement samples $\mathrm{S}_1, \mathrm{S}_2, \mathrm{S}_3$ to extract all six correlation components. S_1 is obtained with B_1 and B_2 as given by the second row of Table A.0.3. All three real components can be extracted from S_1 through three distinct marginalisations, as discussed above, but none of the imaginary parts can be extracted from S_1. Furthermore, the restrictions imposed on B_2 for $\mathrm{Im}\,[C_1]$ and $\mathrm{Im}\,[C_3]$ are distinct, so that they cannot be extracted from the same sample of measurements. S_2 is obtained with B_1 and B_2 as given by the third row of Table A.0.3 and allows for extraction of $\mathrm{Im}\,[C_1]$ as well as $\mathrm{Im}\,[C_2]$. To extract $\mathrm{Im}\,[C_3]$ we require a third sample S_3, obtained with B_1 and B_2 as given by the last row of Table A.0.3 (we can also extract $\mathrm{Im}\,[C_2]$ from S_3, by a marginalising over eigenvalues corresponding to ancilla 2 and lattice site i). The power of the cNIMP lies in the freedom of marginalising the outcome distribution (A.0.6) of a given sample of measurements S_i in various ways, retaining only that pair of eigenvalues which corresponds to the two particles whose states are being correlated. Mathematically these marginalisations are equivalent to measuring only these two particles, due to the projective decomposition of the identity operator. Physically, however, one always measures all four particles.

The ability to measure multiple estimators of real and imaginary parts simultaneously is a potential advantage of the cNIMP over the sNIMP (see Sec. 2.3.3), provided that the total number of measurements n_c making up samples $\mathrm{S}_1, \mathrm{S}_2$ and S_3 does not exceed that of the 6 samples required by the sNIMP n_s.

Correlation component	B_1	B_2	Sample
$\mathrm{Re}\,[C_1]$	$-i(S_a^+ - S_a^-)/2$	$-i(S_b^+ - S_b^-)/2$	S_1
$\mathrm{Im}\,[C_1]$	S^a	$-i(S_b^+ - S_b^-)/2$	S_2
$\mathrm{Re}\,[C_2]$	$-i(S_a^+ - S_a^-)/2$	S^b or $-i(S_b^+ - S_b^-)/2$	S_1
$\mathrm{Im}\,[C_2]$	S^a	S^b or $-i(S_b^+ - S_b^-)/2$	S_2
$\mathrm{Re}\,[C_3]$	S^a or $-i(S_a^+ - S_a^-)/2$	$-i(S_b^+ - S_b^-)/2$	S_1
$\mathrm{Im}\,[C_3]$	S^a or $-i(S_a^+ - S_a^-)/2$	S^b	S_3

Table A.0.3: Summary of constraints on operators B_1, B_2 acting, respectively, on ancilla 1 and 2 during the noninvasive measurements at t_1 and t_2 in the cNIMP.

For the example of Sec. 2.3.3 where $s = 1/2$ and $a = b = z$, we can measure all 6 correlation components with 3 iterations of the cNIMP as follows: Measurement sample S_1 is obtained with $B_1 = \sigma^y$, $B_2 = \sigma^y$, S_2 with $B_1 = \sigma^z$, $B_2 = \sigma^y$ and S_3 with $B_1 = \sigma^y$, $B_2 = \sigma^z$.

- $\mathrm{Re}\,[C_1]$ and $\mathrm{Im}\,[C_1]$ are obtained by respectively marginalising S_1 and S_2 over eigenvalues corresponding to site i and site j.
- $\mathrm{Re}\,[C_2]$ and $\mathrm{Im}\,[C_2]$ are obtained by respectively marginalising S_1 and S_2 over eigenvalues corresponding to ancilla 2 and site i. We can also extract $\mathrm{Im}\,[C_2]$ from S_3 via the same marginalisation.
- $\mathrm{Re}\,[C_3]$ and $\mathrm{Im}\,[C_3]$ are obtained by respectively marginalising S_1 and S_3 over eigenvalues corresponding to ancilla 1 and site j.

Although we require only three measurement samples—as opposed to six with the sNIMP—the example of Sec. 2.3.3 (last paragraph) shows that $n_c \gg n_s$. In terms of resources (time, money, manpower) the sNIMP is therefore superior to the cNIMP, even though the cNIMP requires fewer measurement samples. For the comparison of Sec. 2.3.3; statistical, systematic and total errors incurred by the cNIMP estimators (A.0.14), (A.0.18), (A.0.20) were calculated in the same manner as for the sNIMP (see Sec. 2.2).

B

General Projective Measurement Protocol

Here we report details of the derivation of Eq. (3.2.15). The use of the Γ operator below was introduced by S. Castrignano during joint work on [14]. For $s \in \mathbb{N}/2$, we consider dynamic correlations $C = \langle\psi| S_i^a(t_1) S_j^b(t_2) |\psi\rangle$. The observables S_i^a, S_j^b have eigenvalues $m_a, m_b \in \mathscr{S} = \{-s, -s+1, \ldots, s-1, s\}$. The spectral decomposition of S_i^a is $\sum_{m_a \in \mathscr{S}} m_a \Pi_i^{m_a}$, where $\Pi_i^{m_a}$ denotes the projector onto the eigenspace corresponding to m_a. Similarly, $S_j^b = \sum_{m_b \in \mathscr{S}} m_b \Pi_j^{m_b}$. The projective correlation function (3.2.12) then generalizes to

$$\mathscr{C}^{\text{Proj}} = \sum_{m_a, m_b \in \mathscr{S}} m_a m_b P_{m_a}^{\text{Proj}} P_{m_b|m_a}^{\text{Proj}}. \tag{B.0.1}$$

Upon substituting

$$P_{m_b|m_a}^{\text{Proj}} = \langle\psi|\Pi_i^{m_a}(t_1)\Pi_j^{m_b}(t_2)\Pi_i^{m_a}(t_1)|\psi\rangle / P(m_a) \tag{B.0.2}$$

into (B.0.1) we obtain

$$\begin{aligned} \mathscr{C}^{\text{Proj}} &= \sum_{m_a, m_b \in \mathscr{S}} m_a m_b \langle\psi|\Pi_i^{m_a}(t_1)\Pi_j^{m_b}(t_2)\Pi_i^{m_a}(t_1)|\psi\rangle \\ &= \sum_{m_a \in \mathscr{S}} m_a \langle\psi|\Pi_i^{m_a}(t_1) S_j^b(t_2) \Pi_i^{m_a}(t_1)|\psi\rangle. \end{aligned} \tag{B.0.3}$$

Using the identity

$$\Pi_i^{m_a}(t_1) = \mathbb{1}_i - \sum_{\substack{m_a' \in \mathscr{S}: \\ m_a' \neq m_a}} \Pi_i^{m_a'}(t_1) \tag{B.0.4}$$

to replace the rightmost projector in (B.0.3), we obtain

$$\begin{aligned} \mathscr{C}^{\text{Proj}} &= \sum_{m_a \in \mathscr{S}} m_a \left(\langle\psi| \Pi_i^{m_a}(t_1) S_j^b(t_2) |\psi\rangle - \sum_{\substack{m_a' \in \mathscr{S}: \\ m_a' \neq m_a}} \langle\psi| \Pi_i^{m_a}(t_1) S_j^b(t_2) \Pi_i^{m_a'}(t_1) |\psi\rangle \right) \\ &= \langle\psi| S_i^a(t_1) S_j^b(t_2) |\psi\rangle - \sum_{m_a \in \mathscr{S}} m_a \sum_{\substack{m_a' \in \mathscr{S}: \\ m_a' \neq m_a}} \langle\psi| \Pi_i^{m_a}(t_1) S_j^b(t_2) \Pi_i^{m_a'}(t_1) |\psi\rangle . \end{aligned} \tag{B.0.5}$$

At this point it is convenient to define the operator

$$\Gamma \equiv \sum_{m_a \in \mathscr{S}} m_a \sum_{\substack{m'_a \in \mathscr{S}: \\ m'_a \neq m_a}} \Pi_i^{m_a}(t_1) S_j^b(t_2) \Pi_i^{m'_a}(t_1), \tag{B.0.6}$$

which depends on the measurement outcome at t_1 via the conditional probabilities (B.0.2). These, in turn, depend on the projection operators $\Pi_i^{m_a}$ which define the post-measurement state at t_1. In the proof of the following section we will consider correlations of arbitrary observables A and B (for $s \geq 1/2$), which leads to a more general form of Γ (B.1.1).

Using (B.0.6), the projectively measured correlation (B.0.5) can be expressed in terms of the exact correlation as

$$\mathscr{C}^{\text{Proj}} = C - \langle\psi| \Gamma |\psi\rangle . \tag{B.0.7}$$

Since $\langle\psi| \left[S_i^a(t_1), S_j^b(t_2)\right] |\psi\rangle = 2i\text{Im}\left[C\right]$ we can write

$$\text{Re}\left[C\right] = C - \frac{1}{2} \langle\psi| \left[S_i^a(t_1), S_j^b(t_2)\right] |\psi\rangle . \tag{B.0.8}$$

Therefore, equality between (B.0.7) and (B.0.8) holds when

$$\langle\psi| \left[S_i^a(t_1), S_j^b(t_2)\right] |\psi\rangle = 2 \langle\psi| \Gamma |\psi\rangle . \tag{B.0.9}$$

If we express $S_i^a(t_1)$ in the above commutator by its spectral decomposition and introduce the identity $\mathbb{1} = \sum_{m'_a \in \mathscr{S}} \Pi_i^{m'_a}(t_1)$ at the right of $S_j^b(t_2)$, we find that

$$\langle\psi| \left[S_i^a(t_1), S_j^b(t_2)\right] |\psi\rangle = \langle\psi| \Gamma - \Gamma^\dagger |\psi\rangle . \tag{B.0.10}$$

Therefore, $\text{Re}\left[C\right] = \mathscr{C}^{\text{Proj}}$ holds if and only if

$$\left(\Gamma - \Gamma^\dagger\right) = 2\Gamma, \tag{B.0.11}$$

i.e. if and only if Γ is anti-hermitian. This shows that validity of $\text{Re}\left[C\right] = \mathscr{C}^{\text{Proj}}$ depends on the spectra of the observables which are to be correlated.

For dynamic correlations of local spin-1/2 observables $\langle\psi| S_i^a(t_1) S_j^b(t_2) |\psi\rangle = \langle\psi| \sigma_i^a(t_1) \sigma_j^b(t_2) |\psi\rangle$ (as in Sec. 3.2.2) we have

$$2\Gamma_{1/2} = \Pi_i^{+_a}(t_1) \sigma_j^b(t_2) \Pi_i^{-_a}(t_1) - \Pi_i^{-_a}(t_1) \sigma_j^b(t_2) \Pi_i^{+_a}(t_1) = -2\Gamma_{1/2}^\dagger, \tag{B.0.12}$$

which satisfies (B.0.11) and thus confirms (3.2.14).

In contrast, for correlations of local spin-1 observables we have $m_a, m_b \in \{0, \pm 1\}$ and

$$\Gamma_1 = \left(\Pi_i^+(t_1) S_j^b(t_2) - \Pi_i^-(t_1) S_j^b(t_2)\right) \Pi_i^0(t_1) + \left(\Pi_i^+(t_1) S_j^b(t_2) \Pi_i^-(t_1) - \text{h.c.}\right) \neq -\Gamma_1^\dagger. \tag{B.0.13}$$

Any spin observable which has a 0 eigenvalue will not satisfy (B.0.11). Thus (B.0.11) is not satisfied in general for $s > 1/2$, and is in fact not even satisfied by arbitrary spin-1/2 observables: Γ is anti-hermitian only when the observable A to be correlated at t_1 has exactly two eigenvalues—which may be degenerate—of the same magnitude, but different sign. The proof of this statement is given below.

B.1 Proof

Here we prove the above statement on the validity of (B.0.11). We consider dynamic correlations $\langle\psi| A(t_1)B(t_2) |\psi\rangle$ of arbitrary many-body spin-$s \in \mathbb{N}/2$ observables A and B (not to be confused with the operators appearing in the NIMP's weak-measurement coupling Hamiltonian H_c). This proof was provided by S. Castrignano during joint work on article [14].

The observables A and B can have arbitrary supports (i.e. they need not be single-site observables) and the system Hamiltonian generating time-evolution can be an arbitrary many-body Hamiltonian. We denote the eigenvalues of A by $\{a\}$ and allow for arbitrary degeneracies, as they occur in multi-site observables. The projector corresponding to the eigenspace of a given eigenvalue is denoted as $P(a)$ and has the same (in general multi-site) support as A. The definition of Γ (B.0.6) is then

$$\Gamma \equiv \sum_{a,a'} (1 - \delta_{a,a'}) a P(a, t_1) B(t_2) P(a', t_1), \tag{B.1.1}$$

where $P(a, t_1) = U^\dagger(t_1) P(a) U(t_1)$ and we rewrite (B.0.11) as

$$\Gamma + \Gamma^\dagger = 0. \tag{B.1.2}$$

Since (B.1.2) is an operator identity it must hold that any matrix element of $\Gamma + \Gamma^\dagger$, is zero. Consider then a matrix element with respect to any two eigenstates $|\mu\rangle, |\nu\rangle$ of $A(t_1)$ with respective eigenvalues μ, ν. Then we have $P(a, t_1) |\mu\rangle = \delta_{a,\mu} |\mu\rangle$ for any a, and similarly for $|\nu\rangle$, so that

$$\langle\mu| \Gamma + \Gamma^\dagger |\nu\rangle = \left(\mu + \nu - 2 \sum_a a \delta_{a,\mu} \delta_{a,\nu} \right) \langle\mu| B(t_2) |\nu\rangle . \tag{B.1.3}$$

Eq. (B.1.3) is zero if $\langle\mu| B(t_2) |\nu\rangle = 0$. This will in general not be satisfied since we consider arbitrary many-body observables and Hamiltonians. Instead, we require

$$\left(\mu + \nu - 2 \sum_a a \delta_{a,\mu} \delta_{a,\nu} \right) = 0 \text{ for any eigenvalues } \mu, \nu \text{ of } A. \tag{B.1.4}$$

This implies that (B.1.2) is valid only if the spectral representation of A satisfies condition (B.1.4). This spectral condition is trivially fulfilled if $\mu = \nu$ i.e. if A

has degenerate eigenvalues. When $\mu \neq \nu$ (i.e. when $|\mu\rangle$ and $|\nu\rangle$ live in distinct eigenspaces of $A(t_1)$), the summation in (B.1.4) reduces to 0, and we are left with the condition

$$\mu = -\nu \text{ for all possible pairs of distinct eigenvalues } (\mu, \nu) \text{ of } A. \tag{B.1.5}$$

We thus conclude that $\Gamma + \Gamma^\dagger = 0$ (B.1.2) holds only for observables A which have *exactly two* eigenvalues of equal magnitude and opposite sign. These eigenvalues may be degenerate. Examples of such observables are single-site spin-1/2 observables which are linear combinations of the Pauli matrices. Multi-site observables constructed as a tensor product of these single-site observables also satisfy the (B.1.4)–(B.1.5). Note that there is no restriction on the observable B which is to be correlated at the later time t_2. Therefore, we can use Sec. 3.2.2's projective measurement protocol to measure any spin-1/2 correlation component $\mathrm{Re}\,\langle\psi|\, A(t_1)B(t_2)\,|\psi\rangle$, with B being an arbitrary observable and A either a single-site observable

$$A = S_i = \boldsymbol{n}_i \cdot \boldsymbol{\sigma}_i \text{ for any unit vector } \boldsymbol{n}_i \text{ and lattice spin } i, \tag{B.1.6}$$

or a multi-site observable

$$A = S_D = \prod_{i \in D} S_i \text{ for some subset of lattice sites } D. \tag{B.1.7}$$

Collective spin observables $A = \sum_{i\in D} \boldsymbol{n}_i \cdot \boldsymbol{\sigma}_i$ have more than one eigenvalue pair and thus $\mathrm{Re}\,\langle\psi|\sum_{i\in D}(\boldsymbol{n}_i \cdot \boldsymbol{\sigma}_i)(t_1)B(t_2)\,|\psi\rangle$ cannot be obtained by means of the projective measurement protocol of Sec. 3.2.2. However, one could reconstruct this correlation component from separate implementations of the projective measurement protocol: From the above proof we know that $\mathrm{Re}\,\langle\psi|\,(\boldsymbol{n}_i \cdot \boldsymbol{\sigma}_i)(t_1)B(t_2)\,|\psi\rangle$ can be measured with a projective measurement at t_1, and we denote the corresponding projective correlation (3.2.12) as $\mathscr{C}_i^{\mathrm{Proj}}$. It then follows from linearity that

$$\mathrm{Re}\,\langle\psi|\sum_{i\in D}(\boldsymbol{n}_i \cdot \boldsymbol{\sigma}_i)(t_1)B(t_2)\,|\psi\rangle = \sum_{i\in D}\mathrm{Re}\,\langle\psi|\,(\boldsymbol{n}_i \cdot \boldsymbol{\sigma}_i)(t_1)B(t_2)\,|\psi\rangle = \sum_{i\in D}\mathscr{C}_i^{\mathrm{Proj}}\,. \tag{B.1.8}$$

C

Details for derivation of section 4.1.2

For the spin lattice Λ considered in bound (4.1.37) of Sec. 4.1.2, the lattice dimension is $D = 1$ so that the neighbourhood function $g(r)$ defined in Sec. 4.1.1 by Eq. (4.1.13) becomes

$$g(r) = C(1 + r) \text{ for } r \geq 0. \tag{C.0.1}$$

The function $f(R)$ is defined in terms of a supremum over the interactions within the lattice Λ (see (4.1.11)). For long-range interactions of Hamiltonians (4.1.23) and (4.1.25) the left-hand-side of (4.1.11) becomes

$$\begin{aligned}
\sup_{x\in\Lambda} \sum_{\substack{Z\ni x:\\ \operatorname{diam}(Z)\geq R}} \|\Phi(Z)\| =& \sup_{x\in\Lambda} \sum_{\substack{y\in\Lambda:\\ d(x,y)\geq R}} \|U_{x,y}\sigma_x^z\sigma_y^z\| \\
\leq& \sup_{x\in\Lambda} \sum_{\substack{y\in\Lambda:\\ d(x,y)\geq R}} U_0(1 + (d(x,y)/R_c)^6)^{-1} \\
\leq& 2U_0 \sum_{d\geq R} (1 + (d/R_c)^6)^{-1} \\
\leq& 2U_0 \int_R^\infty dx \left[1 + \left(\frac{x-1}{R_c}\right)^6\right]^{-1}.
\end{aligned} \tag{C.0.2}$$

In the second line we have used property (4.1.20) and $\|\sigma^a\| = 1$ for any $a \in \{x, y, z\}$. In the third line we assume that the system is thermodynamically large, and the resulting translational invariance allows us to drop the supremum. The factor 2 arises because in $D = 1$ dimensions there are always two lattice sites y which are a distance d away from a given site x. In principle the sum in line three suffices as a definition of $f(R)$, however, in order to obtain a closed form which depends only on R, we upper bound this sum with an integral in the last line. To do so we used that for a function $y(x)$ which is non-increasing on $x \in [0, \infty)$

$$\sum_{x\geq R} y(x) = \sum_{x=R}^\infty y(x) \leq \int_R^\infty dx\, y(x-1). \tag{C.0.3}$$

The closed form for $f(R)$ is then

$$\begin{aligned} f(R) =& 2U_0 \int_R^\infty dx(1+((x-1)/R_c)^6)^{-1} = 2U_0 R_c \int_{\frac{R-1}{R_c}}^\infty \frac{du}{1+u^6} \\ =& \frac{2U_0 R_c}{6}\Bigg[2\pi + \arctan(\sqrt{3}-2\frac{R-1}{R_c}) - 2\arctan(\frac{R-1}{R_c}) - \arctan(\sqrt{3}+2\frac{R-1}{R_c}) \\ & - \sqrt{3}\text{arctanh}\left(\frac{\sqrt{3}\frac{R-1}{R_c}}{1+\left(\frac{R-1}{R_c}\right)^2}\right)\Bigg], \end{aligned} \tag{C.0.4}$$

where the integral has been solved using partial fractions. A plot of (C.0.4) is given in Fig. C.0.1 for various Rydberg length scales R_c. The plot verifies that f is decreasing on $R \in [0,\infty)$ and that it captures the behaviour of the long-range interactions of Hamiltonians (4.1.23) and (4.1.25). For the contour plots in the main text (Fig. 4.1.2) we have used $R_c = 1$. Note that $f(R)$ is not unique; a simpler function which also satisfies condition (4.1.11) is $\sum_{d=R}^\infty R_c^6/d^6$. This however diverges as R tends to 0 and this leads to a loose Lieb-Robinson bound (LRB).

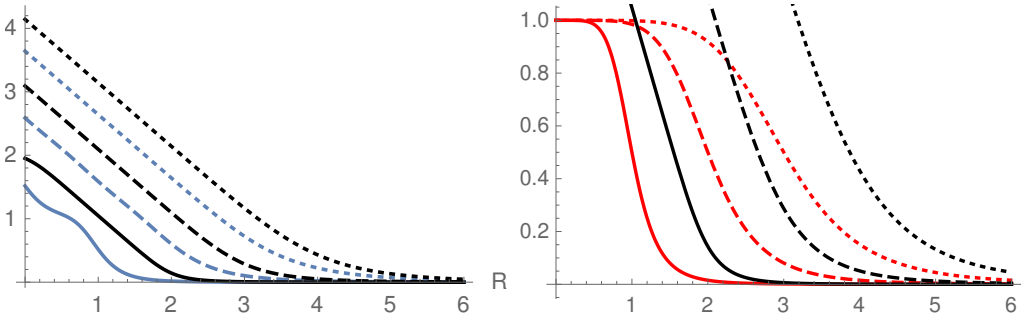

Figure C.0.1: Function $f(R)$ as defined by (C.0.4) for $U_0 = 1$ and different values of the length scale R_c induced by the Rydberg interactions of Ref. [29]: $R_c = 1$, (solid line), $R_c = 2$ (dashed line), $R_c = 3$ (dotted line). Left: Comparison of $f(R)$ to the sum in the third line of (C.0.2), given by blue (grey) lines for different values of R_c. Black and blue curves with the same line-style were calculated with the same value of R_c. The function $f(R)$ lies above the sum for all $R \geq 0$ and decreases as R increases, as is required by definition (4.1.11). Right: Comparison of $f(R)$ to a single interaction strength term $U_0/(1+(d/R_c)^6)$ for $U_0 = 1$. As the Rydberg length scale R_c increases, the soft-core plateau of the interaction strength is extended, but decreases rapidly once $d > R_c$ and then tends to 0. This is reflected in the function $f(R)$ which remains large for longer as R_c increases, but rapidly approaches 0 for $R > R_c$.

Bibliography

[1] Kubo, R.: Statistical-mechanical theory of irreversible processes. I. General theory and simple applications to magnetic and conduction problems. *J. Phys. Soc. Jpn.*, vol. 12, pp. 570–586, 1957.

[2] Glauber, R.J.: The quantum theory of optical coherence. *Phys. Rev.*, vol. 130, pp. 2529–2539, 1963.

[3] Sciolla, B., Poletti, D. and Kollath, C.: Two-time correlations probing the dynamics of dissipative many-body quantum systems: Aging and fast relaxation. *Phys. Rev. Lett.*, vol. 114, p. 170401, Apr 2015.
Available at: https://link.aps.org/doi/10.1103/PhysRevLett.114.170401

[4] Makhlin, Y., Schön, G. and Shnirman, A.: Statistics and noise in a quantum measurement process. *Phys. Rev. Lett.*, vol. 85, pp. 4578–4581, Nov 2000.
Available at: https://link.aps.org/doi/10.1103/PhysRevLett.85.4578

[5] Di Lorenzo, A., Campagnano, G. and Nazarov, Y.V.: Full counting statistics of noncommuting variables: The case of spin counts. *Phys. Rev. B*, vol. 73, p. 125311, Mar 2006.
Available at: https://link.aps.org/doi/10.1103/PhysRevB.73.125311

[6] Oehri, D., Lebedev, A.V., Lesovik, G.B. and Blatter, G.: Projective versus weak measurement of charge in a mesoscopic conductor. *Phys. Rev. B*, vol. 90, p. 075312, Aug 2014.
Available at: https://link.aps.org/doi/10.1103/PhysRevB.90.075312

[7] Knap, M., Kantian, A., Giamarchi, T., Bloch, I., Lukin, M.D. and Demler, E.: Probing real-space and time-resolved correlation functions with many-body Ramsey interferometry. *Phys. Rev. Lett.*, vol. 111, p. 147205, 2013.

[8] Romero-Isart, O., Rizzi, M., Muschik, C.A., Polzik, E.S., Lewenstein, M. and Sanpera, A.: Quantum memory assisted probing of dynamical spin correlations. *Phys. Rev. Lett.*, vol. 108, p. 065302, Feb 2012.
Available at: https://link.aps.org/doi/10.1103/PhysRevLett.108.065302

[9] Svensson, B.: Pedagogical review of quantum measurement theory with an emphasis on weak measurements. *Quanta*, vol. 2, no. 1, pp. 18–49, 2013. ISSN 1314-7374.
Available at: http://quanta.ws/ojs/index.php/quanta/article/view/12

[10] Braginsky, V.B. and Khalili, F.Y.: *Quantum Measurement*. Cambridge University Press, 1992.

[11] Jacobs, K. and Steck, D.A.: A straightforward introduction to continuous quantum measurement. *Contemp. Phys.*, vol. 47, pp. 279–303, 2006.

[12] Wiseman, H.M. and Milburn, G.J.: *Quantum Measurement and Control*. Cambridge University Press, Cambridge, 2010.

[13] Das, D. and Arvind: Estimation of quantum states by weak and projective measurements. *Phys. Rev. A*, vol. 89, p. 062121, 2014.

[14] Uhrich, P., Castrignano, S., Uys, H. and Kastner, M.: Noninvasive measurement of dynamic correlation functions. *Phys. Rev. A*, vol. 96, p. 022127, Aug 2017. Available at: https://link.aps.org/doi/10.1103/PhysRevA.96.022127

[15] Jacobs, K.: *Quantum Measurement Theory and its Appplications*. Cambridge University Press, 2014.

[16] Nielsen, M.A. and Chuang, I.L.: *Quantum Computation and Quantum Information*. Cambridge University Press, 2000.

[17] von Neumann, J.: *Mathematical Foundations of Quantum Mechanics*. Princeton University Press, 1955.

[18] Peres, A.: *Quantum Theory: Concepts and Methods*. Kluwer Academic Publishers, 1993.

[19] Oehri, D., Lebedev, A.V., Lesovik, G.B. and Blatter, G.: Time correlators from deferred measurements. *Phys. Rev. B*, vol. 93, p. 045308, 2016.

[20] Johansen, L.M. and Mello, P.A.: Quantum mechanics of successive measurements with arbitrary meter coupling. *Phys. Lett. A*, vol. 372, pp. 5760–5764, 2008.

[21] Jordan, A.N., Korotkov, A.N. and Büttiker, M.: Leggett-Garg inequality with a kicked quantum pump. *Phys. Rev. Lett.*, vol. 97, p. 026805, 2006.

[22] Goggin, M.E., Almeida, M.P., Barbieri, M., Lanyon, B.P., O'Brien, J.L., White, A.G. and Pryde, G.J.: Violation of the Leggett–Garg inequality with weak measurements of photons. *Proc. Natl. Acad. Sci. USA*, vol. 108, pp. 1256–1261, 2011.

[23] Young, H.: *Statistical Treatment of Experimental Data*. McGraw-Hill Book Company, 1962. Chapter III.8.

[24] Yan, B., Moses, S.A., Gadway, B., Covey, J.P., Hazzard, K.R.A., Rey, A.M., Jin, D.S. and Ye, J.: Observation of dipolar spin-exchange interactions with lattice-confined polar molecules. *Nature (London)*, vol. 501, pp. 521–525, 2013.

[25] Schwarzkopf, A., Sapiro, R.E. and Raithel, G.: Imaging spatial correlations of Rydberg excitations in cold atom clouds. *Phys. Rev. Lett.*, vol. 107, p. 103001, Aug 2011. Available at: https://link.aps.org/doi/10.1103/PhysRevLett.107.103001

[26] Lahaye, T., Menotti, C., Santos, L., Lewenstein, M. and Pfau, T.: The physics of dipolar bosonic quantum gases. *Rep. Prog. Phys.*, vol. 72, p. 126401, 2009.

[27] Britton, J.W., Sawyer, B.C., Keith, A.C., Wang, C.-C.J., Freericks, J.K., Uys, H., Biercuk, M.J. and Bollinger, J.J.: Engineered two-dimensional Ising interactions in a trapped-ion quantum simulator with hundreds of spins. *Nature (London)*, vol. 484, pp. 489–492, 2012.

[28] Zhang, J., Pagano, G., Hess, P.W., Kyprianidis, A., Becker, P., Kaplan, H., Gorshkov, A.V., Gong, Z.-X. and Monroe, C.: Observation of a Many-Body Dynamical Phase Transition with a 53-Qubit Quantum Simulator. *arXiv:1708.01044*, 2017.

[29] Zeiher, J., van Bijnen, R., Schausz, P., Hild, S., Choi, J., Pohl, T., Bloch, I. and Gross, C.: Many-body interferometry of a Rydberg-dressed spin lattice. *Nat Phys*, vol. 12, no. 12, pp. 1095–1099, December 2016. ISSN 1745-2473.
Available at: http://dx.doi.org/10.1038/nphys3835

[30] Steane, A.: The ion trap quantum information processor. *Applied Physics B*, vol. 64, no. 6, pp. 623–643, Jun 1997. ISSN 1432-0649.
Available at: https://doi.org/10.1007/s003400050225

[31] Ozeri, R.: The trapped-ion qubit tool box. *Contemporary Physics*, vol. 52, no. 6, pp. 531–550, 2011.
Available at: http://dx.doi.org/10.1080/00107514.2011.603578

[32] Itano, W.M., Bergquist, J.C., Bollinger, J.J. and Wineland, D.J.: Cooling methods in ion traps. *Physica Scripta*, vol. 1995, no. T59, p. 106, 1995.
Available at: http://stacks.iop.org/1402-4896/1995/i=T59/a=013

[33] James, D.: Quantum dynamics of cold trapped ions with application to quantum computation. *Applied Physics B*, vol. 66, no. 2, pp. 181–190, Feb 1998. ISSN 1432-0649.
Available at: https://doi.org/10.1007/s003400050373

[34] Sawyer, B.C., Britton, J.W., Keith, A.C., Wang, C.-C.J., Freericks, J.K., Uys, H., Biercuk, M.J. and Bollinger, J.J.: Spectroscopy and thermometry of drumhead modes in a mesoscopic trapped-ion crystal using entanglement. *Phys. Rev. Lett.*, vol. 108, p. 213003, May 2012.
Available at: http://link.aps.org/doi/10.1103/PhysRevLett.108.213003

[35] Bakr, W.S., Gillen, J.I., Peng, A., Folling, S. and Greiner, M.: A quantum gas microscope for detecting single atoms in a Hubbard-regime optical lattice. *Nature*, vol. 462, no. 7269, pp. 74–77, November 2009. ISSN 0028-0836.
Available at: http://dx.doi.org/10.1038/nature08482

[36] Boll, M., Hilker, T.A., Salomon, G., Omran, A., Nespolo, J., Pollet, L., Bloch, I. and Gross, C.: Spin- and density-resolved microscopy of antiferromagnetic correlations in Fermi-Hubbard chains. *Science*, vol. 353, no. 6305, pp. 1257–1260, September 2016.

[37] Haller, E., Hudson, J., Kelly, A., Cotta, D.A., Peaudecerf, B., Bruce, G.D. and Kuhr, S.: Single-atom imaging of fermions in a quantum-gas microscope. *Nat Phys*, vol. 11, no. 9, pp. 738–742, September 2015. ISSN 1745-2473.
Available at: http://dx.doi.org/10.1038/nphys3403

[38] Lieb, E.H. and Robinson, D.W.: The Finite Group Velocity of Quantum Spin Systems. *Commun. Math. Phys.*, vol. 28, pp. 251–257, 1972.

[39] Aliprantis, C.D. and Border, K.C.: *Infinite Dimensional Analysis: A hitchhikers guide*. Springer, 2006.

[40] Bachmann, S., Michalakis, S., Nachtergaele, B. and Sims, R.: Automorphic equivalence within gapped phases of quantum lattice systems. *Commun. Math. Phys.*, vol. 309, no. 3, pp. 835–871, 2 2012. ISSN 0010-3616.

[41] Hastings, M.B. and Koma, T.: Spectral Gap and Exponential Decay of Correlations. *Commun. Math. Phys.*, vol. 265, pp. 781–804, 2006.

[42] Eisert, J., van den Worm, M., Manmana, S.R. and Kastner, M.: Breakdown of quasilocality in long-range quantum lattice models. *Phys. Rev. Lett.*, vol. 111, p. 260401, 2013.

[43] Foss-Feig, M., Gong, Z.-X., Clark, C.W. and Gorshkov, A.V.: Nearly Linear Light Cones in Long-Range Interacting Quantum Systems. *Phys. Rev. Lett.*, vol. 114, p. 157201, 2015.

[44] Matsuta, T., Koma, T. and Nakamura, S.: Improving the Lieb–Robinson bound for long-range interactions. *Annales Henri Poincaré*, vol. 18, no. 2, pp. 519–528, 2017. ISSN 1424-0661.
Available at: http://dx.doi.org/10.1007/s00023-016-0526-1

[45] Gallagher, T.F. and Pillet, P.: Dipole-dipole interactions of Rydberg atoms. *Advances in Atomic, Molecular, and Optical Physics*, vol. 56, pp. 161–218, 2008.

[46] Glaetzle, A.W., Dalmonte, M., Nath, R., Gross, C., Bloch, I. and Zoller, P.: Designing Frustrated Quantum Magnets with Laser-Dressed Rydberg Atoms. *Phys. Rev. Lett.*, vol. 114, p. 173002, Apr 2015.
Available at: https://link.aps.org/doi/10.1103/PhysRevLett.114.173002

[47] Kastner, M.: Entanglement-enhanced spreading of correlations. *New Journal of Physics*, vol. 17, no. 12, p. 123024, 2015.
Available at: http://stacks.iop.org/1367-2630/17/i=12/a=123024

[48] Mølmer, K. and Sørensen, A.: Multiparticle entanglement of hot trapped ions. *Phys. Rev. Lett.*, vol. 82, pp. 1835–1838, Mar 1999.
Available at: http://link.aps.org/doi/10.1103/PhysRevLett.82.1835

[49] Leibfried, D., DeMarco, B., Meyer, V., Lucas, D., Barrett, M., Britton, J., Itano, W.M., Jelenkovic, B., Langer, C., Rosenband, T. and Wineland, D.J.: Experimental demonstration of a robust, high-fidelity geometric two ion-qubit phase gate. *Nature*, vol. 422, no. 6930, pp. 412–415, March 2003. ISSN 0028-0836.
Available at: http://dx.doi.org/10.1038/nature01492

[50] Kim, K., Chang, M.-S., Islam, R., Korenblit, S., Duan, L.-M. and Monroe, C.: Entanglement and Tunable Spin–Spin Couplings between Trapped Ions Using Multiple Transverse Modes. *Phys. Rev. Lett.*, vol. 103, p. 120502, 2009.

[51] Zhu, S.-L., Monroe, C. and Duan, L.-M.: Trapped ion quantum computation with transverse phonon modes. *Phys. Rev. Lett.*, vol. 97, p. 050505, Aug 2006.
Available at: http://link.aps.org/doi/10.1103/PhysRevLett.97.050505

[52] Derzhko, O. and Krokhmalskii, T.: Numerical Approach for the Study of the Spin-1/2 XY Chains Dynamic Properties. *Physica Status Solidi B: Basic Solid State Physics*, vol. 208, pp. 221–248, 1998.

[53] Suzuki, S., Inoue, J. and Chakrabarti, B.K.: *Quantum Ising Phases and Transitions in Transverse Ising Models*. Springer, 2013.

[54] Lieb, E., Schultz, T. and Mattis, D.: Two soluble models of an antiferromagnetic chain. *Annals of Physics*, vol. 16, pp. 407–466, 1961.

[55] Campisi, M. and Goold, J.: Thermodynamics of quantum information scrambling. *Phys. Rev. E*, vol. 95, p. 062127, Jun 2017.
Available at: https://link.aps.org/doi/10.1103/PhysRevE.95.062127

[56] Bohrdt, A., Mendl, C.B., Endres, M. and Knap, M.: Scrambling and thermalization in a diffusive quantum many-body system. *New Journal of Physics*, vol. 19, no. 6, p. 063001, 2017.
Available at: http://stacks.iop.org/1367-2630/19/i=6/a=063001

[57] Hosur, P., Qi, X.-L., Roberts, D.A. and Yoshida, B.: Chaos in quantum channels. *Journal of High Energy Physics*, vol. 2016, no. 2, p. 4, Feb 2016. ISSN 1029-8479.
Available at: https://doi.org/10.1007/JHEP02(2016)004

[58] Swingle, B., Bentsen, G., Schleier-Smith, M. and Hayden, P.: Measuring the scrambling of quantum information. *Phys. Rev. A*, vol. 94, p. 040302, Oct 2016.
Available at: https://link.aps.org/doi/10.1103/PhysRevA.94.040302

[59] Yao, N.Y., Grusdt, F., Swingle, B., Lukin, M.D., Stamper-Kurn, D.M., Moore, J.E. and Demler, E.A.: Interferometric Approach to Probing Fast Scrambling. *ArXiv e-prints*, July 2016. 1607.01801.